Spring 2018

Reprocessing of the 2 Hz P-P data from the Blackfoot 3C-2D survey with special reference to multicomponent seismic processing

Onur Akturk

Department:

REPROCESSING OF THE 2 HZ P-P DATA FROM THE BLACKFOOT 3C-2D SURVEY WITH SPECIAL REFERENCE TO MULTICOMPONENT SEISMIC PROCESSING

by

ONUR AKTURK

A THESIS

Presented to the Graduate Faculty of the

MISSOURI UNIVERSITY OF SCIENCE AND TECHNOLOGY

In Partial Fulfillment of the Requirements for the Degree

MASTER OF SCIENCE

in

GEOLOGY AND GEOPHYSICS

2018

Approved by

Dr. Kelly Liu, Advisor
Dr. Stephen Gao
Dr. Neil Anderson

ABSTRACT

The 3C-2D multicomponent seismic survey was acquired in the Blackfoot Field, which is located 15 km southeast of Strathmore, Alberta. The 2 Hz vertical component data were reprocessed to better image the target reservoir, the Glauconitic sand formation at approximately 1150 ms. The zone of the major reflector at about 1550 ms was also taken into consideration to determine the better seismic section for further processing. The main characteristics of the converted wave processing, such as common conversion point (CCP), asymptotic binning, gamma ratios, receiver statics, rotation of the data, positive/negative offsets, and anisotropy, were also summarized in this study.

The processing chart was determined by testing a number of parameters and methods. Different types of deconvolution, static corrections, and migrations were applied to the seismic data to better image the target zone. The noise attenuation steps reduced the ground roll noise and increased the signal-to-noise ratio. Two-dimensional Kirchhoff prestack and poststack time migration were utilized to image the subsurface. Since the lithology discrimination between the target reservoir and the neighboring shales is the main issue in the study area, the spectral whitening was applied to the migrated sections to increase the resolution and the appearance of the reservoir. In this context, the obtained results suggest that the prestack time migration offered stronger amplitudes in the target zone, and the channel cuts were observed clearer than the poststack migration.

ACKNOWLEDGMENTS

I am thankful to my advisor, Dr. Kelly Liu, for her suggestions and assistance to improve my thesis during my research. I also would like to thank Dr. Stephen Gao and Dr. Neil Anderson for accepting to be members of the Master Thesis Committee.

I am grateful to my sponsors, Turkish Ministry of National Education and Turkish Petroleum Corporation (TPAO), for providing me this opportunity to pursue a master's degree in the United States.

I would like to acknowledge Emily Seals, who assisted in the editing of the grammar of my thesis.

Thank you to all my relatives and friends who shared their support and encouragement.

I would like to thank Gorkem Yagci and Fulya Yagci for their positive contributions during my study. It was really helpful to have their assistance since they went through the same way.

I would like to thank Havva Malone, whose guidance and kindness has been invaluable to me since I met her.

I will always be grateful to my family, especially my mother and my father, for their endless support throughout my life.

DEDICATION

To our scientists, academicians, and teachers who make valuable contributions to the development of the Republic of Turkey.

To our martyrs and veterans, who we owe much.

To our soldiers who fight for our country without hesitation.

To my brother, Yasin Akturk, who is an honorable naval officer working for the Turkish Navy.

TABLE OF CONTENTS

Page

LIST OF ILLUSTRATIONS

LIST OF TABLES

NOMENCLATURE

Symbol	Description
2D	Two-dimensional
3C	Three-component
3D	Three-dimensional
AGC	Automatic gain control
BCF	Billion Cubic Feet
CCP	Common conversion point
CMP	Common midpoint
CVG	Constant velocity gather
CVS	Constant velocity stack
HTI	Horizontally transverse isotropy
MMbbls	Million barrels
Qa	Directional azimuth
PSTM	Prestack time migration
RMS	Root-mean square
SEG	Society of Exploration Geophysics
SH	Horizontal S-wave
SV	Vertical S-wave
Vp	P-wave velocity
Vs	S-wave velocity
VTI	Vertically transverse isotropy

1. INTRODUCTION

The 3C-2D broadband seismic data used in this study were acquired in 1995 through the CREWES Project in the Blackfoot Field, which is located in Township 23, Range 23, 15 km southeast of Strathmore, Alberta (Figure 1.1). The field is operated by Encana Petroleum Ltd (Lu and Maier, 2009).

The primary objectives of this survey were to 1) image the Glauconitic sandstone reservoir, which is the target zone, 2) analyze the differences among a variety of geophones, and 3) obtain the best probable broadband seismic data. Additionally, the 3C-2D seismic data were utilized to plan the optimal parameters for a subsequent 3C-3D survey over the same area in the Blackfoot Field (Stewart, 1995).

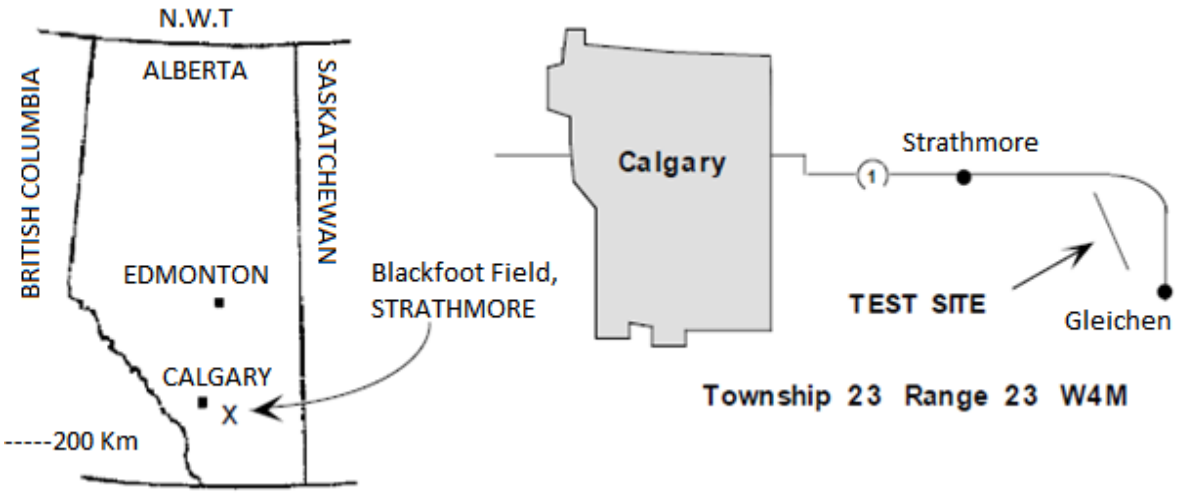

Figure 1.1. Location of the Blackfoot Field (Stewart et al., 1996).

The Blackfoot 3C-2D broadband seismic project (Line 950278) consists of five lines, which correspond to various geophones (1C-10 Hz, 3C-10 Hz, 3C-4.5 Hz, 2 Hz vertical and radial) used in the survey. The distance between each line is 1 m. The length of the line is 4 km, trending southeast to northwest. The receiver and source interval is 20 m. The shots are taken at every half receiver interval using 6 kg dynamite at 18 m depth. There are

200 receiver and source stations in the survey, and all of the receiver stations are live for each shot. There are 16 wells in the study area, and one of them, i.e., well 14-09 intersects with the survey line at shot point 156 (Figure 1.2). These wells include sonic and density logs as well (Gallant et al., 1996).

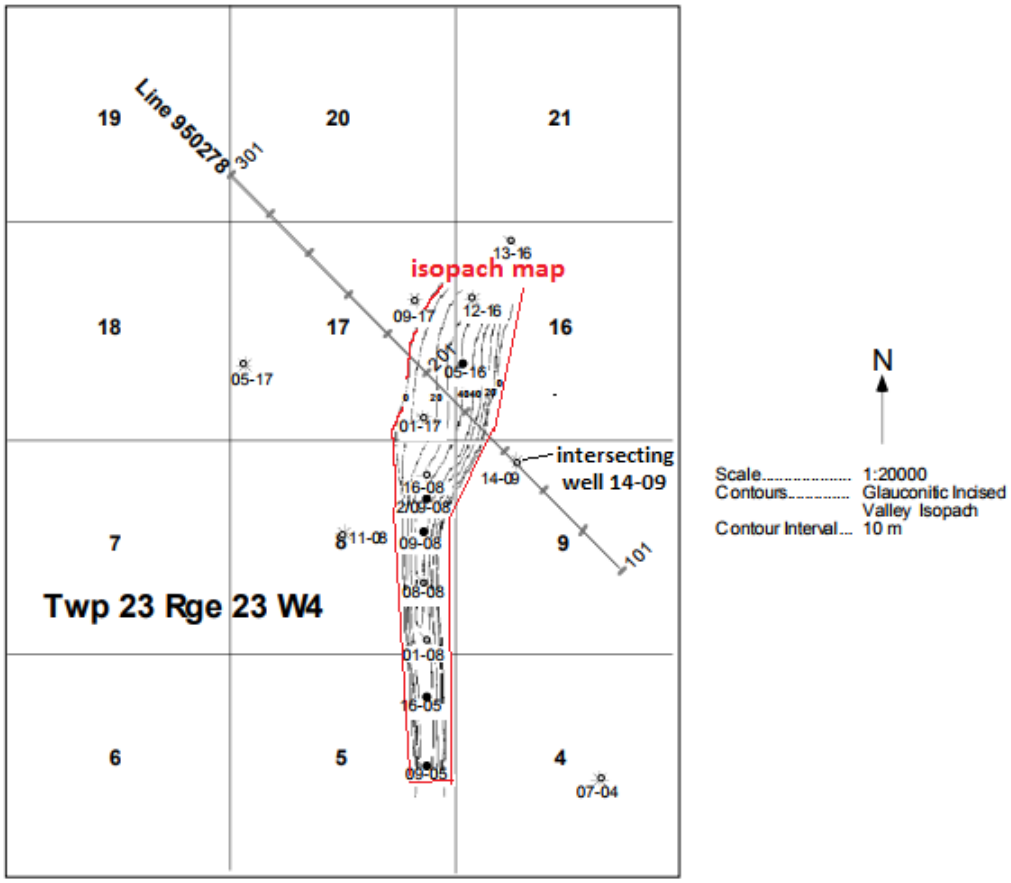

Figure 1.2. Location of the survey line. The contours indicate the incised valley isopach (Miller et al., 1995).

The main objective of this study is to reprocess the 2 Hz vertical component data to increase the quality and resolution of the seismic image in the Glauconitic sand reservoir in particular, which is approximately at 1150 ms. A previous study indicated that the neighboring shales around the reservoir have very similar P-wave anomalies to those of the reservoir (Stewart et al., 1996). As a result, it is hard to observe the reservoir on the P-wave seismic sections. For this reason, the zone of the major reflector at about 1550 ms is also

taken into consideration to determine a seismic section with the better quality during the processing stages. Several parameters are tested to obtain optimum results regarding the quality of seismic sections, and each step is followed by a stacked section to determine the better results when different processing methods and algorithms are applied.

The Blackfoot 3C-2D survey includes multicomponent geophone arrays, which contain vertical, radial, and transverse components. The main aspects of the multicomponent seismic data processing such as common conversion point (CCP), asymptotic binning, gamma ratios, positive/negative offsets, receiver statics, rotation of the data, and anisotropy are also discussed in this study. Several examples of the applications of the multicomponent seismic method are presented by comparing P-P and P-S seismic sections.

1.1. GEOLOGICAL BACKGROUND

A chart of the stratigraphic sequence in the Blackfoot Field is shown in Figure 1.3. The target reservoir is the Glauconitic sand formation, a member of the Upper Mannville Group of the Lower Cretaceous in the Alberta Basin (Yang et al., 1996).

The Alberta Basin, a part of the Western Canadian Sedimentary Basin, extends from the Rocky Mountain Thrust Belt in the west to the Precambrian Canadian Shield in the northeast, and to the Sweetgrass Arch in the southwest (Connolly et al., 1990) (Figure 1.4).

During the Lower Cretaceous, older miogeoclinal rocks were compressed by the accretion of allochthonous terrains and thrusted towards the continental margin. The pile of accumulated thrust layers (sheets) caused the craton edge to subside, reserving accommodation in the foredeep for the huge amount of sediments separated (segregated) from upthrusted layers or sheets. As a result, the deposition of the Mannville Group was initiated by the introduction of these sediments to the foreland basin (Mossop and Shetsen, 1994).

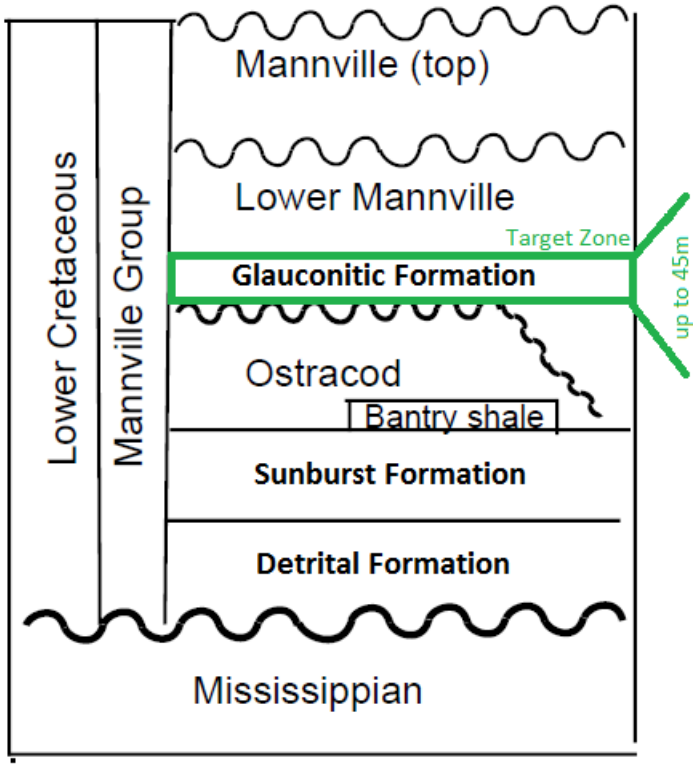

Figure 1.3. Stratigraphic sequence in the study area (Modified from (Miller et al., 1995)).

There were three regional tectonic elements that affected the sedimentation of the Mannville Group within the foreland basin, i.e., the foredeep, Peace River Arch, and Liard Basin (Mossop and Shetsen, 1994) (Figure 1.5). Base level rose prior to the Lower Cretaceous transgression of the Boreal Sea. The Mannville Group thickens suddenly from the east toward the foredeep. The thickest section of the Mannville Group is conserved where the foredeep and the Peace River Arch converge in the northeast of British Columbia (Mossop and Shetsen, 1994). The overall tectonic setting of the Upper Mannville Group is assumed to be transgressional from the northwest with progradations counteracting from the northeast (Christopher, 2002).

The target reservoir in the study area is at a depth of approximately 1550 m, and with a thickness up to 45 m. A previous study indicated that these kinds of sand formations have the capability to produce the most prolific hydrocarbon reservoirs in the southeast of

Figure 1.4. Tectonic setting of the study area (Regulator, 2015).

Strathmore (Stewart et al., 1996). Oil is the primary hydrocarbon source in the study area. The Glauconitic sands are productive and lucrative reservoirs and have produced over 200 MMbbls and 400 BCF of gas in the southern Alberta (Miller et al., 1995).

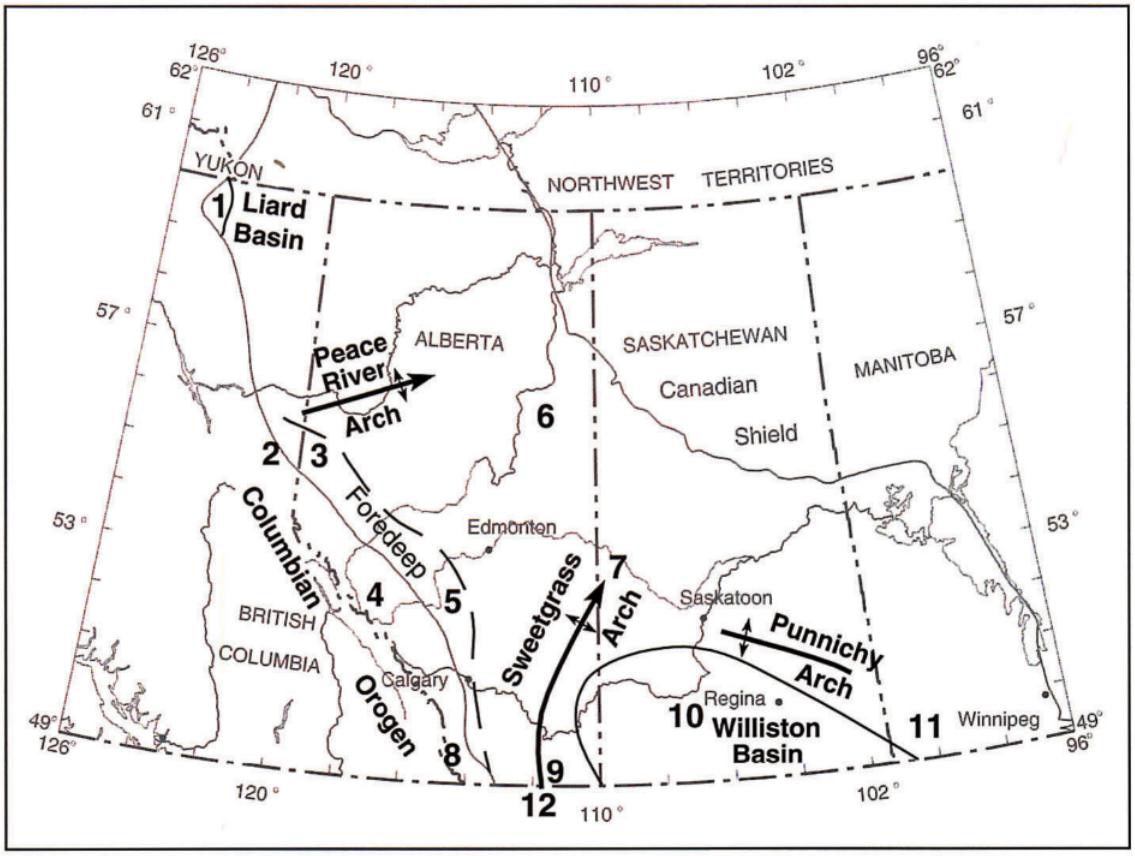

Figure 1.5. Tectonic elements affecting the Mannville deposition (Mossop and Shetsen, 1994).

The Glauconitic sand formation in the Blackfoot Field consists of quartz sandstones from very fine to medium grain with salt and pepper sandstones. The hydrocarbon sources are stratigraphtically trapped within these quartz sandstones of the Glauconitic member of the Lower Cretaceous (Yang et al., 1996).

The target is located in the incised valley fill or channel fill sediments that were formed in a fluvial/estuarine environment (Miller et al., 1995). Incised valley systems are assumed to form in two different phases. The first phase includes erosion into coastal plain or shelf sediments as opposed to a relative fall in sea level, which is followed by sediment

bypass with the aid of the valley that is eroded and deposition that occurs at the lowstand shoreline. The second phase includes deposition of fine-grained fluvial/estuarine sediments within the valleys as opposed to a relative rise in sea level (Dyson and Christopher, 1994).

A previous study showed that the Glauconitic sand formation in the study area is an unconformity bounded sequence formed by sea level fluctuations on an ancient coastal plain (Wood and Hopkins, 1992). There are a number of incised valley systems filled with fluvial/esturaine facies in this region, which is trending in the northwest direction. The sediments of the channel are divided into three parts, i.e., Upper, Lithic, and Lower incised valleys, which correspond to three stages of the valley incision (Miller et al., 1995). The main reservoirs are the Upper and the Lower incised valleys (Dufour et al., 1998).

The problem associated with the exploration of the Lower Cretaceous incised valley sandstone reservoir in the study area arises from the difficulty to differentiate the shale from the sandstone due to their similar acoustic impedance (Mawdsley et al., 1996). As mentioned before, it is essential to note that since the neighboring shales around the Glauconitic sand reservoirs have similar P-wave anomalies to the reservoirs. This leads to an obstacle to observe the reservoir on P-wave seismic sections (Stewart et al., 1996).

1.2. SURVEY ACQUISITION

The 3C-2D Blackfoot broadband survey has two main objectives. One is to confirm ratios of sand/shale within an incised valley, and another objective is to determine the optimal parameters for the subsequent 3C-3D survey (Miller et al., 1995). The survey includes five lines, which correspond to various of geophones (1C-10 Hz, 3C-10 Hz, 3C-4.5 Hz, 1C-2 Hz vertical and radial) used during the acquisition of the data (Figure 1.6). There is a 1 m interval between each line.

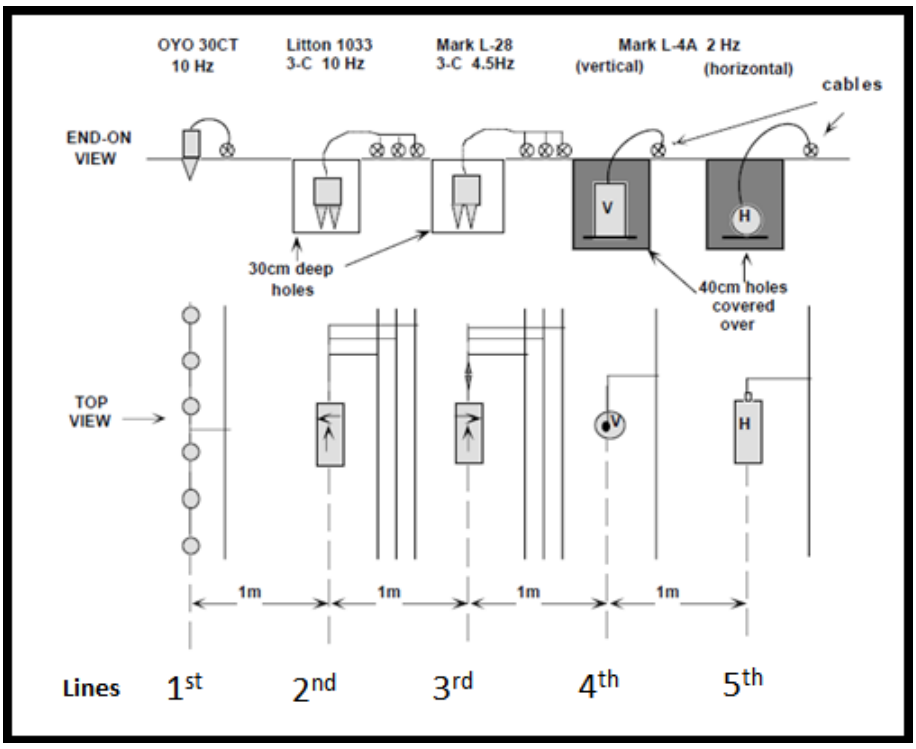

Figure 1.6. The geophone and cable layout for each receiver line (Gallant et al., 1996).

The first line consists of 200 strings of Oyo GS-30 CT 10 Hz vertical geophones. The interval between each geophone is 20 m. The second line contains Litton 1033 3-C 10 Hz geophones that are spread out in 30 cm deep holes. These geophones have individual cables and 200 channels per component (Gallant et al., 1996).

For the third line, Mark L-28 4.5 Hz 3-C geophones are deployed in 30 cm deep holes and have individual cables with a total of 600 live channels. For the fourth line, Mark L-4A 2 Hz vertical geophones are placed in holes 40 cm deep. The fifth line, a shorter line of 60 channels Mark L-4A 2 Hz horizontal geophones, is laid out one meter from the fourth line, and the geophones are put in 40 cm deep holes. These 2 Hz horizontal geophones are deployed in the center of the spread from stations 153 to 213 (Gallant et al., 1996).

There are 200 receiver and source stations in this survey, and the geophones are spread out over 4 km line (Gallant et al., 1996). Seismic sources are mostly from 6 kg dynamite at a depth of 18 m. Using the 6 kg dynamite source is preferred to capture

the most broadband seismic data possible, particularly the low frequencies (Gallant et al., 1996). The source and receiver interval is 20 m and shots are taken at every half interval, which gives the minimum offset 10 m and the maximum offset 3990 m (Figure 1.7).

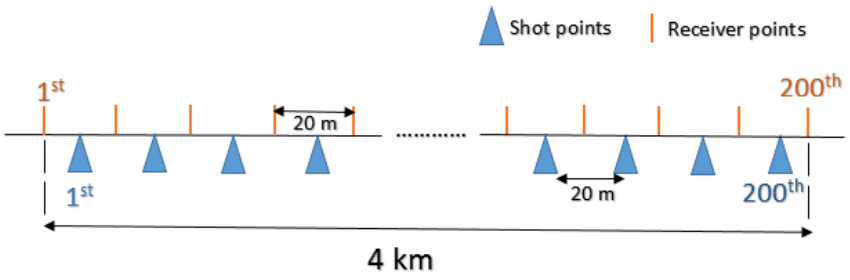

Figure 1.7. Schematic diagram of the layout of sources and geophones for the 4th line used in this study.

The 4 km survey line being live for each shot results in an end-on spread with a 3990 m maximum offset at the end of the line and a split-spread with an approximately 2000 m offset in the center of the line (Margrave, 1995). Table 1.1 shows the acquisition parameters used in the survey.

Table 1.1. The acqusition parameters for the Blackfoot 3C-2D survey (Gallant et al., 1996).

Line length	4 km
Shot interval	20 m
Receiver interval	20 m
Shot depth	18 m
Source	Dynamite
Shot numbers	200
Receiver numbers	200
Sample rate	1 ms
Number of channels	200
Record length	6 s
Minimum offset	10 m
Maximum offset	3990 m
Spread	Fixed split-spread
Geophones	Mark L-4A 2 Hz vertical

1.3. DATA QUALITY

In this study, the data analyses were performed on the seismic data acquired using Mark L-4A 2 Hz vertical geophones. Since this survey was conducted using a broadband recording system, which is referred to as a wider frequency content, there was an observable increase in the signal energy of the seismic data (Gorek et al., 1995). The amplitude spectrum of shots 1–3 suggests that the frequency content of the data is adequate (Figure 1.8).

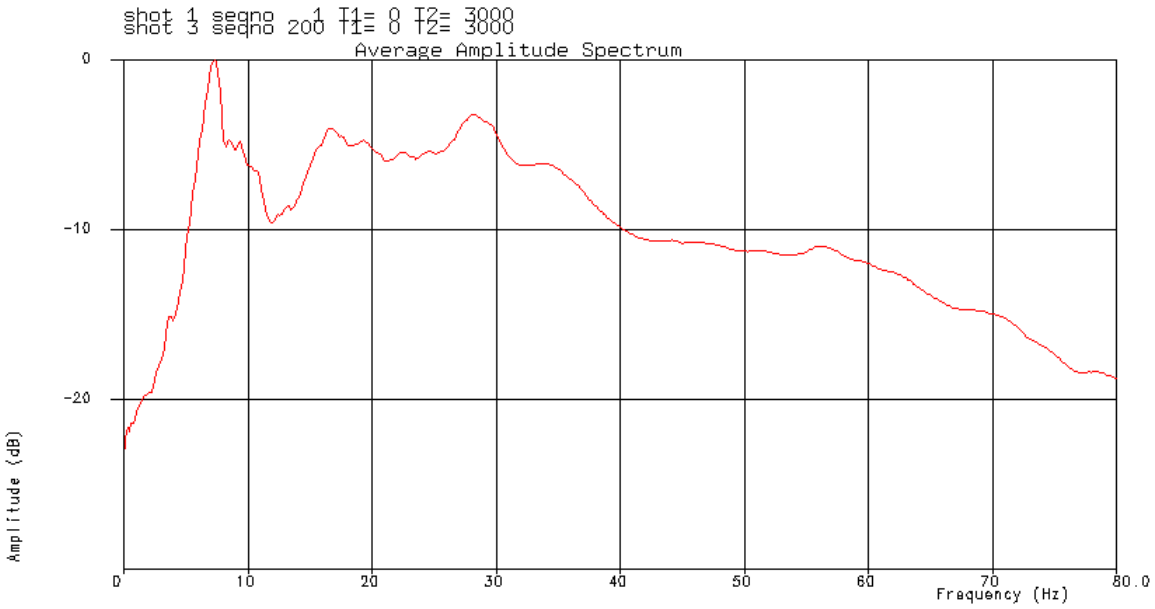

Figure 1.8. Amplitude spectrum of shot gathers 1–3.

The shot gathers of the 2 Hz vertical component raw data selected from the first, middle, and last records are shown in Figure 1.9. Automatic gain control (AGC) was applied to the seismic data to examine seismic events. AGC is generally used to observe the late-arriving seismic events. Figure 1.10 illustrates the shot record 100 prior to applying AGC. Figure1.11 displays the same shot record after applying AGC. These figures demonstrate that the data are improved significantly, and the late arrivals are observed more clearly.

Strong reflections are recorded on the vertical component despite the fact that the seismic data are contaminated by heavy ground-roll noise. There were low levels of wind noise and other surface noises (Gorek et al., 1995). To reduce the noise caused by wind, the

2 Hz geophones were installed in holes at 40 cm deep. The Blackfoot survey was conducted in a rugged prairie field, and it was rainy and windy most of the time during the acquisition of the data (Gallant et al., 1996).

The processing parameters were tested using a representative subset of the data. The obtained results were examined to determine the optimal parameters to be applied to entire seismic data.

1.4. OBJECTIVES

In this study, the main objective is to reprocess the 2 Hz vertical component data to obtain a better image of the subsurface and enhance the quality and resolution of the the target reservoir, which is the Glauconitic sand formation at approximately 1150 ms. Since the reservoir and the neighboring shales have very similar P-wave anomalies, it is difficult to recognize and distinguish the reservoir from the neighboring shales. Therefore, the major reflector at approximately 1550 ms on the vertical component is also taken into consideration in determining the better seismic section for further processing stages.

Another objective is to summarize the main characteristics of the multicomponent processing. The essential concepts involved in the converted wave processing such as common conversion point (CCP), asymptotic binning, gamma ratios, positive/negative offsets, receiver statics, rotation of the data, and anisotropy are also presented in this study.

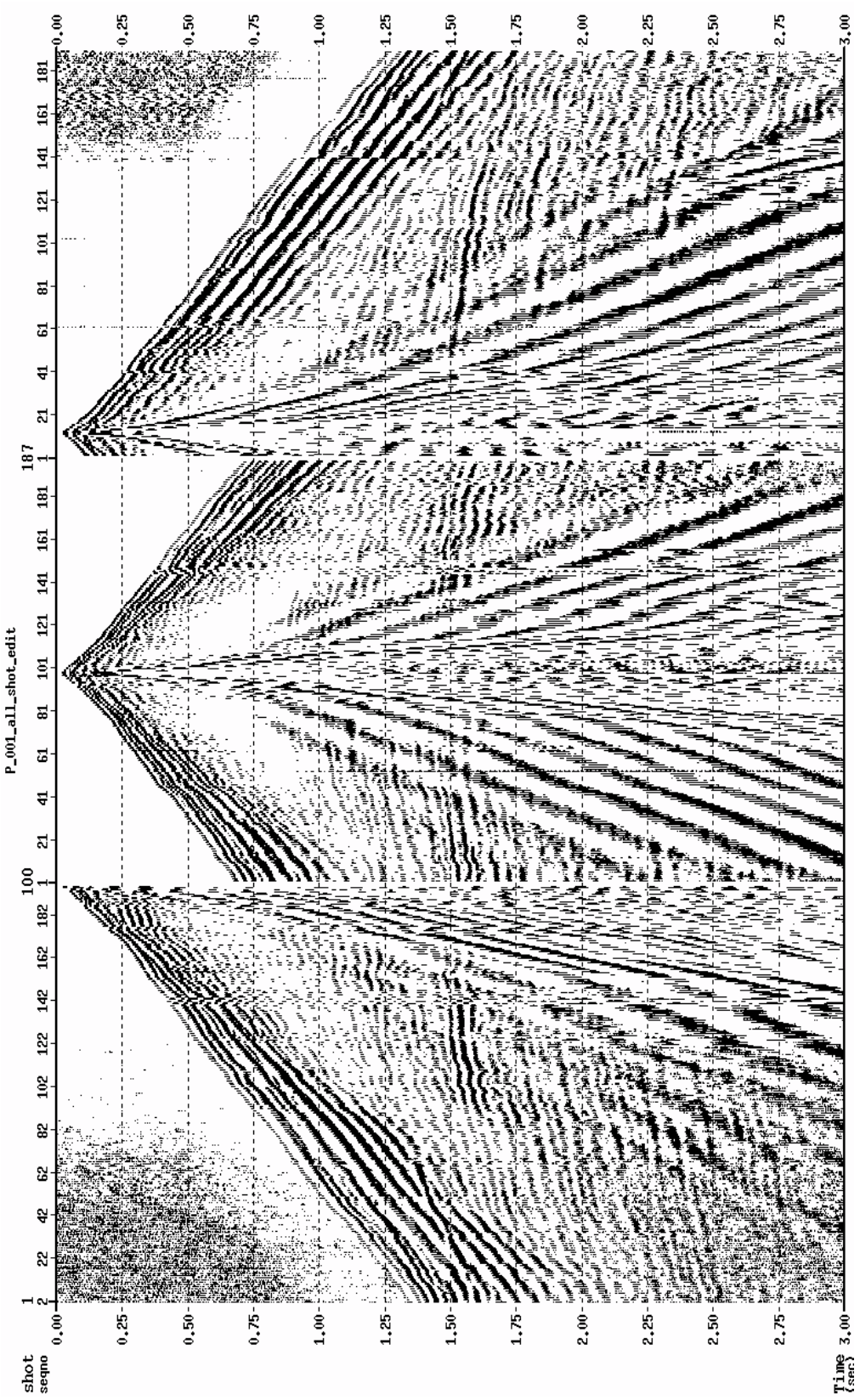

Figure 1.9. Field records of shots 1, 100, and 187 with AGC applied.

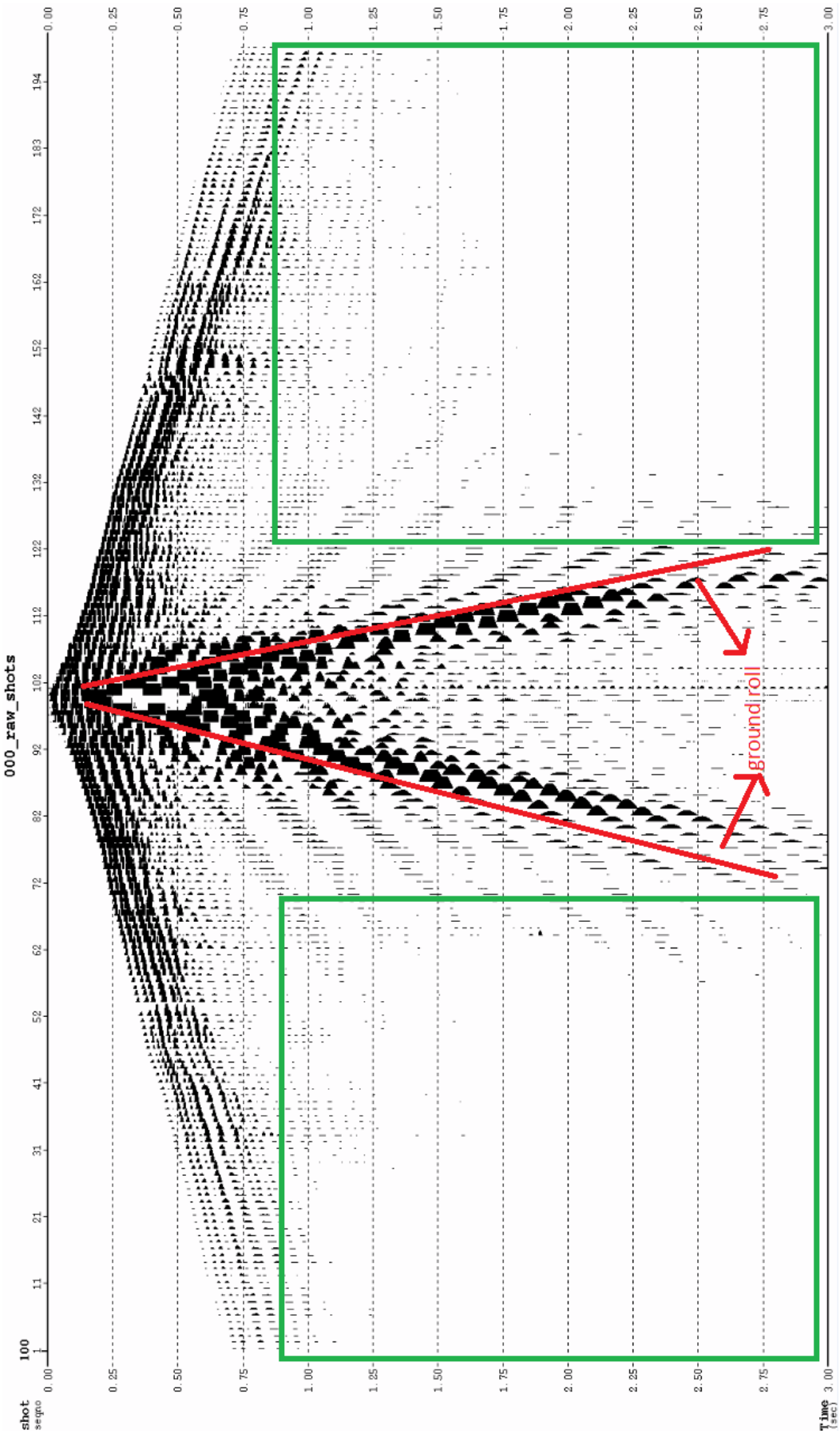

Figure 1.10. Field record of the shot gather 100 without applying AGC. The areas indicated by green rectangles are presented to indicate the changes caused by AGC.

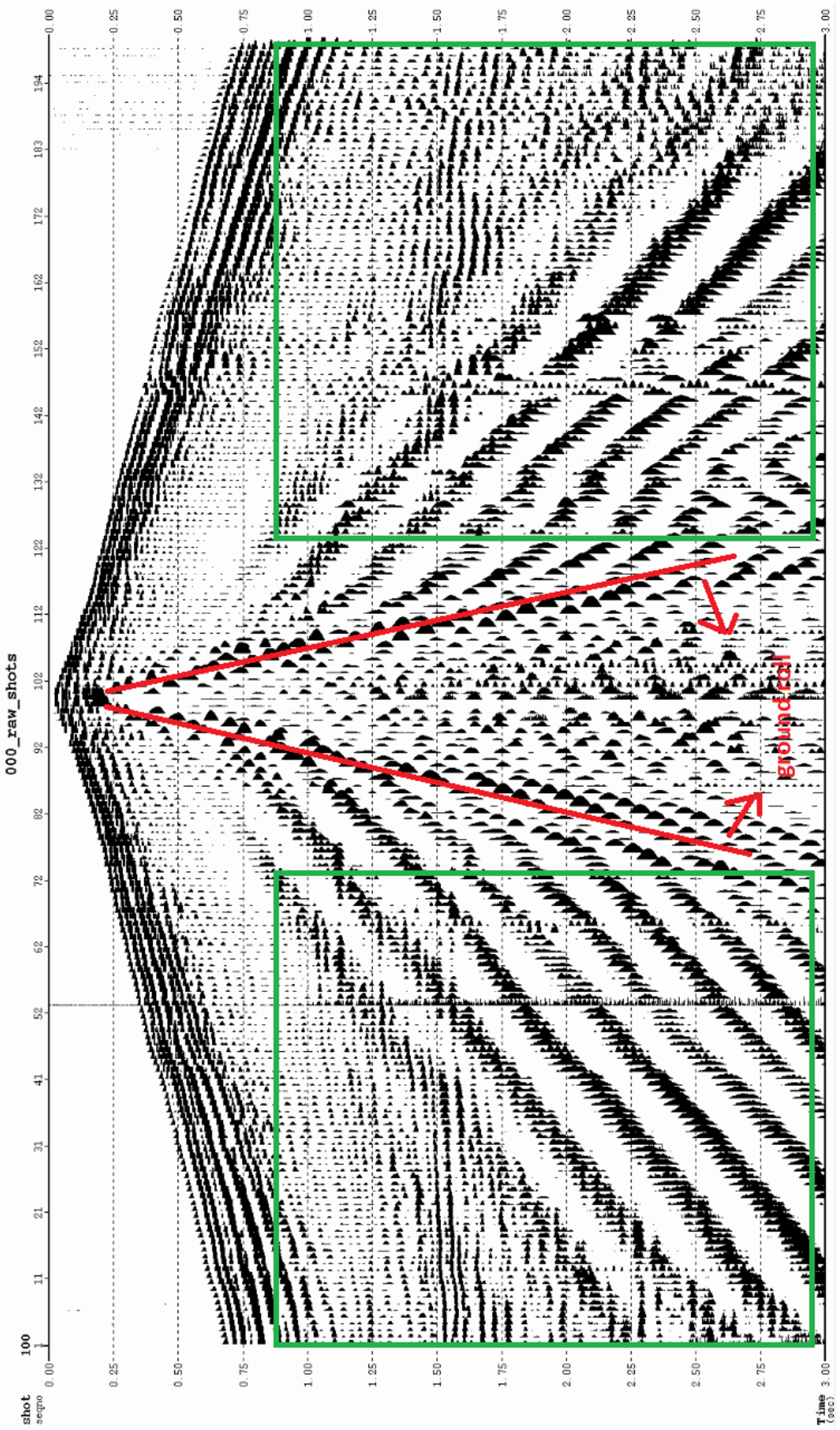

Figure 1.11. Field record of the shot gather 100 after AGC. The areas specified by the green rectangles indicate that the data are improved, and the late-arriving seismic events can be observed more clearly.

2. METHODOLOGY

The 2 Hz vertical component data were reprocessed using the software Echos by Paradigm. Each of the processing methods and parameter optimizations were performed on a representative subset of the data. After determining the optimal parameters in the testing stage, the data processing was conducted for the entire dataset.

The optimum processing chart was determined by testing various parameters, methods, and algorithms (Figure 2.1). Different types of deconvolutions, i.e., predictive and surface consistent, static corrections, i.e., refraction and elevation statics, and migrations, i.e., 2D Kirchhoff prestack time and 2D Kirchhoff poststack time were applied to the data to better image the subsurface.

The two important zones analyzed to determine better seismic sections are the Glauconitic sand formation (reservoir) at approximately 1150 ms and the major reflector at about 1550 ms. The areas below 2000 ms are not taken into consideration during the processing of the seismic data.

There are two significant issues encountered in the Blackfoot Field. One is the lithology discrimination between the neighboring shales and the target sandstone reservoir because of that they have similar P-wave anomalies (or acoustic impedance). Another is the stratigraphically thin incised valley (or channel fill). The frequency bandwidth of the seismic data and bed thickness are the main parameters to reveal seismic thin beds. For this reason, a poststack enhancement method, spectral whitening (which is also known as broadening or balancing), was applied to the migrated sections to improve the appearance and resolution of the incised valley.

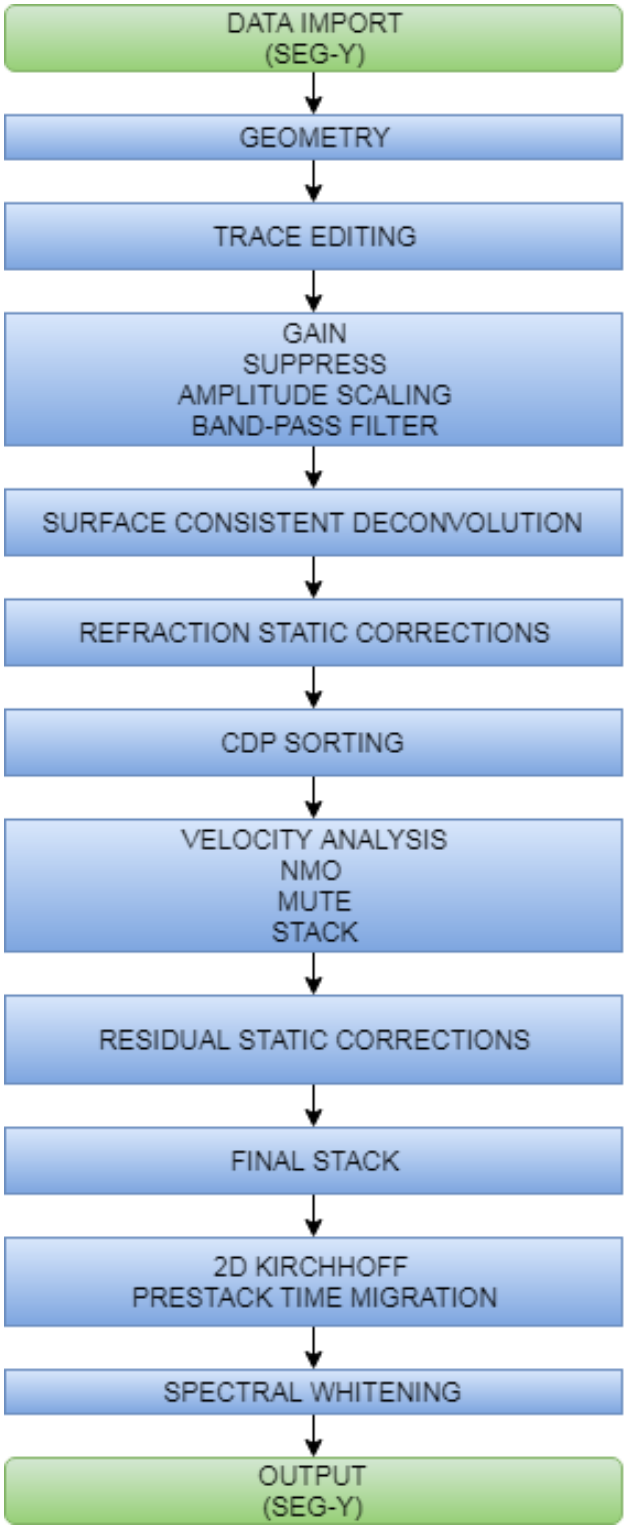

Figure 2.1. Processing chart for the 2 Hz vertical component seismic data.

2.1. GEOMETRY

Setting geometry is defined as the association of the recorded traces with specific shot and receiver locations through the unique identifiers. In this step, the seismic data were incorporated with the coordinates in the seismic database that includes all the information about the survey such as coordinates and elevations of shot and receiver stations. Since a number of processing steps such as CMP binning and refraction statics are required to access the database, it is essential to set the geometry correctly.

Quality control (QC) is performed to verify that the geometry is set correctly. The first step is to control and match the headers of seismic data with the headers of the software in case there are differences between the headers.

The Blackfoot 3C-2D dataset had the geometry information in the trace headers. However, there were several inconsistencies between the headers of the data and the software regarding the byte number in the SEGY format. These differences were fixed and adjusted to the standard SEGY format. Figures 2.2 and 2.3 show the locations and elevations for the seismic survey, respectively.

The survey includes 200 channels, and the source and receiver intervals are 20 m, which gives the maximum fold of 100. Since the split-spread layout is used to acquire the data in this survey, fold coverages in the near offsets and far offsets are low but are high in the mid-offsets.

There are several ways to perform geometry QC. In this context, the offset plot for selected shot gathers is presented to verify that the offset-geometry is consistent (Figure 2.4). It is expected that the offset increases by the distance from the shot station to the receiver station. In the figure, the offset plot indicates that the offset geometry shows consistency and increases by the distance.

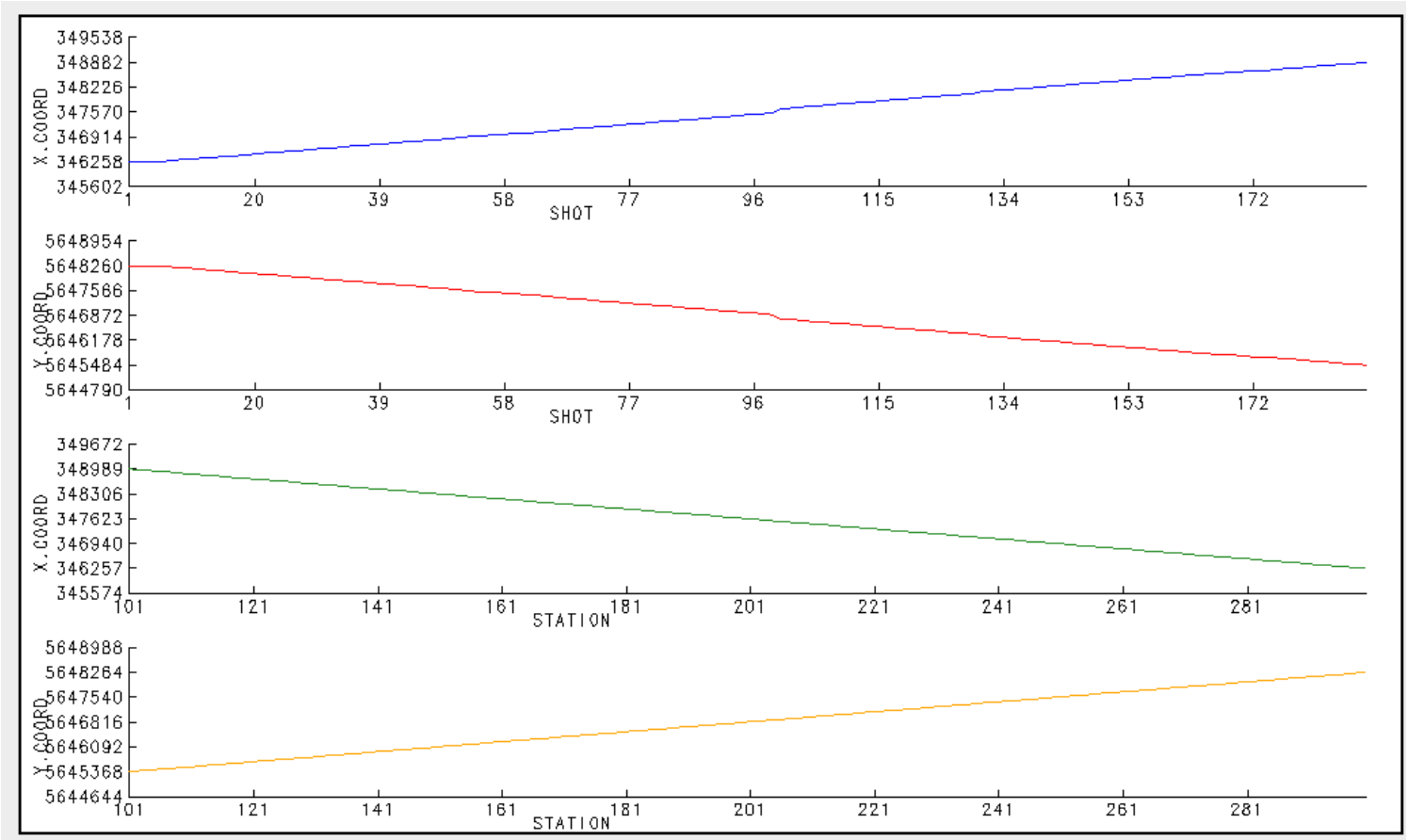

Figure 2.2. Diagram showing the shot and receiver locations. X-axis represents the number of shots and stations while Y-axis indicates the coordinates.

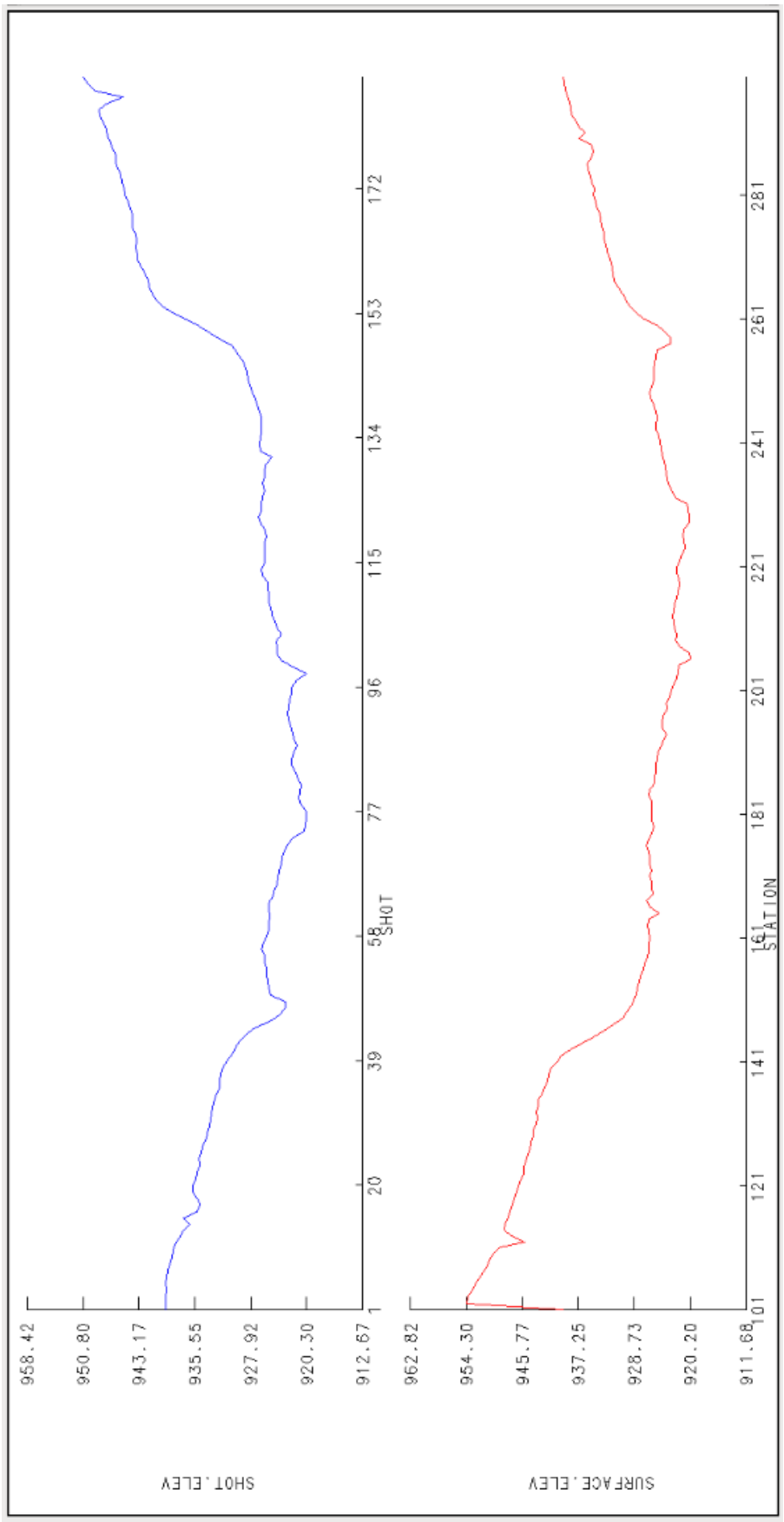

Figure 2.3. Diagram displaying the shot and receiver elevations. X-axis indicates the shot and receiver station numbers, and Y-axis shows the elevations in meter.

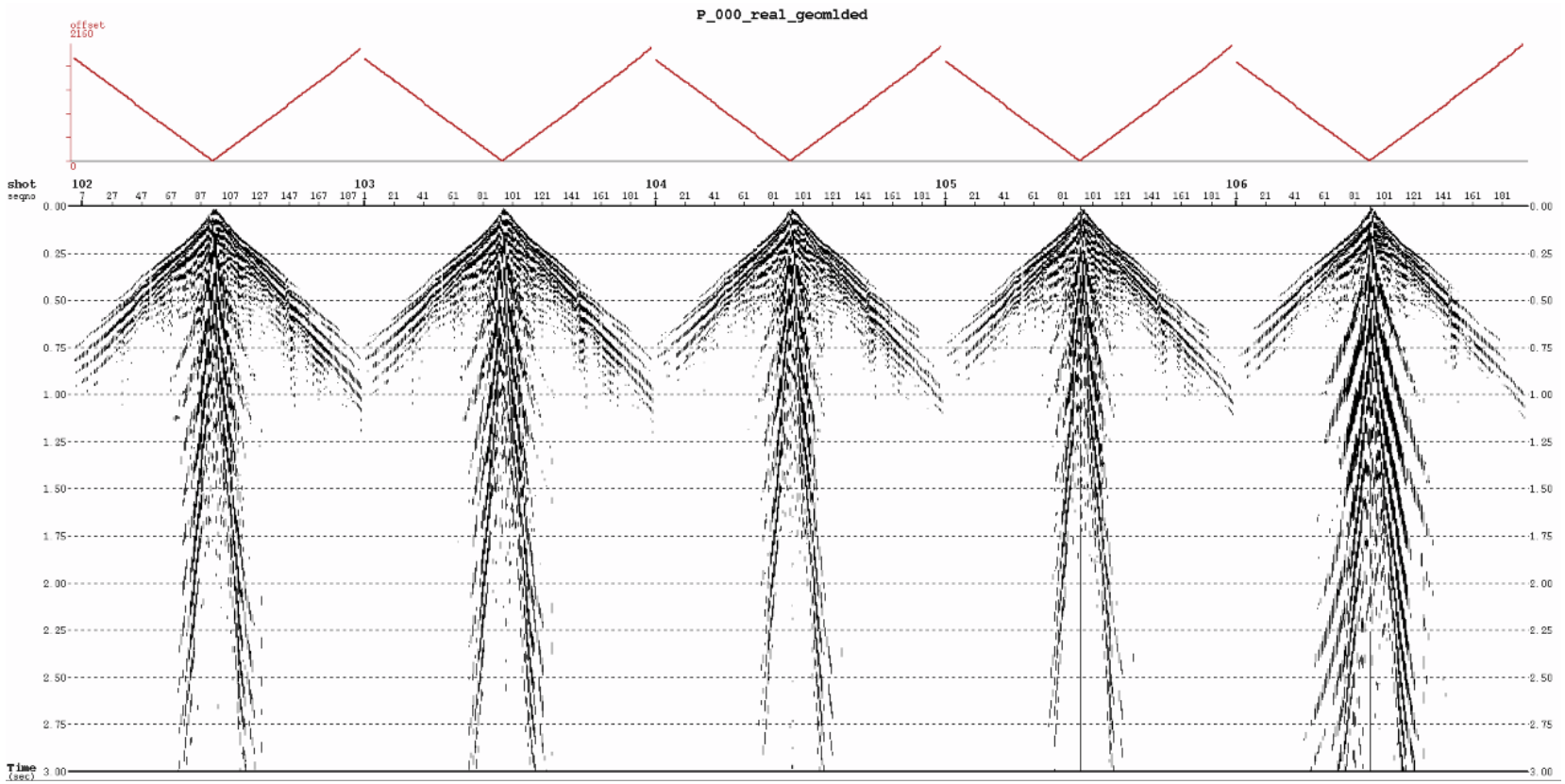

Figure 2.4. Offset plot for selected shot gathers 102–106. The offset is consistent. It increases as the distance from the shot to receiver station increases.

2.2. TRACE EDITING

Noises contaminating the seismic data are first addressed in the trace editing step by examining seismic records. Trace editing was one of the main steps to control noise in seismic data. Bad records, dead shots, and noisy traces are edited or omitted from the records so that the edited prestack data are utilized for further processing steps such as velocity analysis and migration.

In the early years of seismic processing, when a seismic trace was obscured by noise, the seismic trace was removed if the stacking fold was significantly high.

Afterwards, seismic traces that were concealed by high-amplitude noises were given special attention since relatively bad traces usually do not influence the stacked section significantly in the case of high fold numbers.

After the advancement and progress of the technology involved in the acquisition and processing of seismic data, the manual editing of seismic traces is no longer preferable since the volume of seismic data is large. It is not possible to visually examine all traces in a feasible time. For this reason, automatic trace editing is more practical, especially in 3D surveys.

In the Blackfoot survey, the observer logs indicate that the first four shots and the last three shots were test shots. There were several missing shots (shot 17, 54, 166, and 173) along with the test shots, and they were omitted from the seismic data during the editing stage.

The reversal polarities were corrected, and the dead traces and the noisy traces were removed from the records. Figure 2.5 shows an example of trace editing for a dead trace and a polarity reversal.

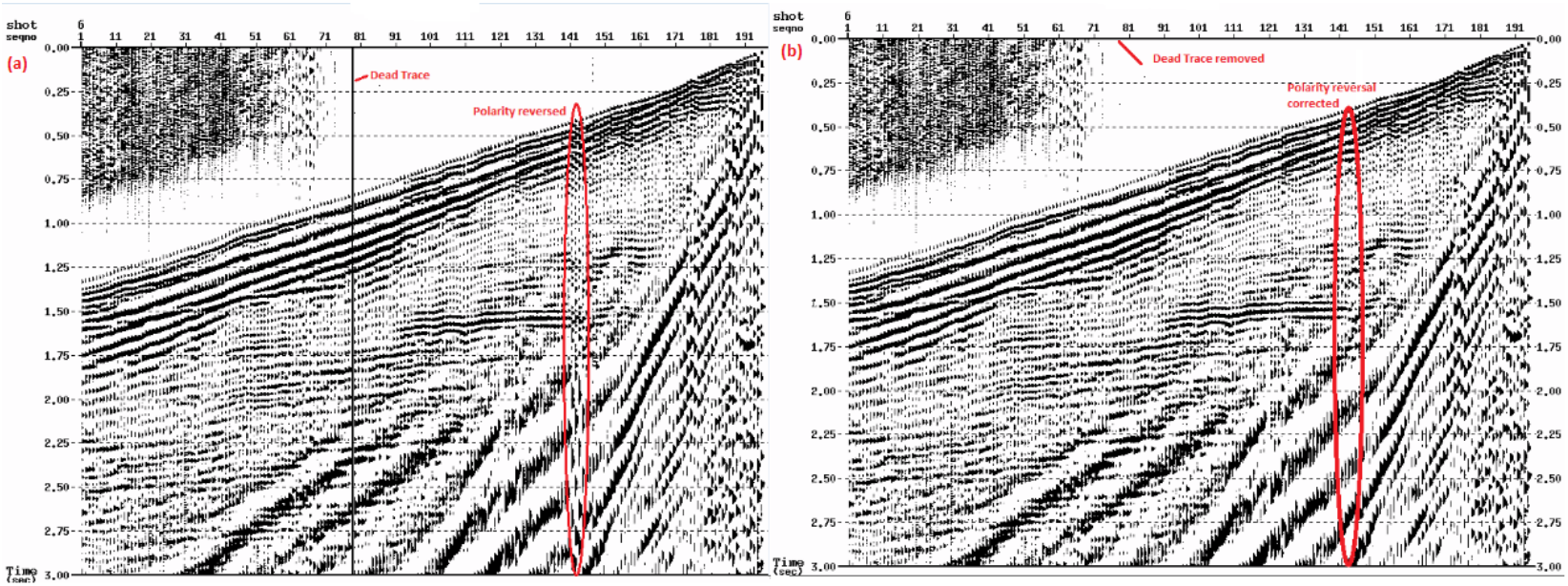

Figure 2.5. Shot gather 6. a) Before trace editing. b) After trace editing. The dead trace was removed, and polarity reversals were corrected.

2.3. NOISE REMOVAL

The spherical divergence corrections, i.e., gain, were applied to the seismic data to compensate for decreases in seismic wave amplitude due to the geometrical spreading of wavefronts (Figure 2.6). As the distance of the signal from the energy source increases, the amplitude of the wavelet decreases. Following gain application, gain analyses were performed to observe the amplitude recovery (Figure 2.7).

Several noise attenuation methods were applied to the seismic data to obtain the section with the better quality. A module was used to suppress bandlimited types of seismic noises such as ground roll, swell noise, and air blasts (Figure 2.8). The data were divided into good (signal) and bad (noise) signal bands, and time-variant noise suppression was applied by matching the noise window (envelope) with the signal window. The Butterworth filter was used to decompose the traces into their signal and noise components.

To eliminate possible noises such as cable slashes and air blasts, another noise elimination module was used by analyzing the data across small overlapping spatial and temporal windows. This was conducted by comparing the window amplitude with the amplitude of the corresponding window on the neighboring traces in the data (Dutta et al., 2010) (Figure 2.9). Finally a bandpass filter was applied to the data and the obtained results are shown in Figure 2.10.

As mentioned previously in the data quality section, the 2 Hz vertical component seismic data were contaminated by heavy ground-roll noises. Accordingly, a number of parameters were tested to attenuate the noise. Only a few shots showed strong ground-roll noises after testing (shot 139 in particular). The obtained results suggest that some tested parameters caused the loss of the seismic data along with the noise. Consequently, the ground roll attenuation was successful, and the optimal parameters that offered the most favorable balance between the signal and noise ratio were preferred for further processing.

As a result, the obtained results from applying these noise elimination methods to the seismic data are shown in Figure 2.11. The reflections were revealed significantly.

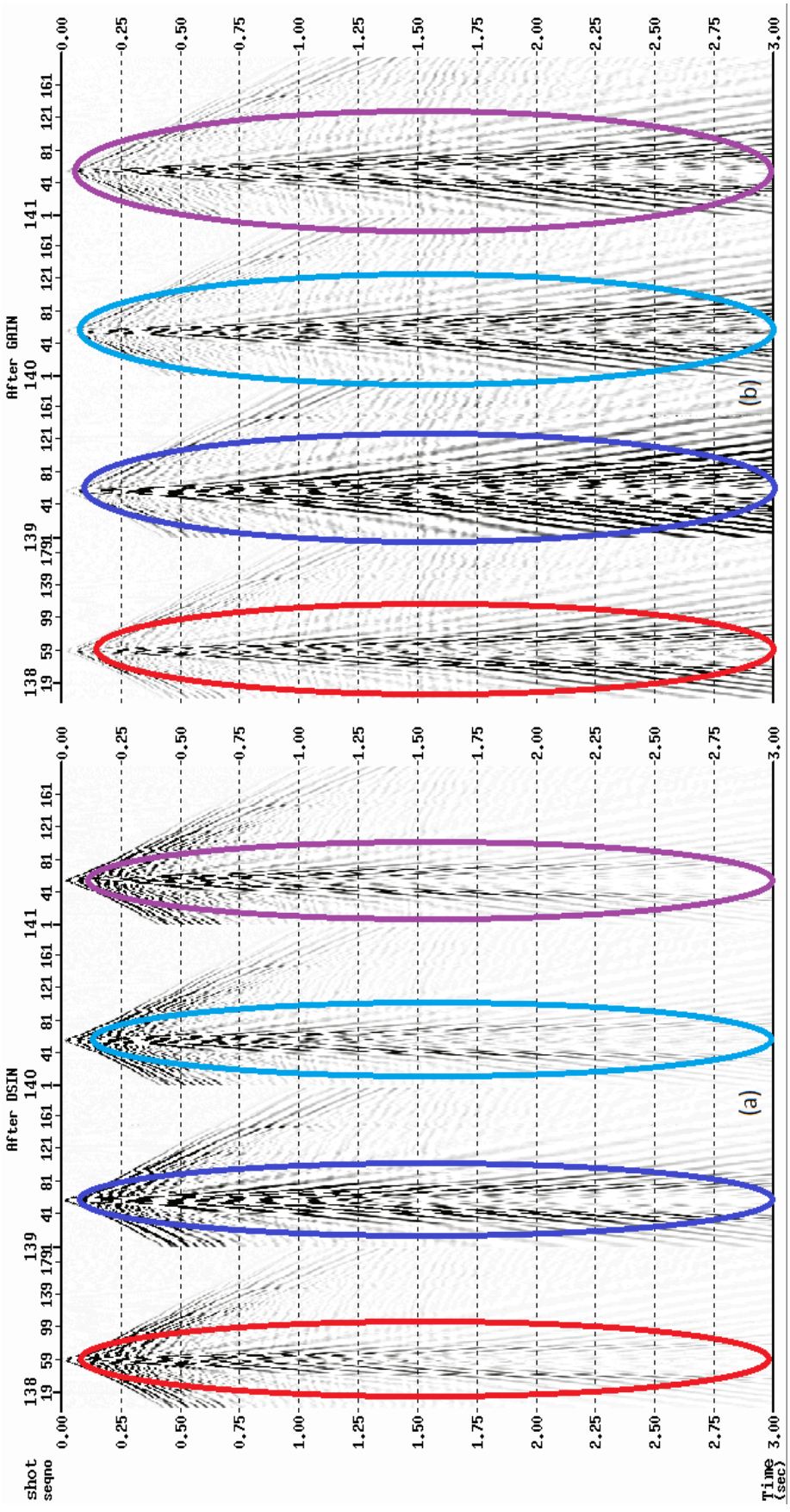

Figure 2.6. Shot records from 138 to 141. a) Amplitudes before gain. b) Amplitudes after gain. The values of amplitudes have been improved.

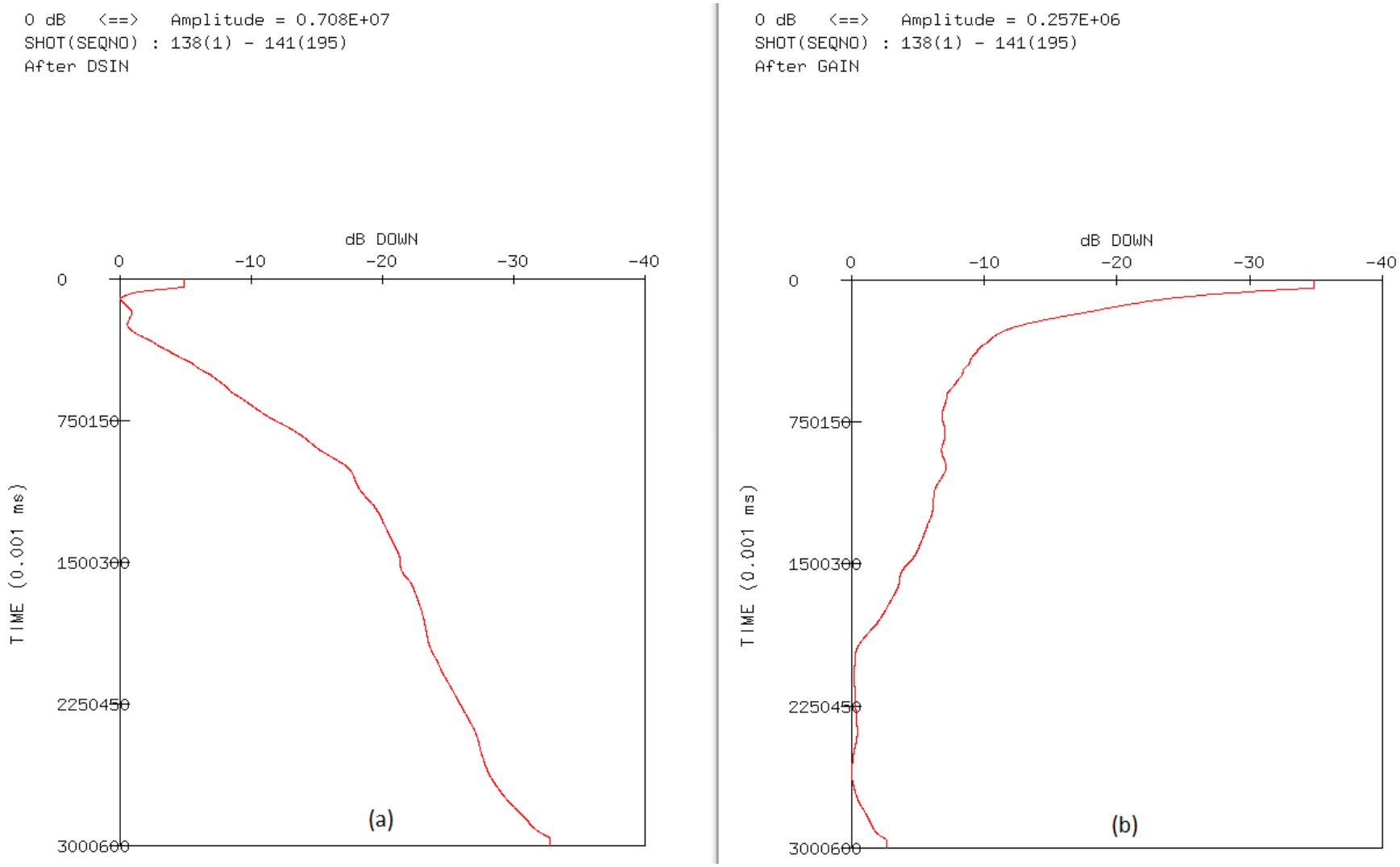

Figure 2.7. Gain analysis results for the shots from 138 to 141. a) Amplitudes values in decibel (dB) before gain. b) Amplitude values after gain. The amplitudes were recovered notably.

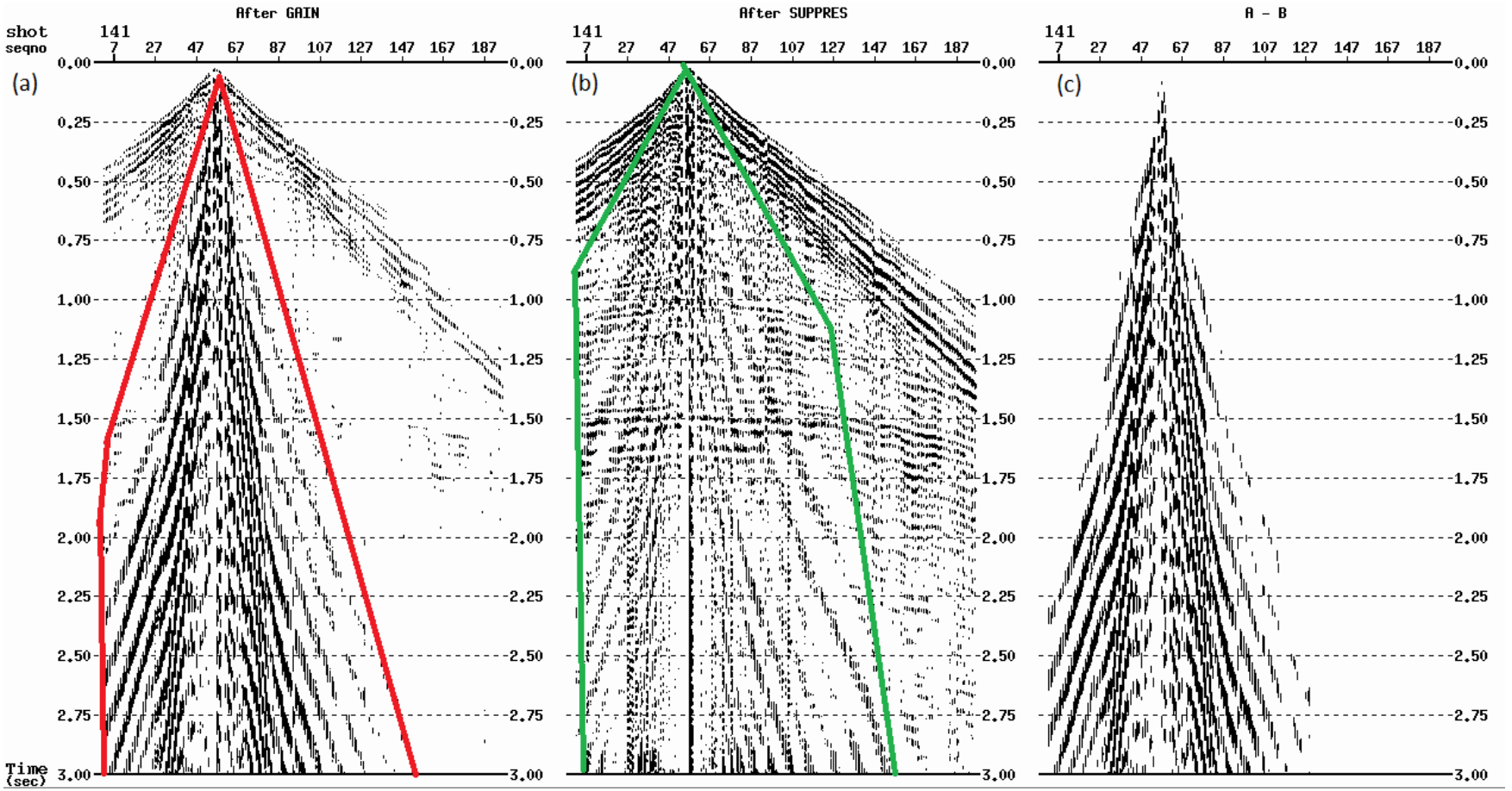

Figure 2.8. Shot gather 141. a) The input of the gather before suppressing the ground roll. b) The output of the shot gather after suppressing the ground roll. c) The removed data displayed as the difference between the input and output. The ground roll noise was significantly reduced.

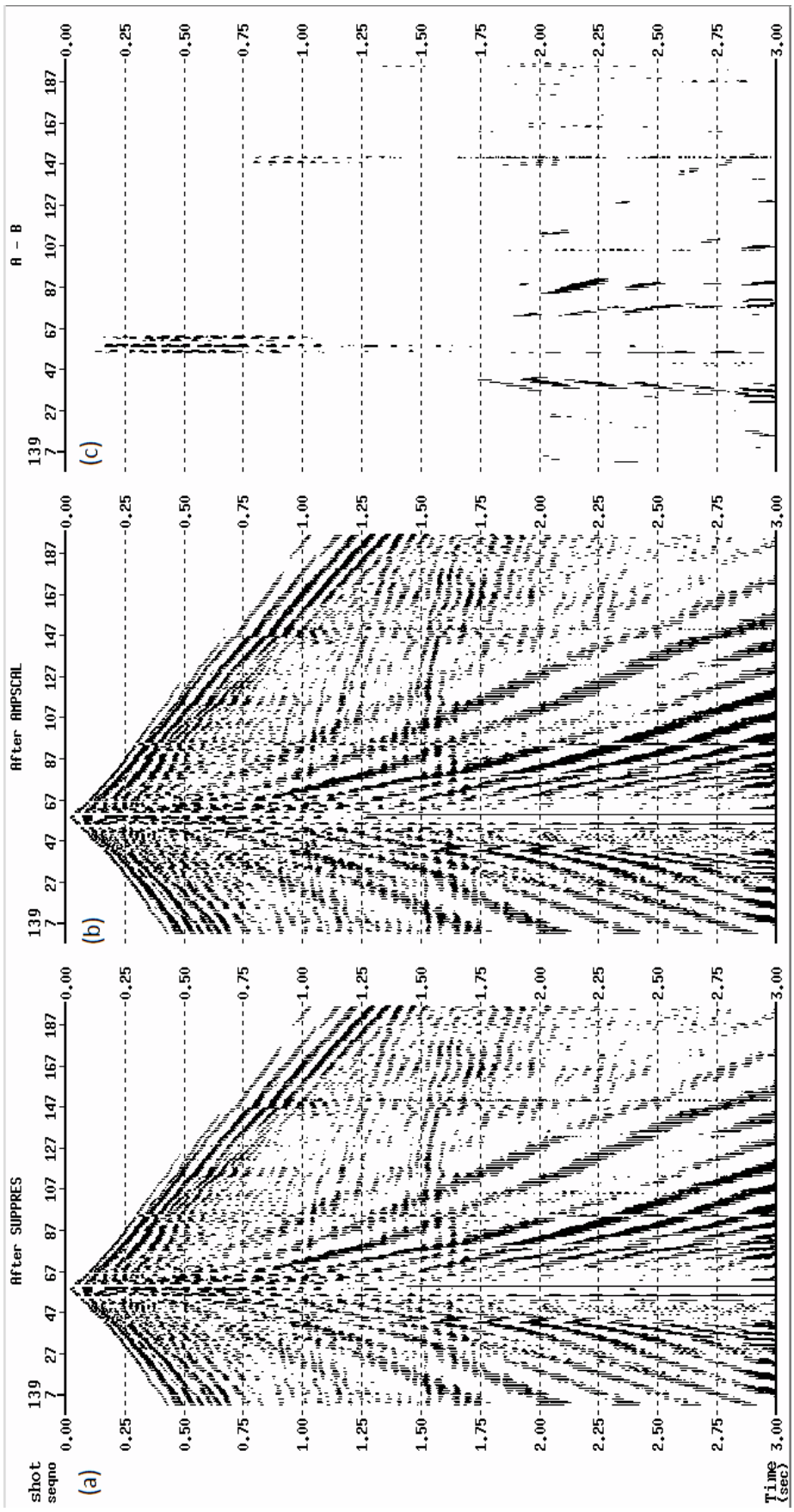

Figure 2.9. Shot gather 139. a) Before amplitude scaling (input). b) After amplitude scaling (output). c) The difference between the input and the output.

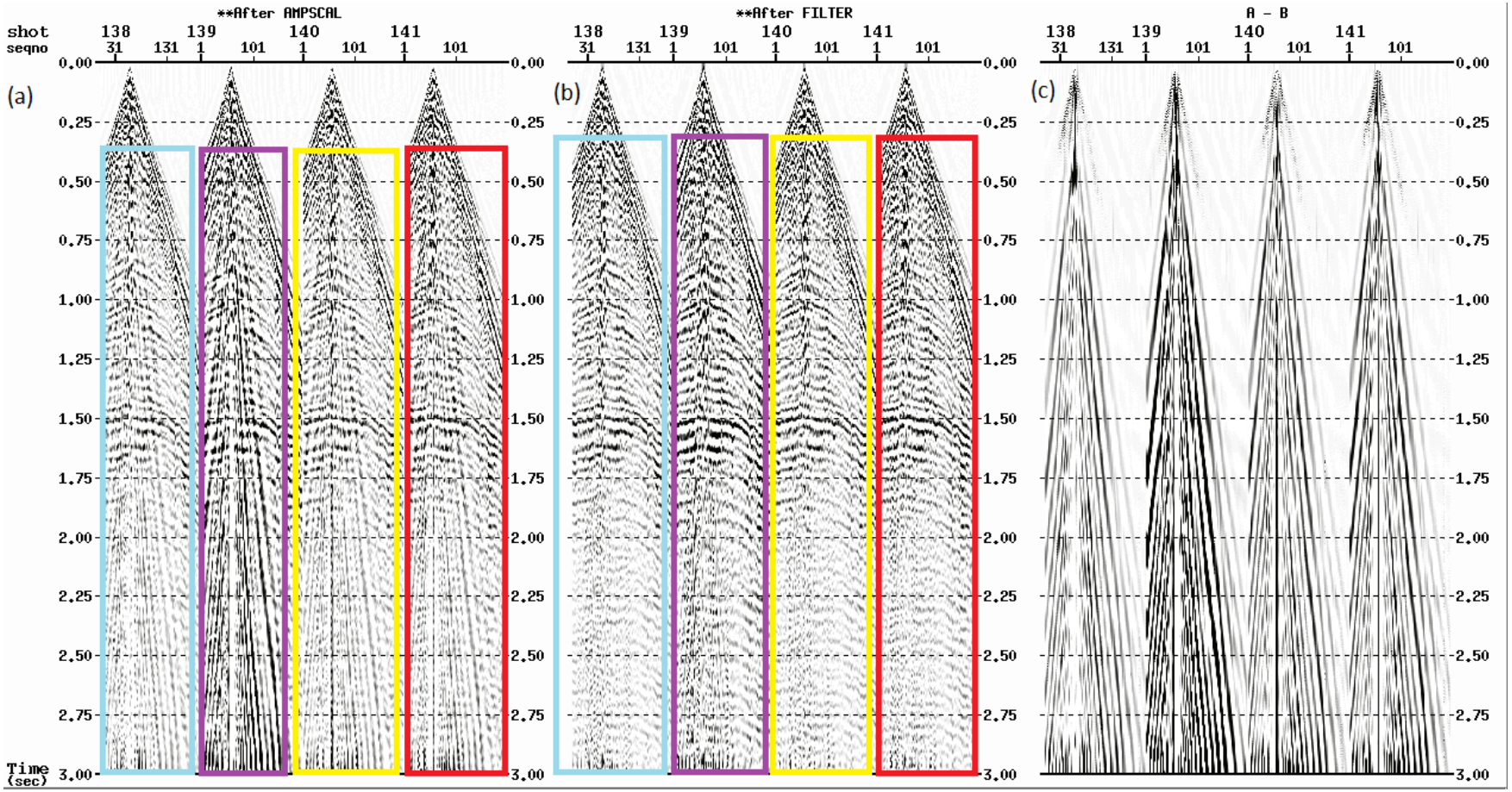

Figure 2.10. Shot gathers from 138 to 141. a) Before filter (input). B) After filter (output). c) The difference between the input and output. The bandpass filter applied has improved the data. The ground roll noise was reduced significantly.

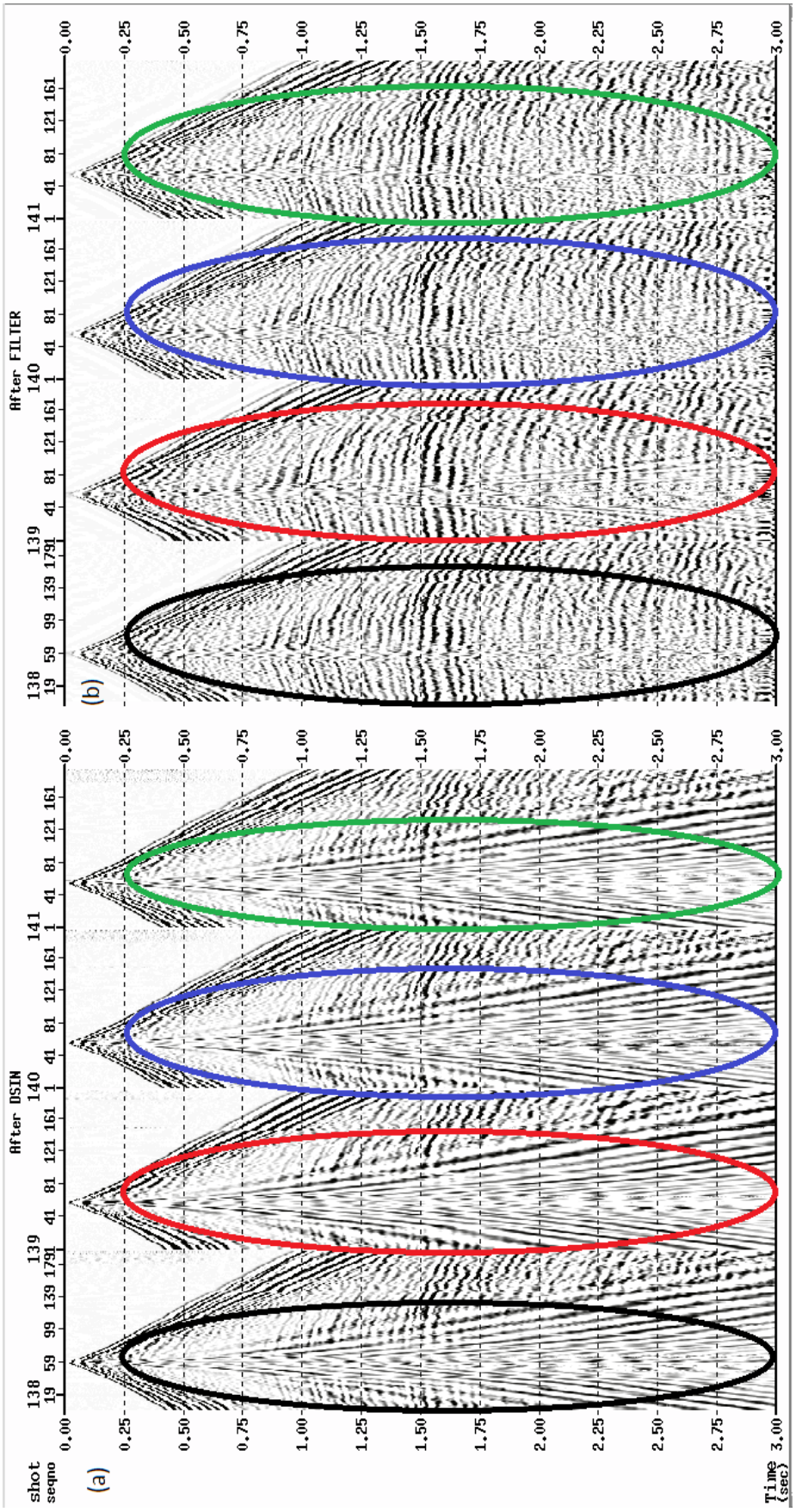

Figure 2.11. Representative shots from 138 to 141. a) Before noise attenuation. b) After noise attenuation. The results indicate that the noises related to the seismic data have been attenuated notably.

2.4. DECONVOLUTION

Deconvolution is the mathematical process of reversing the effects of convolution on the data (O'Haver, 2007). A seismic signal is assumed to be a convolution of the source signal with other instruments, such as geophones or the earth. Deconvolution is performed to remove or undo the effects of filters applied such as the recording system (the geophones) or the earth itself. The temporal resolution is increased, and the better interpretable seismic section is obtained by deconvolution (Sheriff, 2004).

In this study, two types of deconvolutions, surface consisted and predictive (gapped) deconvolution, were tested. Both types use the Wiener-Levinson algorithm (the main factor used for the noise attenuation methods to suppress ground roll in seismic data) to determine and sharpen seismic events. The Wiener algorithm is an effective filter used in the digital reduction of traces (Peacock and Treitel, 1969).

The predictive deconvolution method is widely used to suppress multiple reflections in seismic data (Ulrych and Matsuoka, 1991). The prediction filter is used in this method to eliminate repetitive events with specific periods. The length of the output wavelet can be controlled in the predictive deconvolution (Peacock and Treitel, 1969).

The surface consistent deconvolution benefits from shot, receiver station, and offset autocorrelations in designing filters and compensating attenuation of high frequencies at long offsets and irregular geophone coupling. It is also important to realize that the surface-consistent deconvolution is mainly used for correcting the amplitude spectrum instead of widening the amplitude spectrum. Thus, the increase in temporal resolution will not be significant (Li, 2017).

Figures 2.12 and 2.13 show the obtained results from predictive deconvolution and surface consistent deconvolution for shot gather 132, respectively.

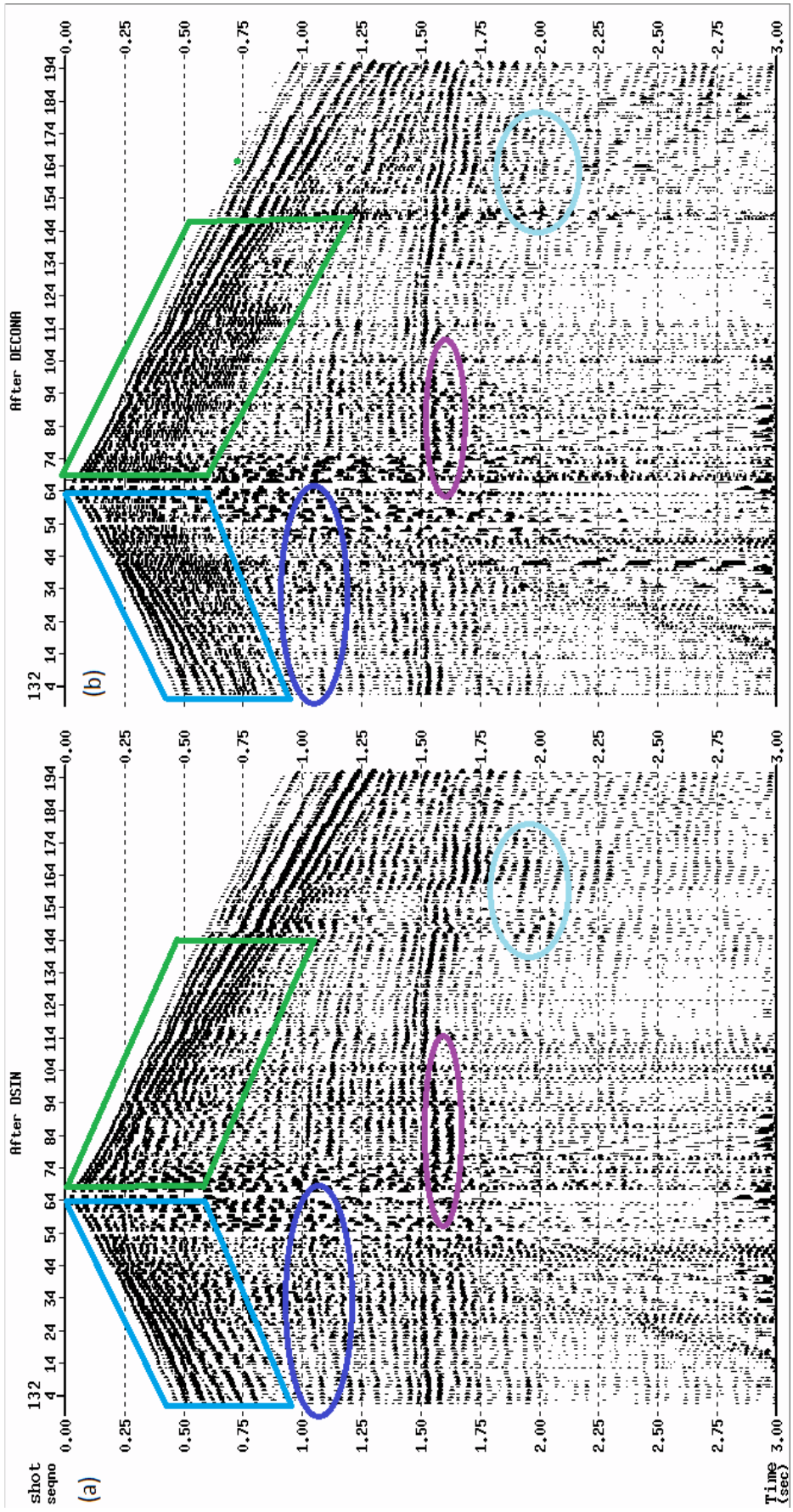

Figure 2.12. Shot gather 132. a) Before predictive deconvolution. b) After predictive deconvolution. The areas shown by different colors specify the changes over the same area.

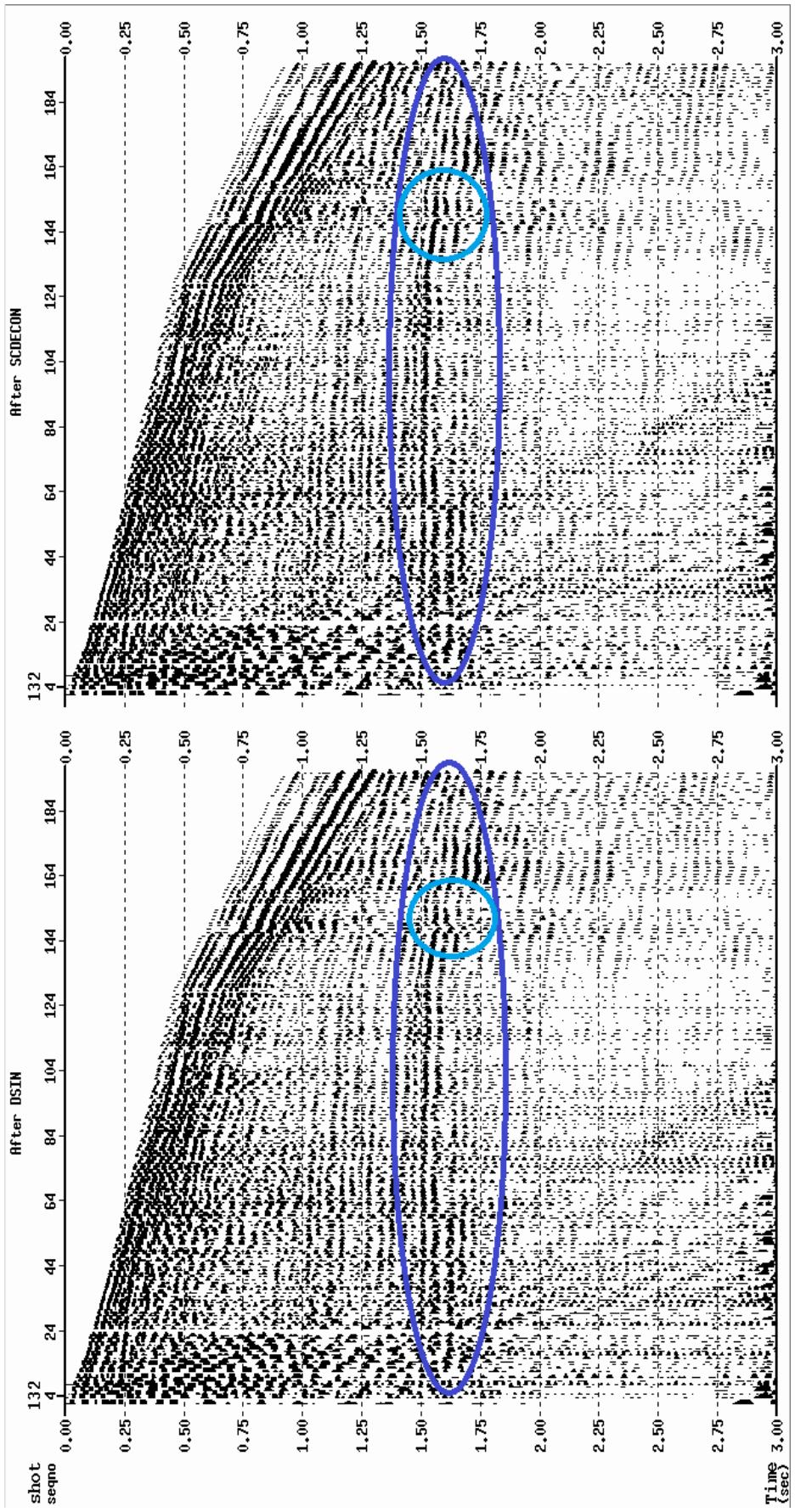

Figure 2.13. Shot gather 132. a) Before surface consistent deconvolution. b) After surface consistent deconvolution. The areas specified indicate the variations on the shot gather.

Comparing these seismic shot gathers obtained from applying predictive (gapped) deconvolution (Figure 2.12) and surface consistent deconvolution (Figure 2.13) to the seismic data, the surface consistent deconvolution method provides a better image of the subsurface when the target zone is taken into account.

The predictive deconvolution generated a low signal noise ratio (SNR) near the subsurface, and the major reflector at a depth of around 1500 ms was distorted after the predictive deconvolution. However, the surface consistent deconvolution offered more SNR near the subsurface, and the major reflector was slighlty more visible than it was before.

The seismic data with these two deconvolution processes were then stacked to determine the better one for further processing. Figures 2.14 and 2.15 show the stacked sections after the predictive and the surface consistent deconvolution, respectively.

Additionally, the spectral analyses were performed for the seismic section before (Figure 2.16) and after predictive deconvolution (Figure 2.17) and surface consistent deconvolution (Figure 2.18) to analyze the extension (recovery) in the frequency bandwidth.

The amplitude spectra show that there is an observable recovery in the frequency bandwidth for both deconvolutions. According to these analyses, it appeared that the recovery in the frequency content is wider in the predictive deconvolution. However, in the interpretation, the seismic data with the surface consistent deconvolution method worked better and offered a more interpretable section in the target zone. The areas near the surface and the major reflector also indicate the improvements notably.

In addition to this, there are several other areas which are indicated by different colors show improvements in the stacked section with the surface consistent deconvolution applied. As a result, the surface consistent deconvolution method was preferred for further processing.

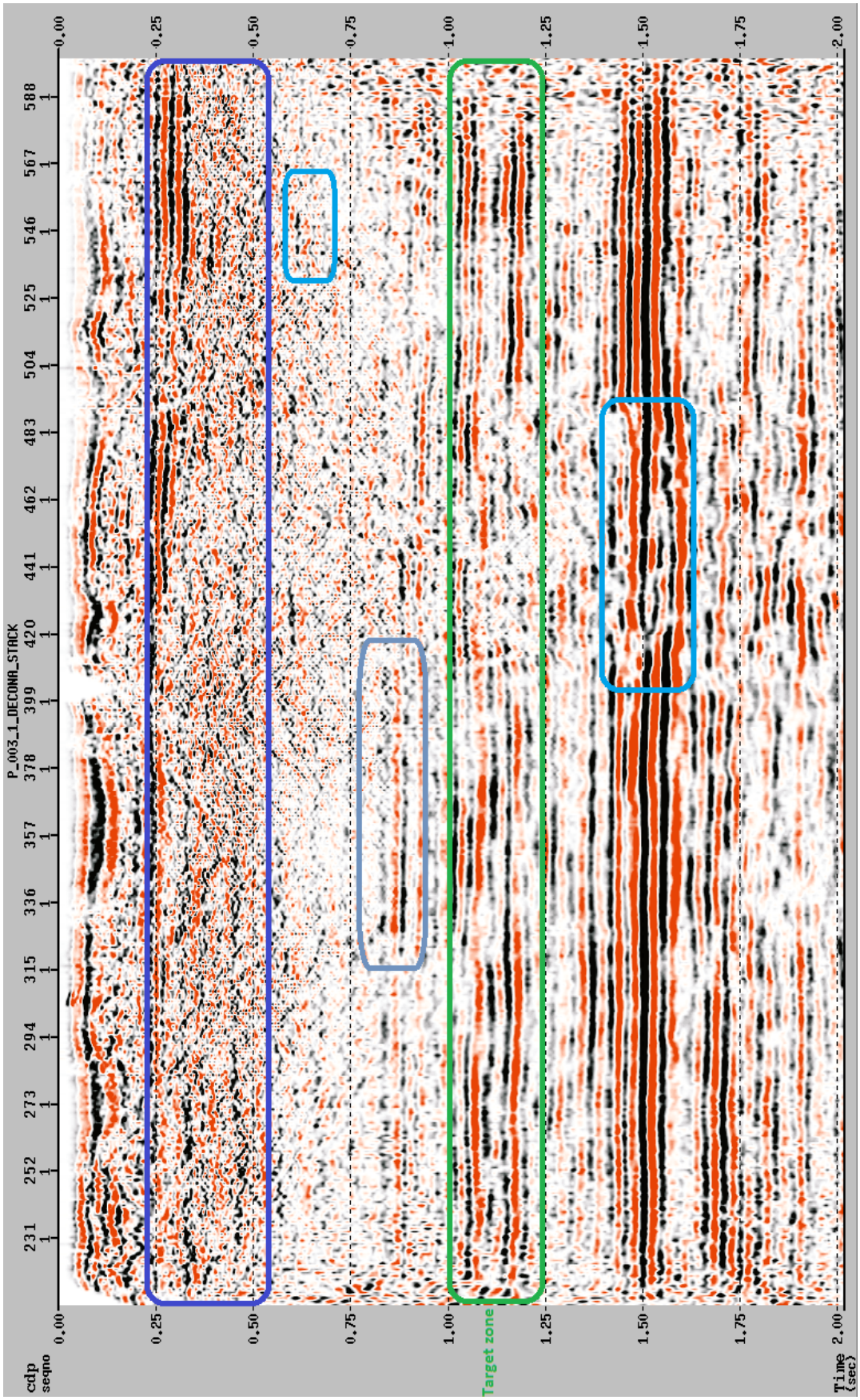

Figure 2.14. Stacked section after the predictive (gapped) deconvolution. The areas specified indicate the changes.

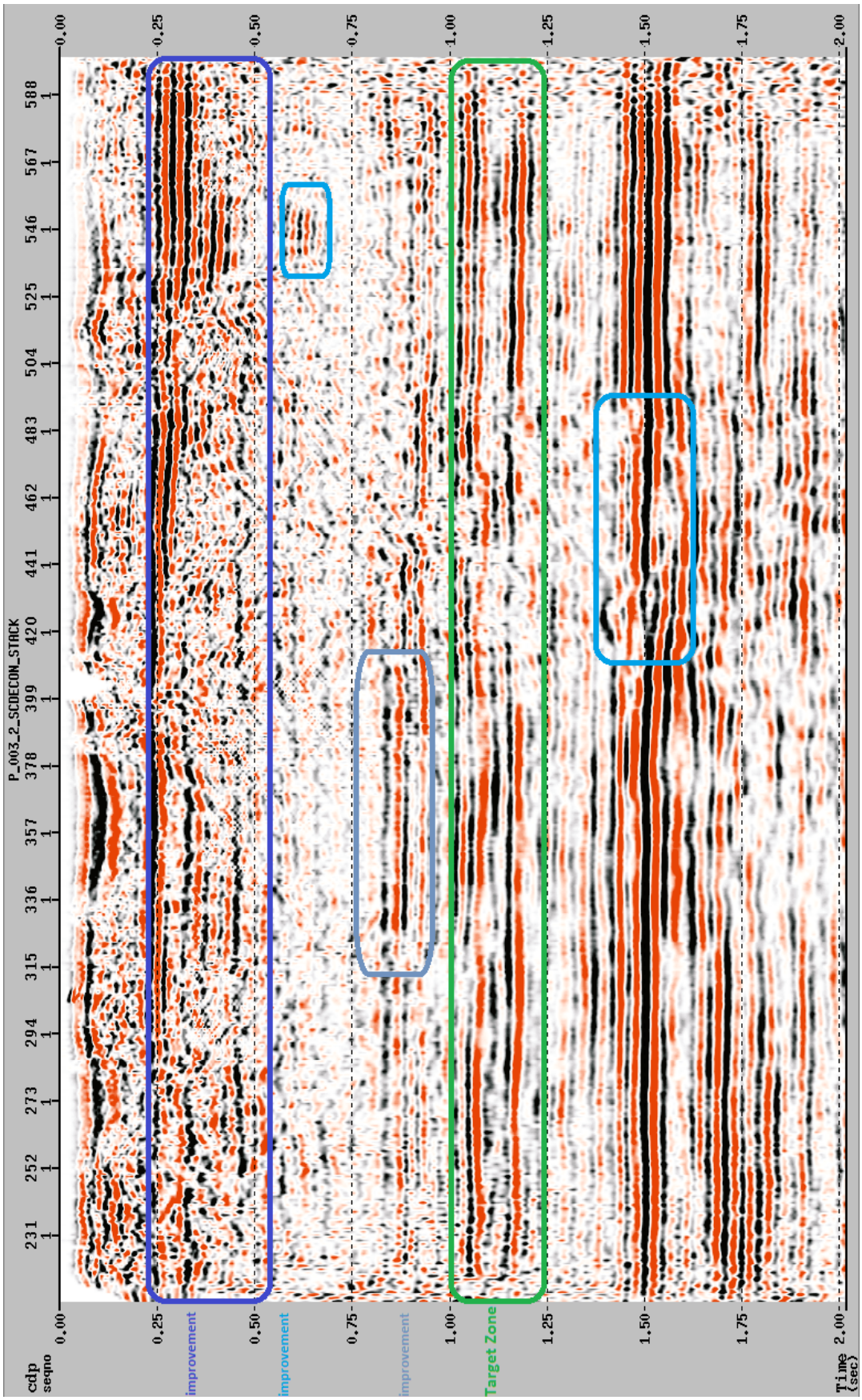

Figure 2.15. Stacked section after the surface consistent deconvolution. The areas specified indicate the improvements.

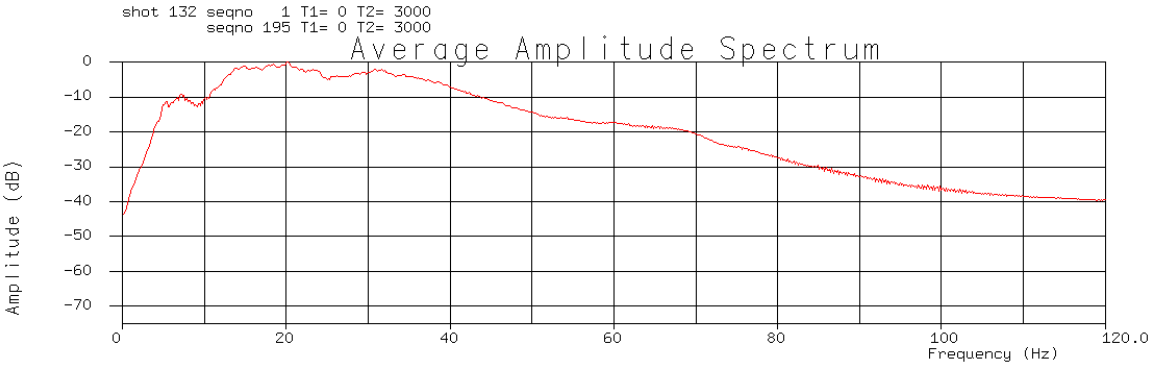

Figure 2.16. Amplitude spectrum of the shot gather 132 before deconvolution.

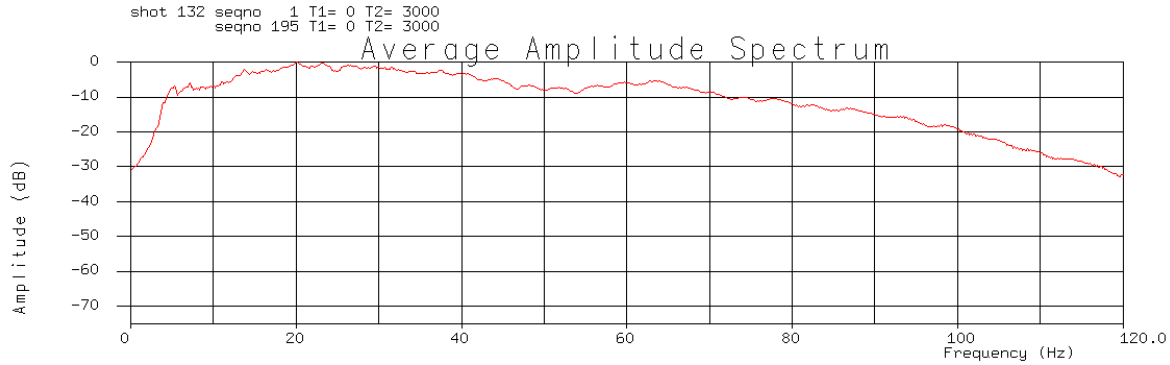

Figure 2.17. Amplitude spectrum after the predictive deconvolution applied.

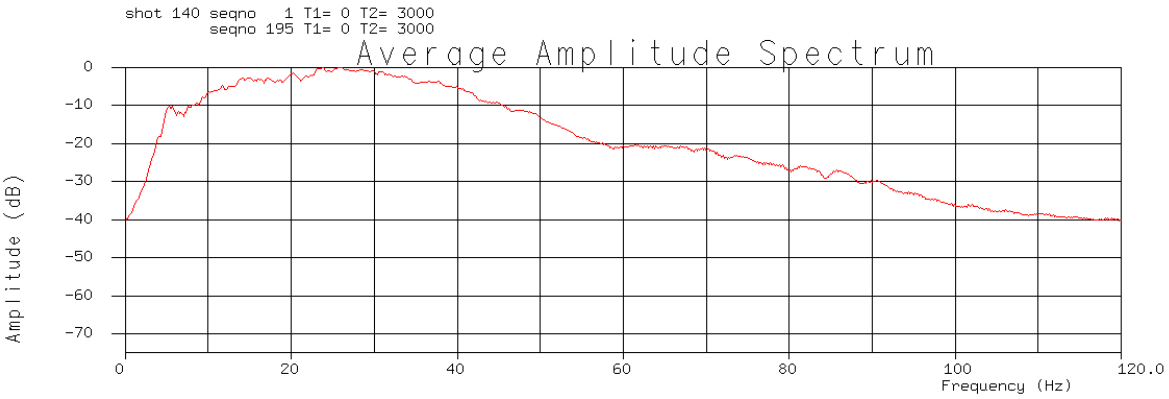

Figure 2.18. Amplitude spectrum after the surface consistent deconvolution applied.

2.5. STATIC CORRECTIONS

Static corrections or ‘statics‘ are essential in the processing of land data since they can affect the quality of processing steps. Statics influence directly the resolution of the data (Hatherly et al., 1994). Two main factors for applying static corrections are to correct near-surface velocity anomalies beneath the source and receivers, and align shots and receivers on a specified datum plane.

Processing seismic data without applying static corrections and errors encountered in this stage cause decreases in both temporal and spatial resolution. Thus, it may lead to severe complications in the interpretation stage (Zhu et al., 2014).

Several factors such as near-surface velocity anomalies and changes in lateral velocity of weathering layers lead to the static problems (Zhu et al., 2014). The corrections of these factors are handled in two aspects, i.e., short wavelengths (small shifts in time), and long wavelengths (larger time shifts). Residual static corrections are applied to seismic data to correct short-wavelengths. Field statics, also known as datum statics or elevation statics, and refraction statics were applied to the data to correct long wavelengths.

Figures 2.19 and 2.20 display the elevation static corrections computed for receivers and shot stations, respectively. The refraction statics calculated for receiver (Figure 2.21) and shot stations (Figure 2.22) are also presented.

After applying elevation and refraction statics to the seismic data, the obtained results were then stacked to determine what kind of static corrections offered the better image. Figures 2.23 and 2.24 show the stacked sections after elevation and refraction static corrections, respectively. The decisions were made based on the areas specified. The obtained results suggest that the refraction static corrections worked better than the elevation statics method, and the refraction statics were used for further processing.

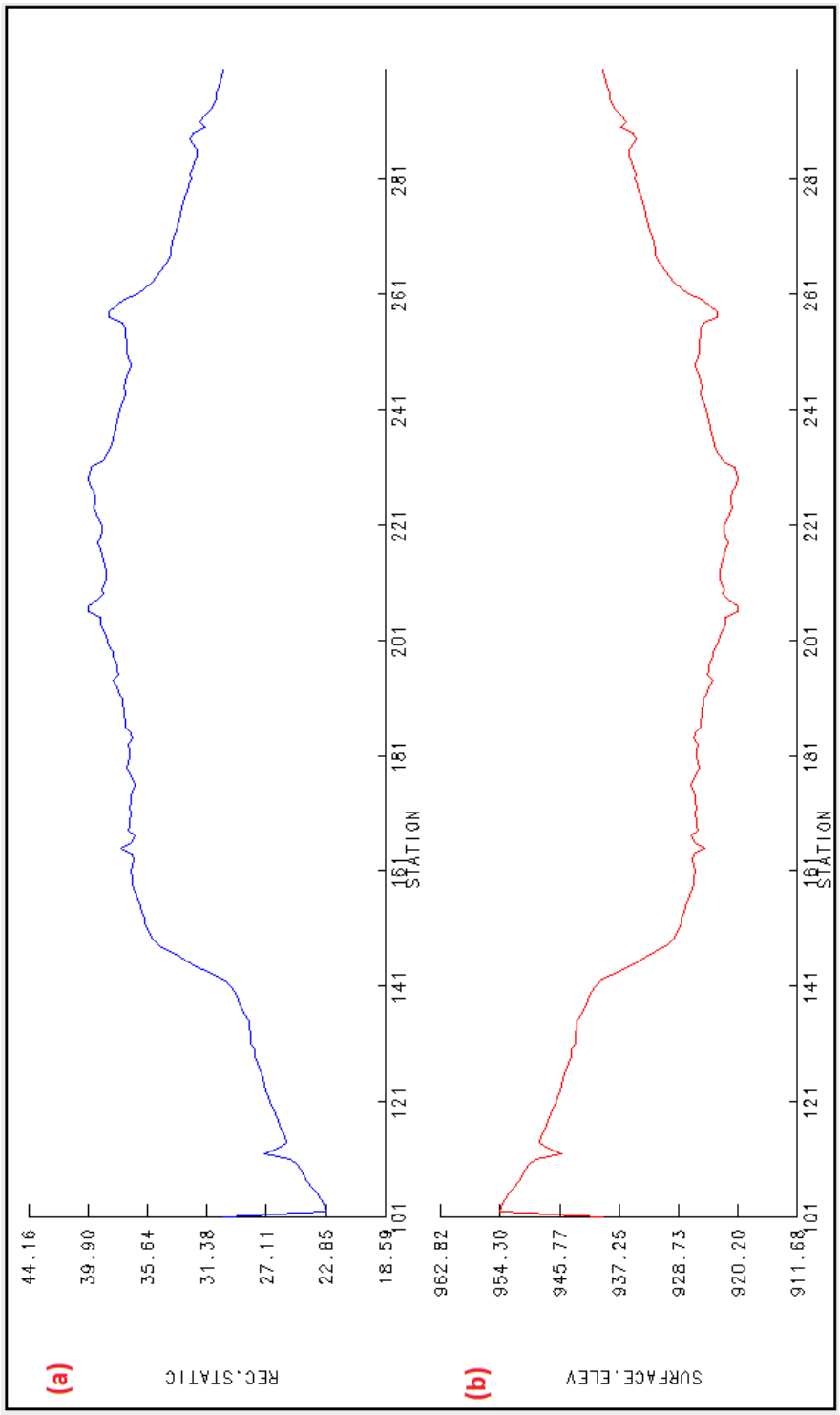

Figure 2.19. Elevation static corrections for receivers. a) Calculated elevation statics for receivers. b) Elevations of the receivers. Datum was determinded as 1000 m.

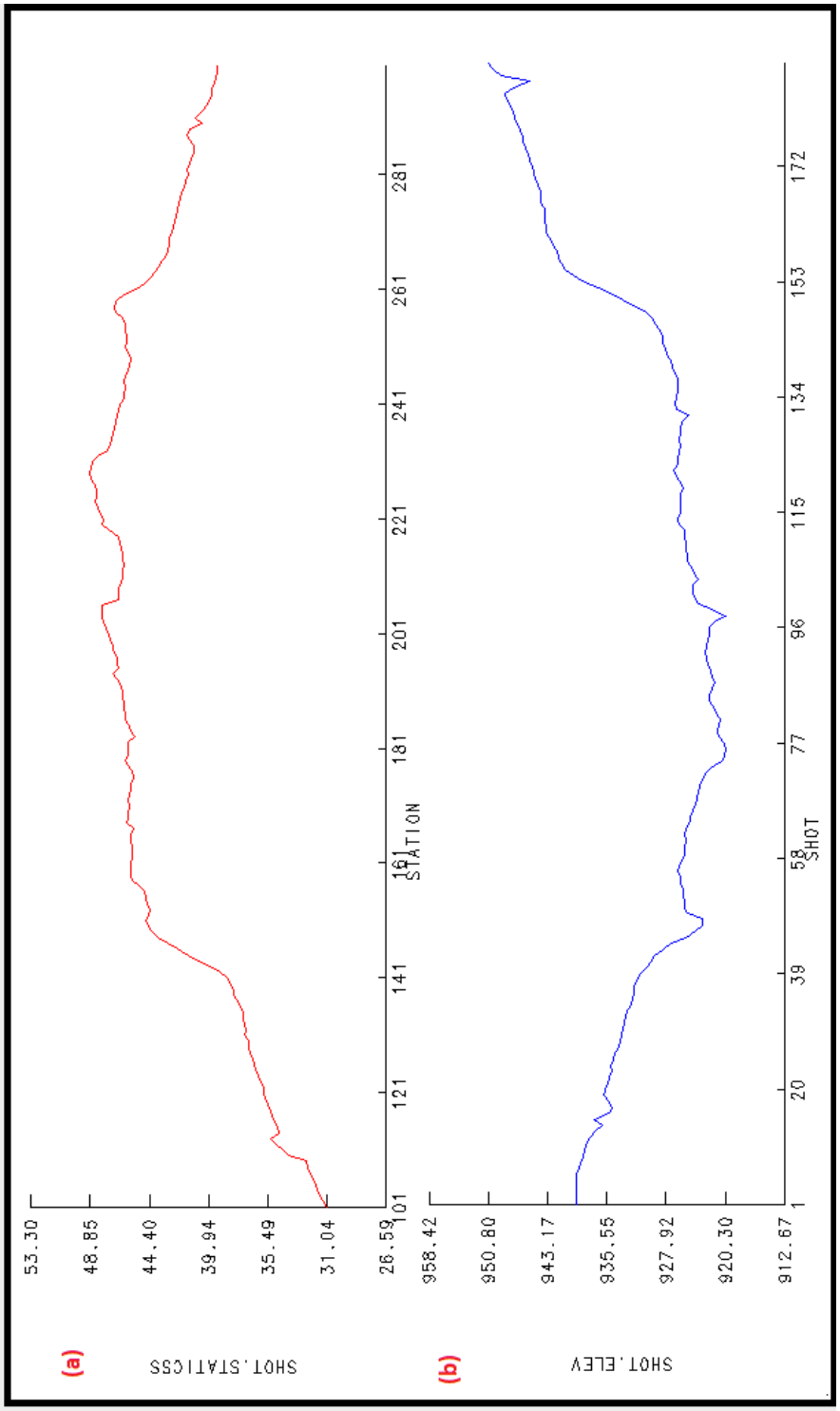

Figure 2.20. Elevation static corrections for shots. a) Calculated elevation statics for shots. b) Elevations of shots.

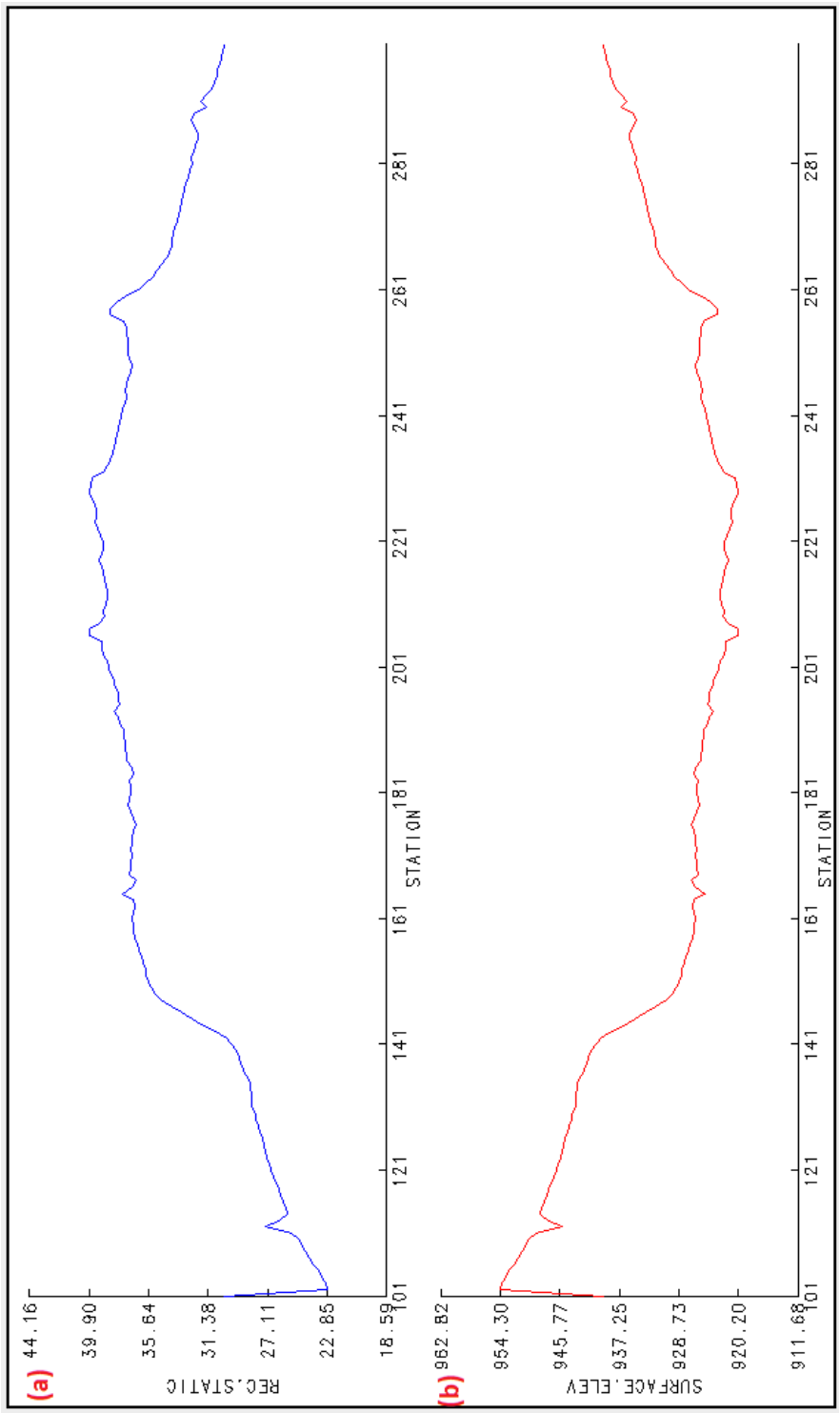

Figure 2.21. Refraction static corrections for receivers. a) Calculated refraction statics for receivers. b) Elevation of receivers.

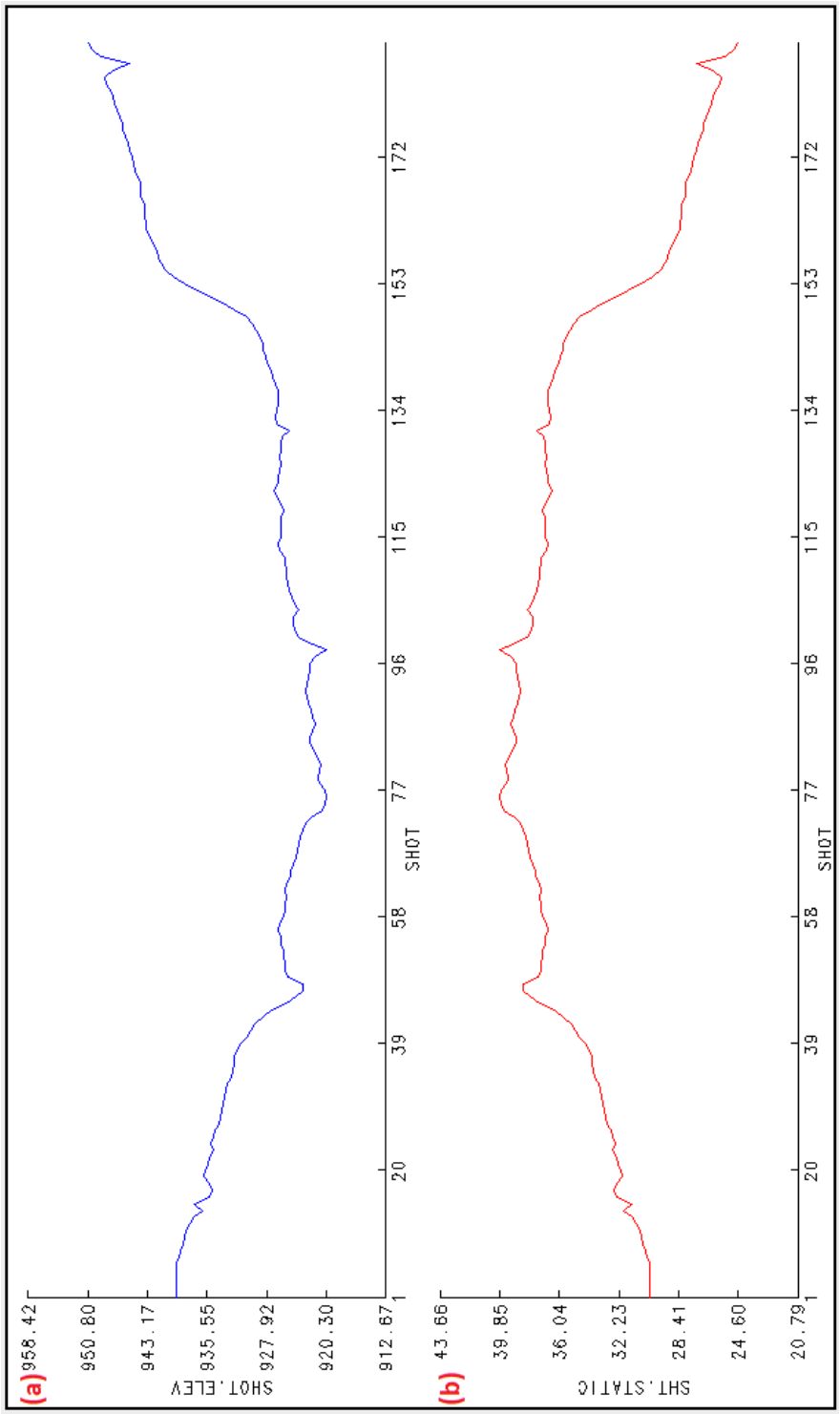

Figure 2.22. Refraction static corrections for shots. a) Elevation of shots. b) Calculated refraction statics for shots.

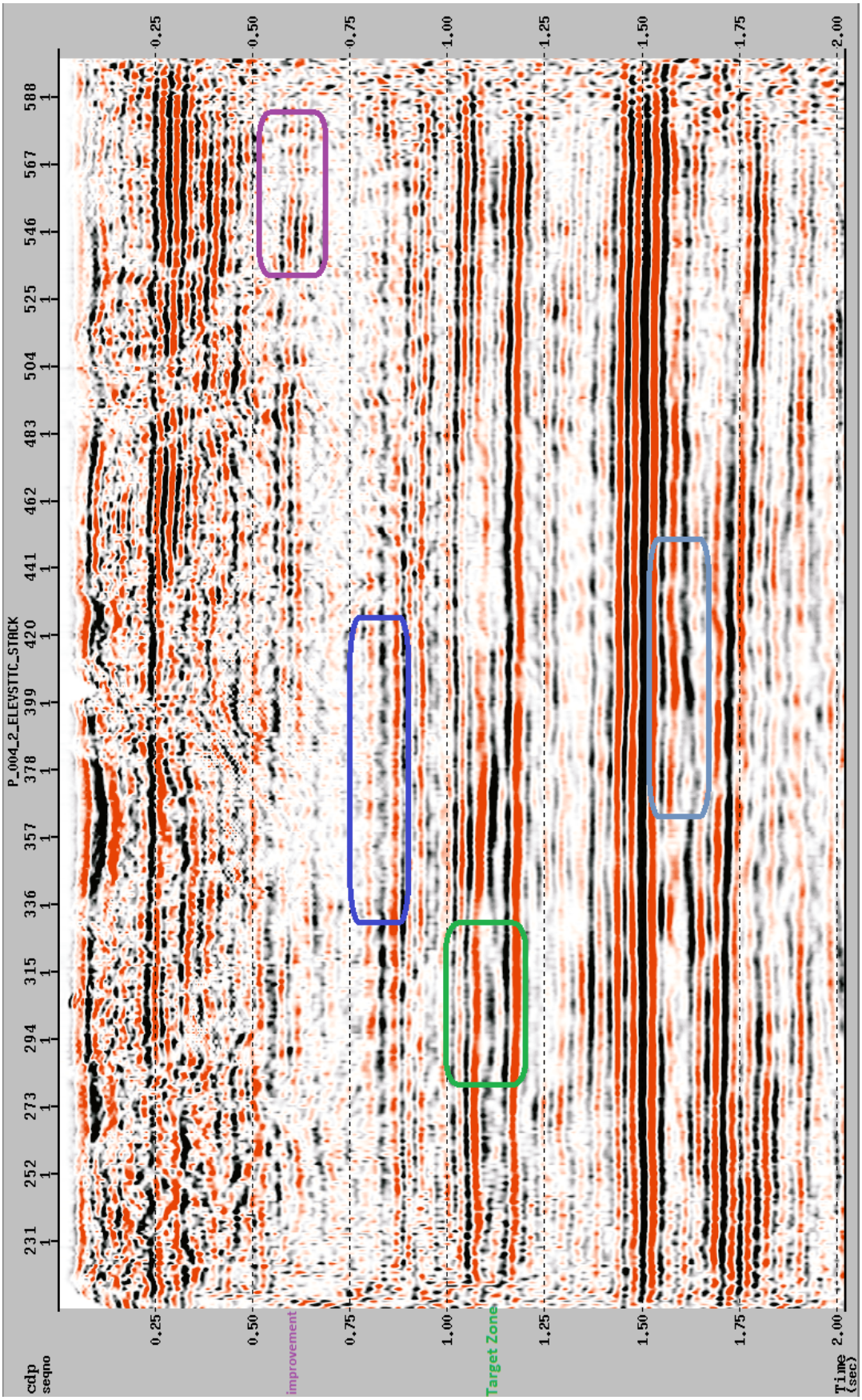

Figure 2.23. Stacked section after elevation static corrections. The areas that reveal the changes are displayed with different colors.

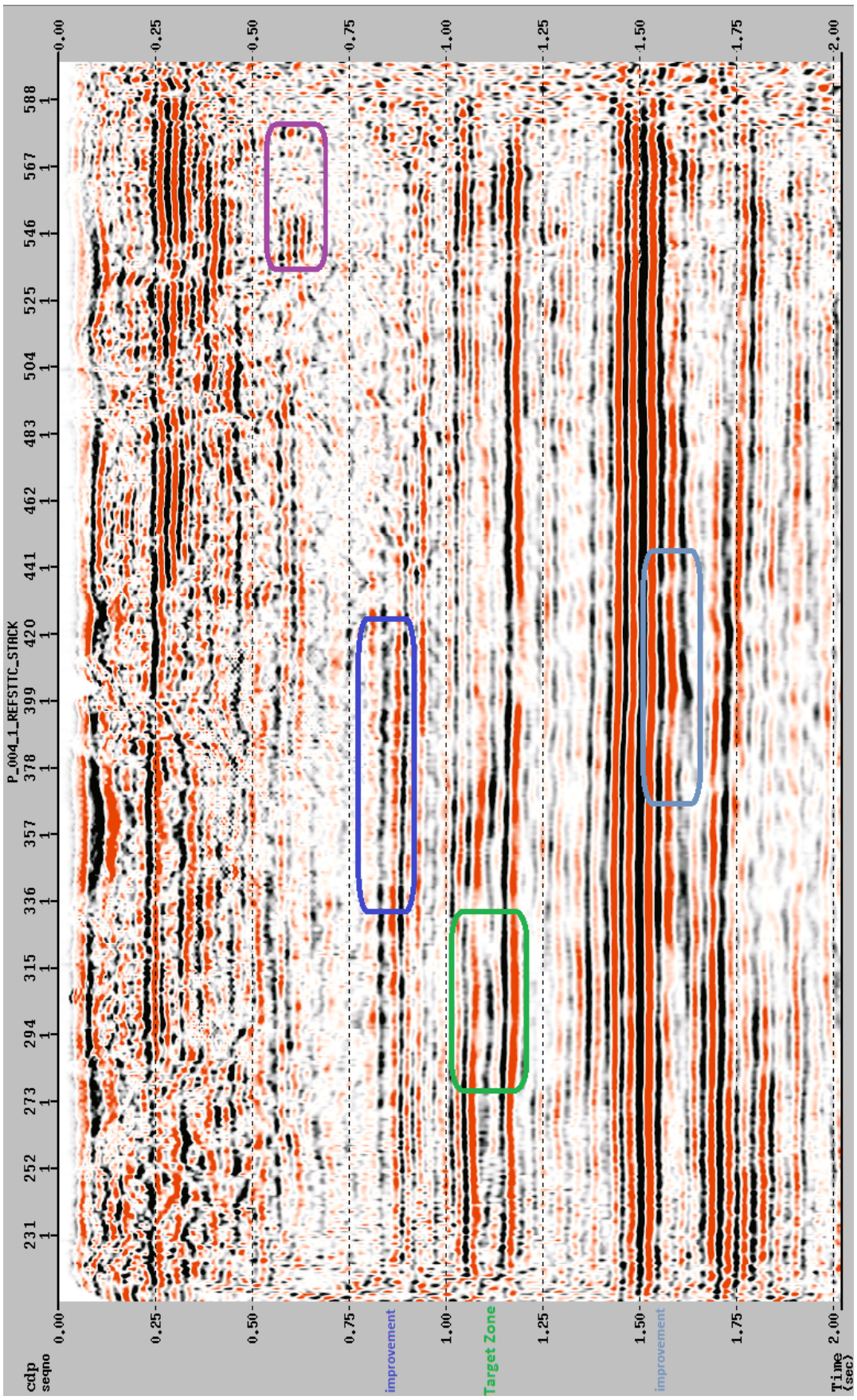

Figure 2.24. Stacked section after refraction static corrections. The areas specified show the improvements. The results indicate that the refraction static method is superior to the elevation static method.

2.6. VELOCITY ANALYSIS AND NORMAL MOVE-OUT (NMO) CORRECTION

Seismic velocity is the most important parameter in the seismic method since it is used in a number of processing steps such as stacking and NMO corrections, migrations, and time-to-depth conversion. The mathematical equations of velocity functions are used to acquire information that is associated with a specific velocity function, for instance, average velocities as function of depth and time (Kaufman, 1953). In this framework, the seismic velocities consist of average, interval, NMO, RMS, stacking, and Dix velocities. Each one is computed differently and used for various purposes.

There are several factors that affect seismic velocities. These are porosity, density, and composition of the rock (temperature-pressure) (Eberhart-Phillips et al., 1989). Of all these factors, porosity has the highest influence on seismic velocity. Other factors that affect seismic velocity include frequency of the seismic energy source, voids, and the characteristics of cracks in the subsurface.

The resolution and accuracy in velocity analysis depend on several factors, such as cable length, frequency bandwidth of signal, and the two-way travel time at zero offset related to seismic reflection events. In this context, a prestack deconvolution is applied to seismic data to improve the resolution, which helps to have a better velocity resolution in the velocity spectrum (Yilmaz, 2001).

There are several approaches of stacking velocity analysis such as constant velocity stack (CVS), constant velocity gather (CVG) and velocity spectrum. Almost all of these methods are performed interactively on a screen by utilizing a combination display configured by user preference.

In this study, the velocity spectrum method was preferred to determine the stacking velocities. Figures 2.25 and 2.26 show examples of velocity analyses in the selected CMP gathers. To have more CMP gathers when velocity analysis is performed offers more accurate velocity picks.

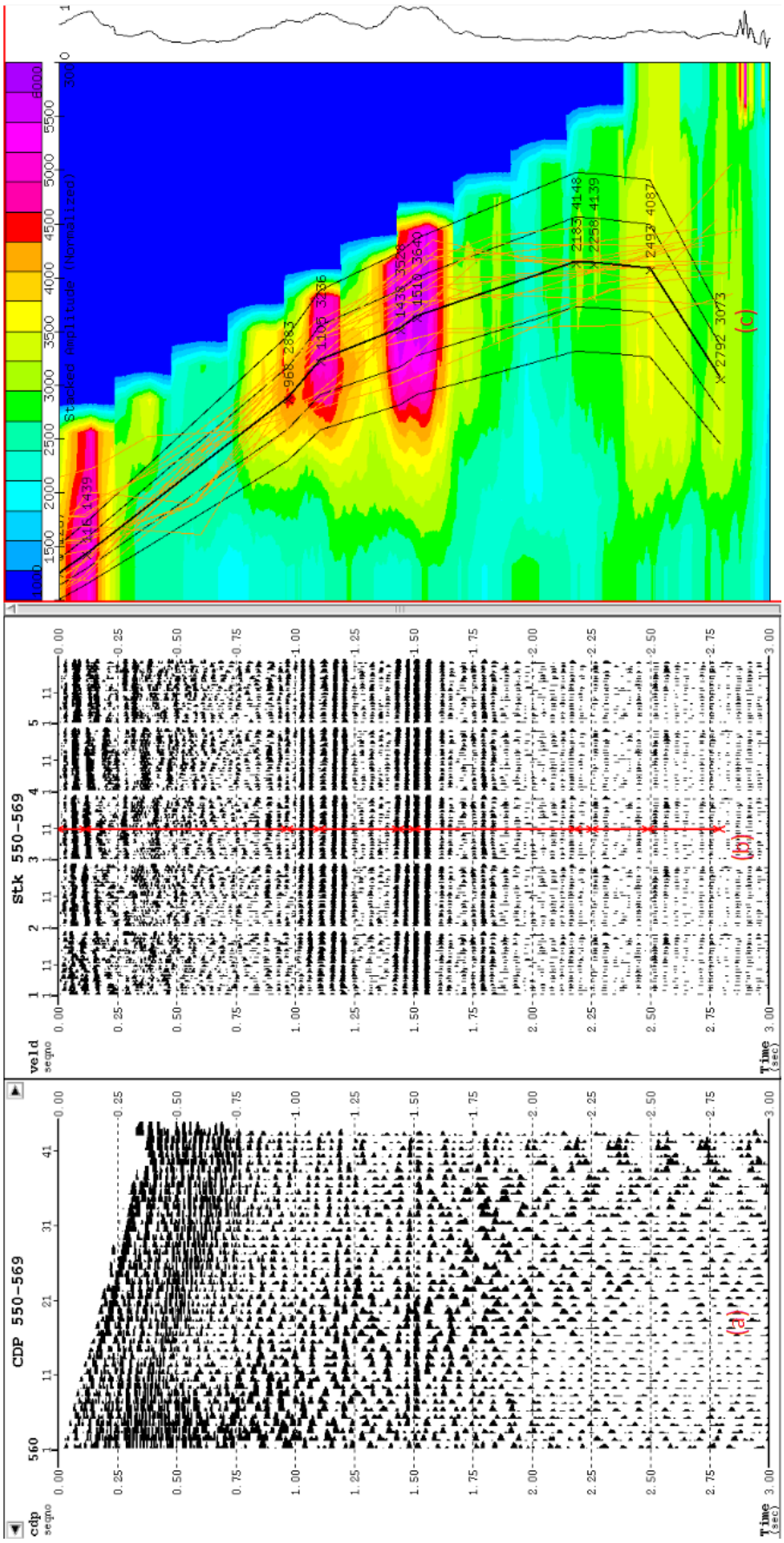

Figure 2.25. Diagram showing velocity analysis. a) Selected cdp gathers 550-569. b) Stacked section. c) NMO semblance of the gathers. The higher amplitudes were picked.

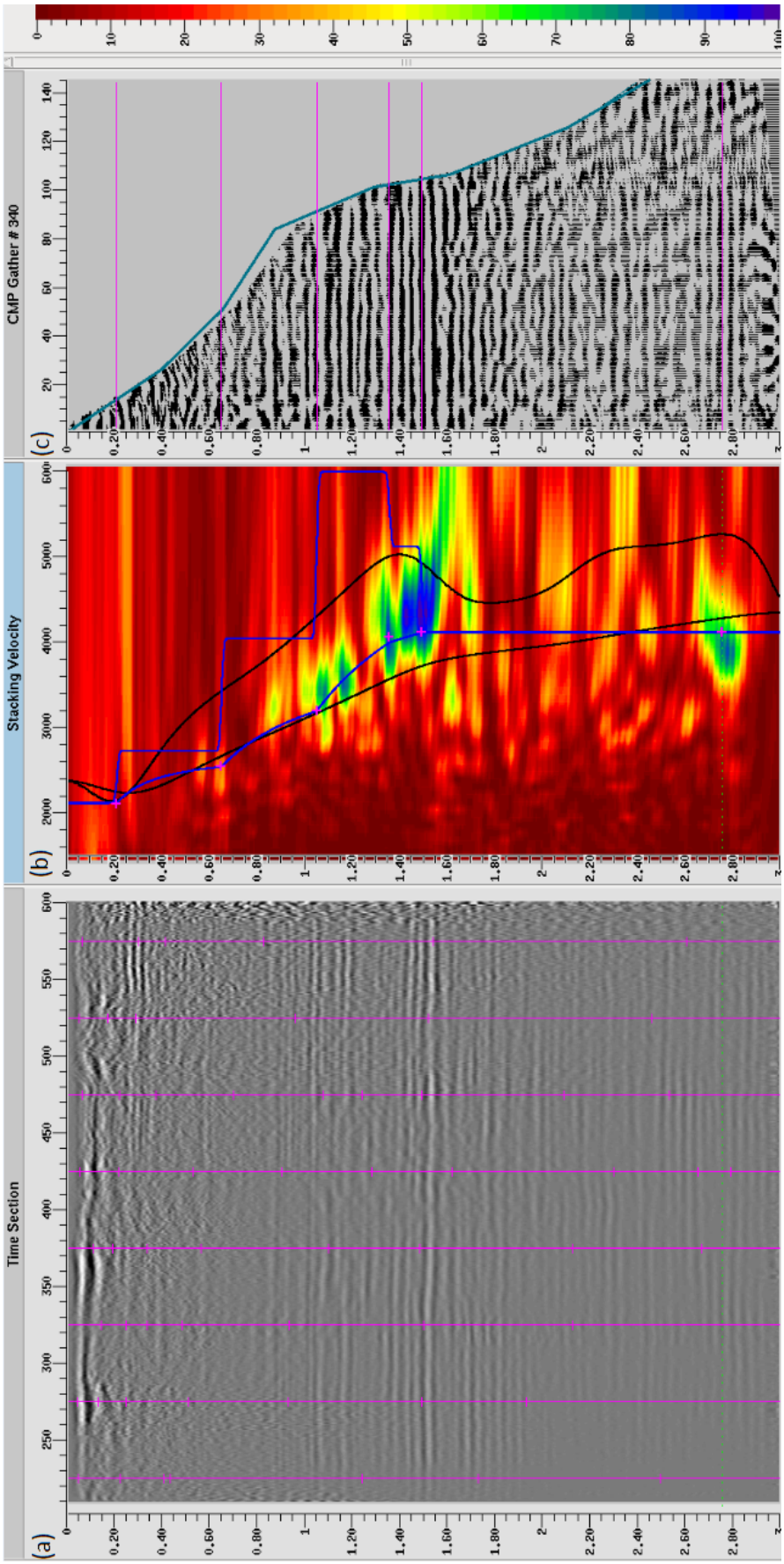

Figure 2.26. Velocity analysis. a) Stacked section. b) NMO semblance of CMP gathers. c) CMP gather 340 to examine the changes of picked velocities for NMO and mute.

The most common method used to generate a velocity spectrum is the conventional NMO semblance method (Taner and Koehler, 2001). The principle is to apply the NMO correction on selected CMP gathers over a velocity spectrum. The stacked section is then generated for each picked velocity (Stockwell, 2012).

Selected gathers before applying NMO are shown in Figure 2.27 and after NMO in Figure 2.28. As shown in the figures, the primary reflections of the seismic data were flattened.

2.7. RESIDUAL STATICS CORRECTIONS

Residual static corrections are to correct the short wavelength (small time shifts) anomalies and valid in the processing land and shallow marine data. Residual static corrections have an influence on the quality of stacked section (Yilmaz, 2001). Approximations to estimate and correct the time shifts are surface consistent. In other words, the corrections depend on the locations of shots or receivers (Zhu et al., 2014).

Seismic sections with only datum statics applied do not thoroughly fulfill the requirements of seismic data processing due to difficulties in the near subsurface model (Faquan and Yusheng, 2011).

Residual statics are applied to data to correct small time shifts in the near subsurface model, and the application of residual corrections improves the final seismic section more than when only datum statics applied (Cox, 1999).

The residual static corrections are first applied to the original gathers without applying NMO. At least two iterations of residual corrections are generally needed in processing land data. Following each residual static correction, velocity analysis is performed to improve the velocity picks (Gadallah and Fisher, 2005).

In this study, the two iterations of the residual static corrections were applied to the seismic data.

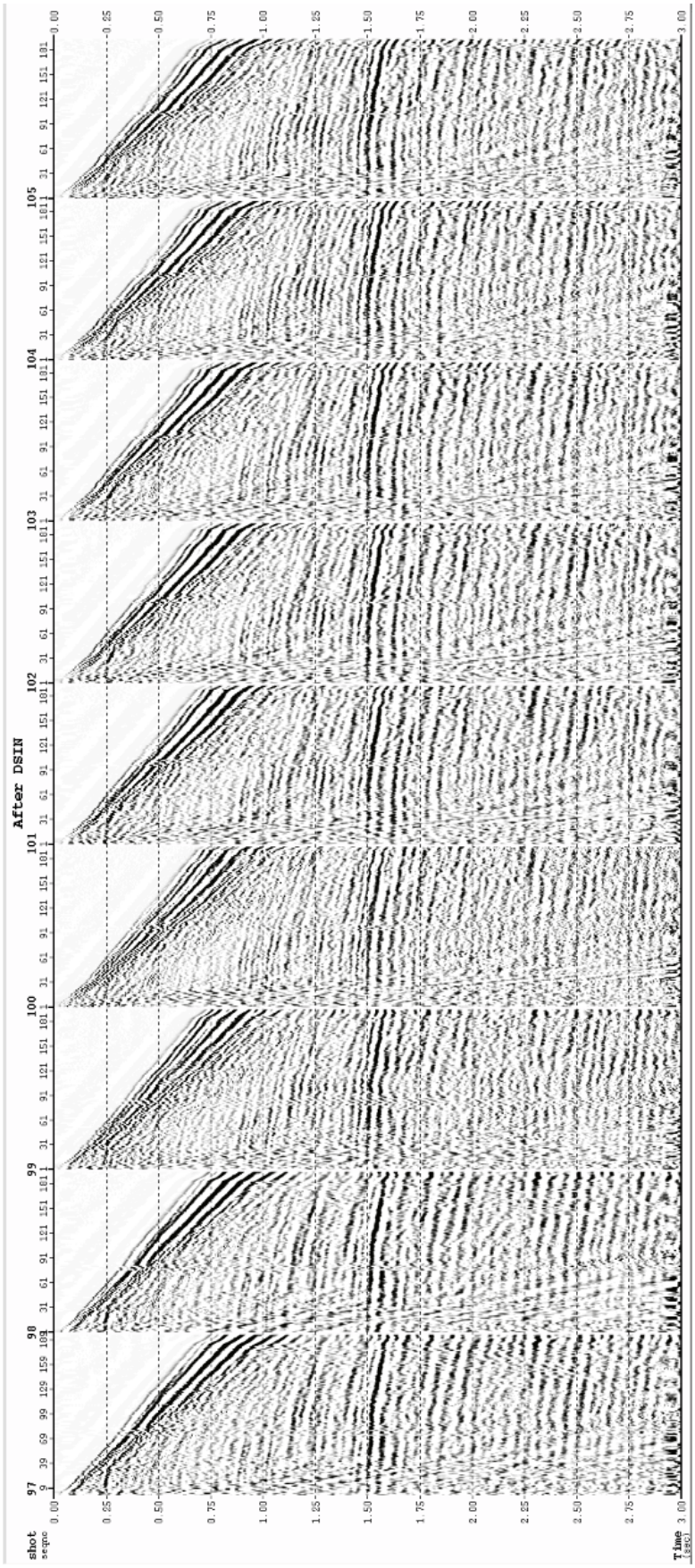

Figure 2.27. Gathers 97-105 before applying NMO.

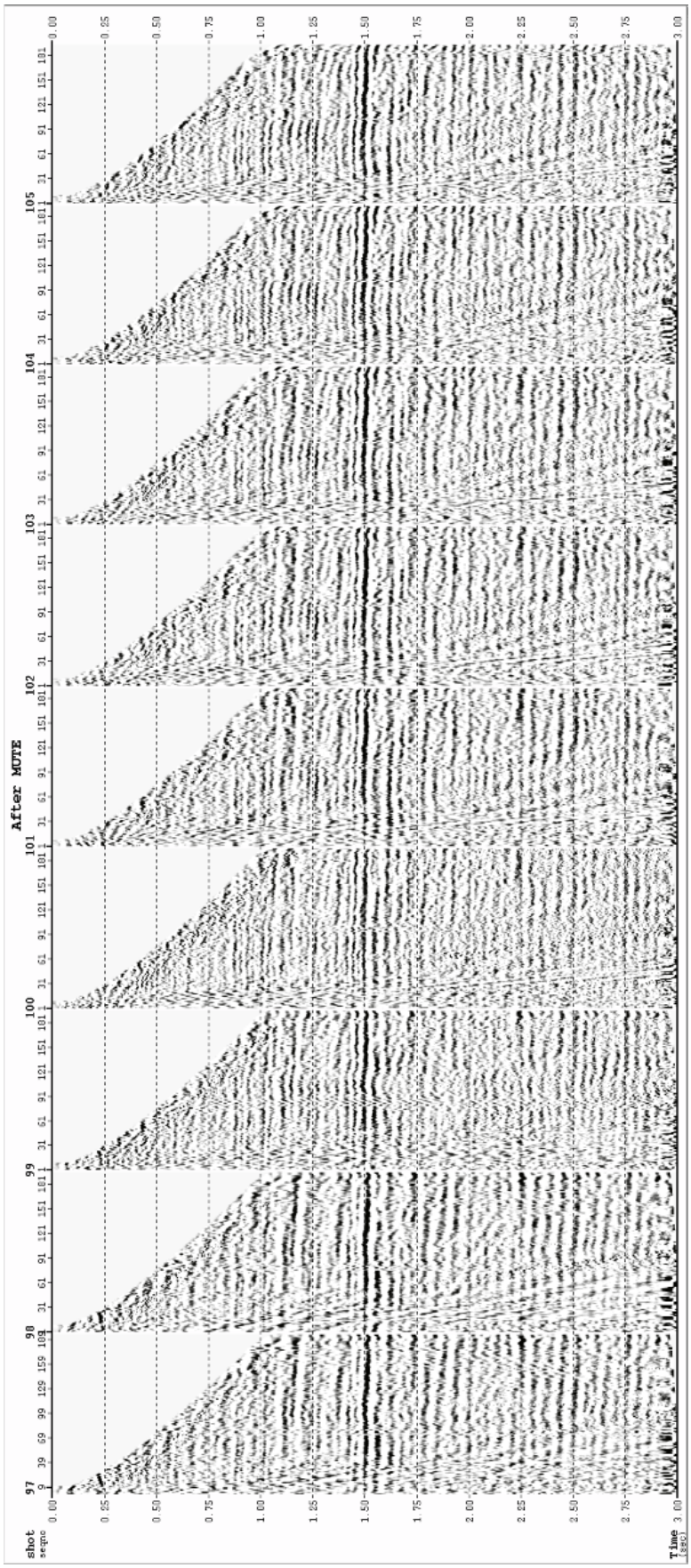

Figure 2.28. Gathers 97-105 after applying NMO. The primary reflections were flattened.

Figure 2.30 shows the stacked section before residual static corrections. The first iteration of residual static corrections is shown in Figure 2.31. After the first residual static correction, the second iteration was performed with improved velocities (Figure 2.32). The target zone and several areas are observed clearer after each iteration of the residual static corrections, and the areas that are specified by different colors show significant improvements.

2.8. STACKING

Summing traces from different records that have a common midpoint (CMP) to form a single trace is called stacking. Stacking is performed to reduce noise and improve the quality of seismic data by compressing the volume of data in the offset direction (Yilmaz, 2001). Figure 2.29 illustrates the three keystones of seismic data processing in their processing domains. Stacking is performed by applying NMO correction to the traces, and then by compressing these traces in the offset domain (Yilmaz, 2001).

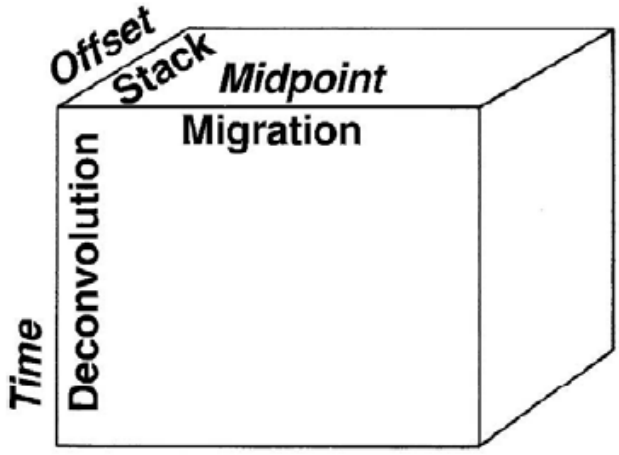

Figure 2.29. Demonstration of the three main steps with their processing coordinates in seismic data processing (Yilmaz, 2001).

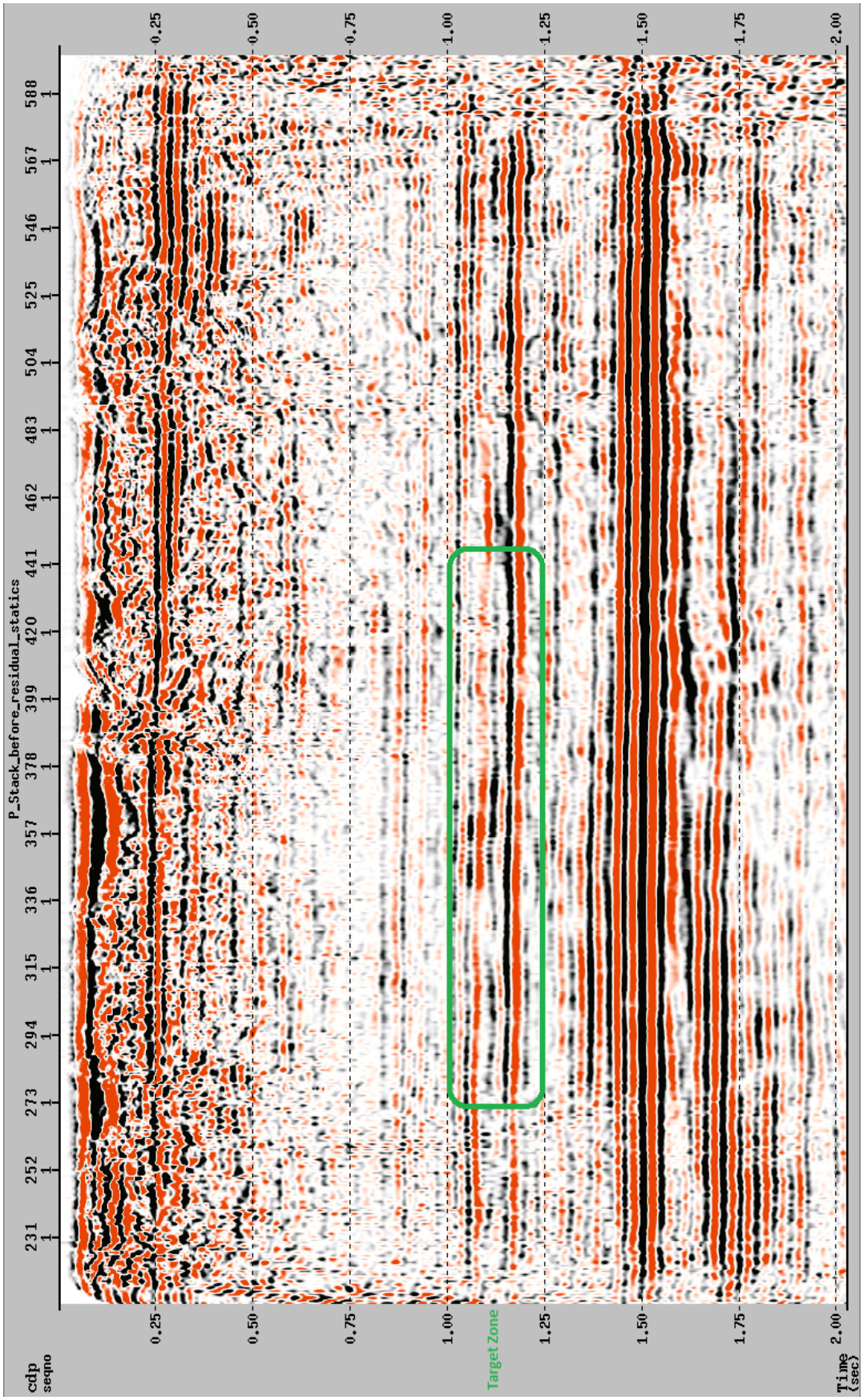

Figure 2.30. Stacked section before applying residual static corrections.

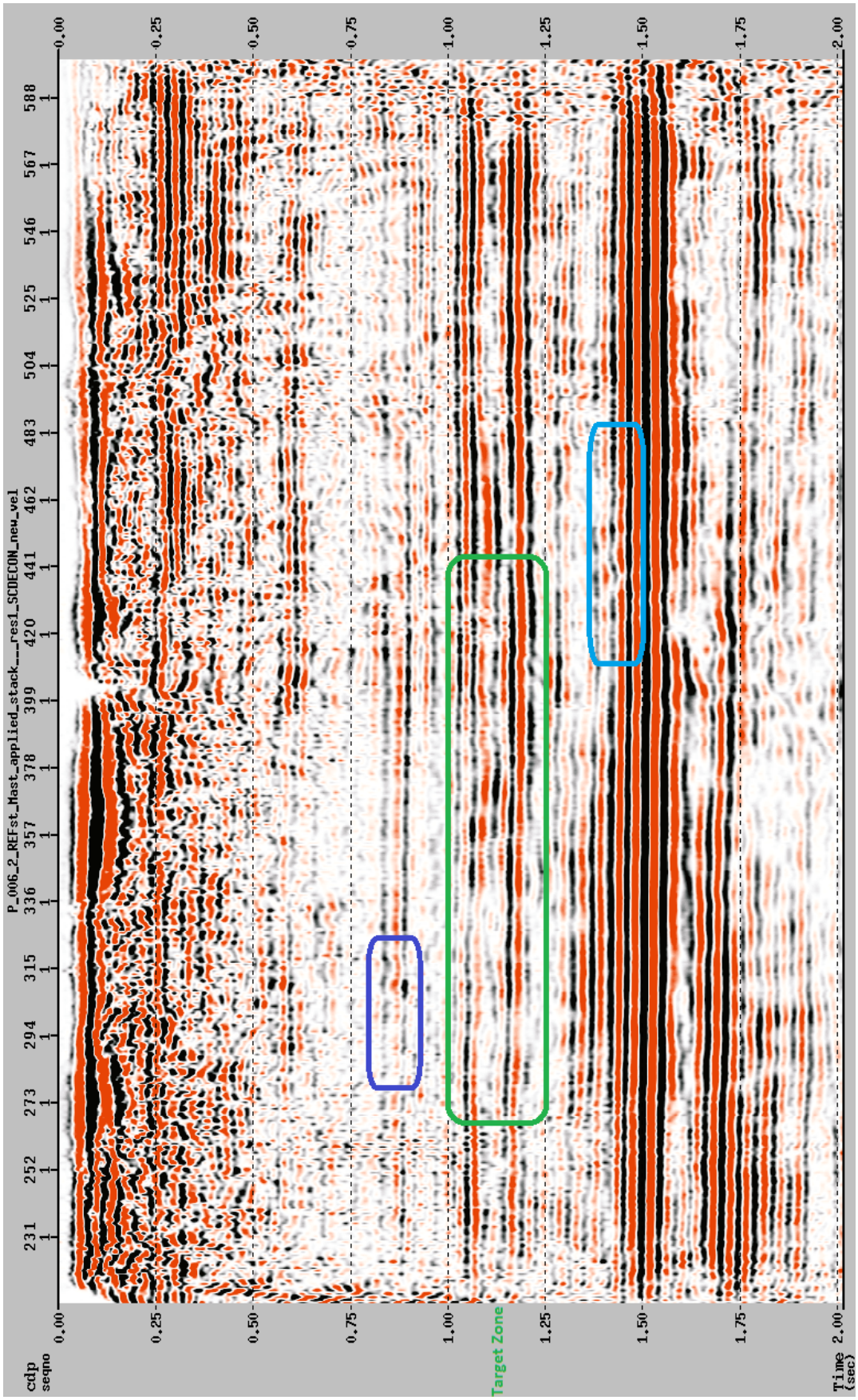

Figure 2.31. Stacked section after the first residual static correction.

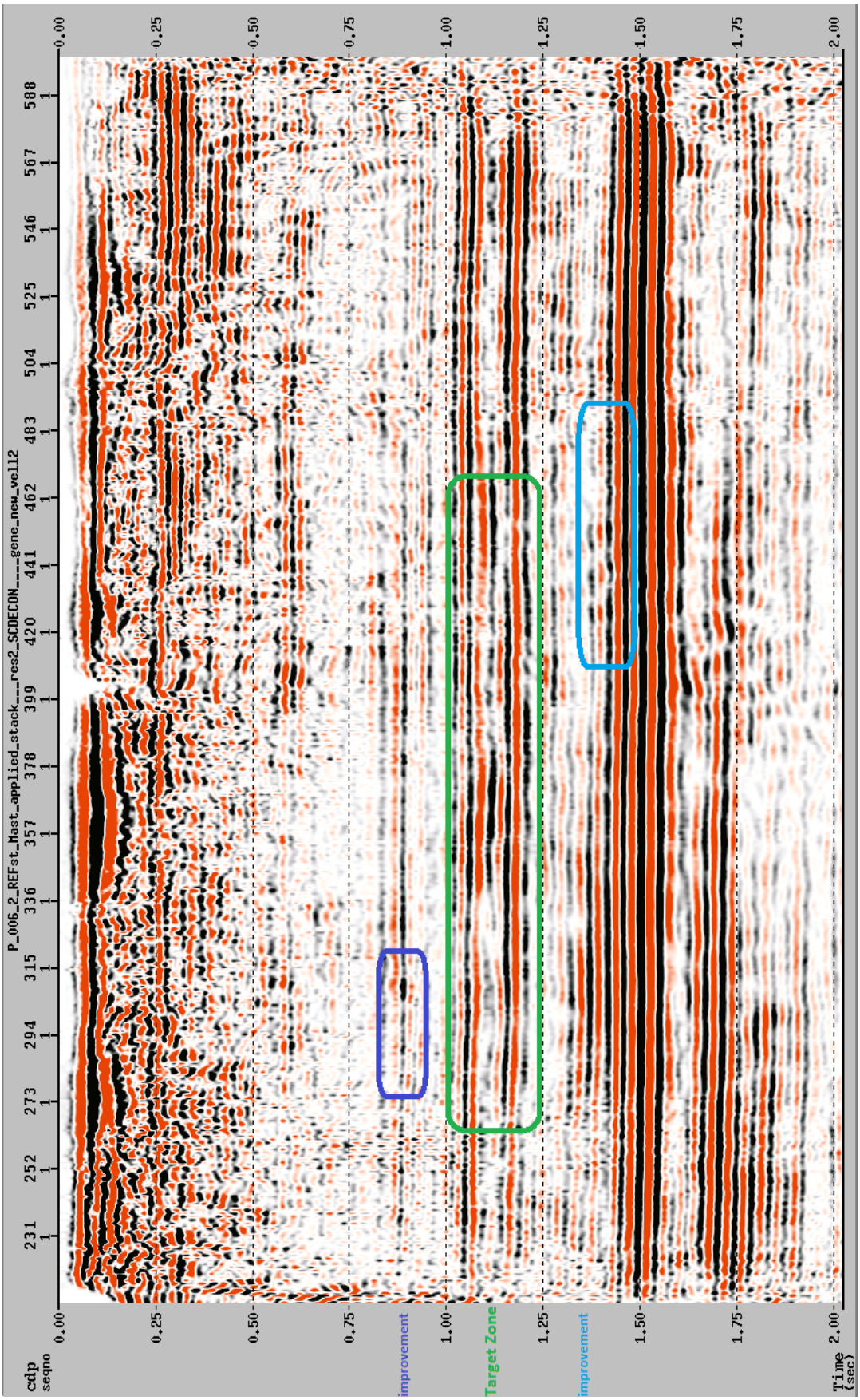

Figure 2.32. Stacked section after the second residual static correction. The areas specified were improved notably.

The conventional stacking algorithm is based on the summation of the traces to produce an optimal trace in which the source and receiver stations are placed at the same CMP point (Covre et al., 2014).

The seismic traces are usually stored at the surface until the NMO correction, which is applied from a floating datum, i.e., the smoothed version of the surface topography (Figure 2.33). A flat datum, i.e., the shift to a reference flat datum, is performed after NMO correction. Several migration algorithms are based on the assumption that the input seismic data are obtained on a horizontal (flat) plane. For this reason, the seismic data are shifted back from a floating datum to a flat datum to efficiently run these migraton algorithms (Zheng et al., 2000). Another stacked section of the flat datum is shown in Figure 2.34. The seismic data were shifted back to a flat datum for the spatial interpolation.

2.9. MIGRATION

Of all the seismic processing steps, migration is one of the most significant parts in seismic imaging since it moves dipping events to their correct temporal and spatial positions, increases spatial resolution, and removes diffractions. It is an important and expensive step in seismic data processing. The migration strategies are used to effectively image the subsurface. These strategies include the following (Yilmaz, 2001):

1. Dimensionality, 2D or 3D migration
2. Prestack or poststack migration
3. Time or depth migration

In this context, any combination of these migration strategies is determined based on the geology of the area (the nature of the subsurface) (Yilmaz, 2001).

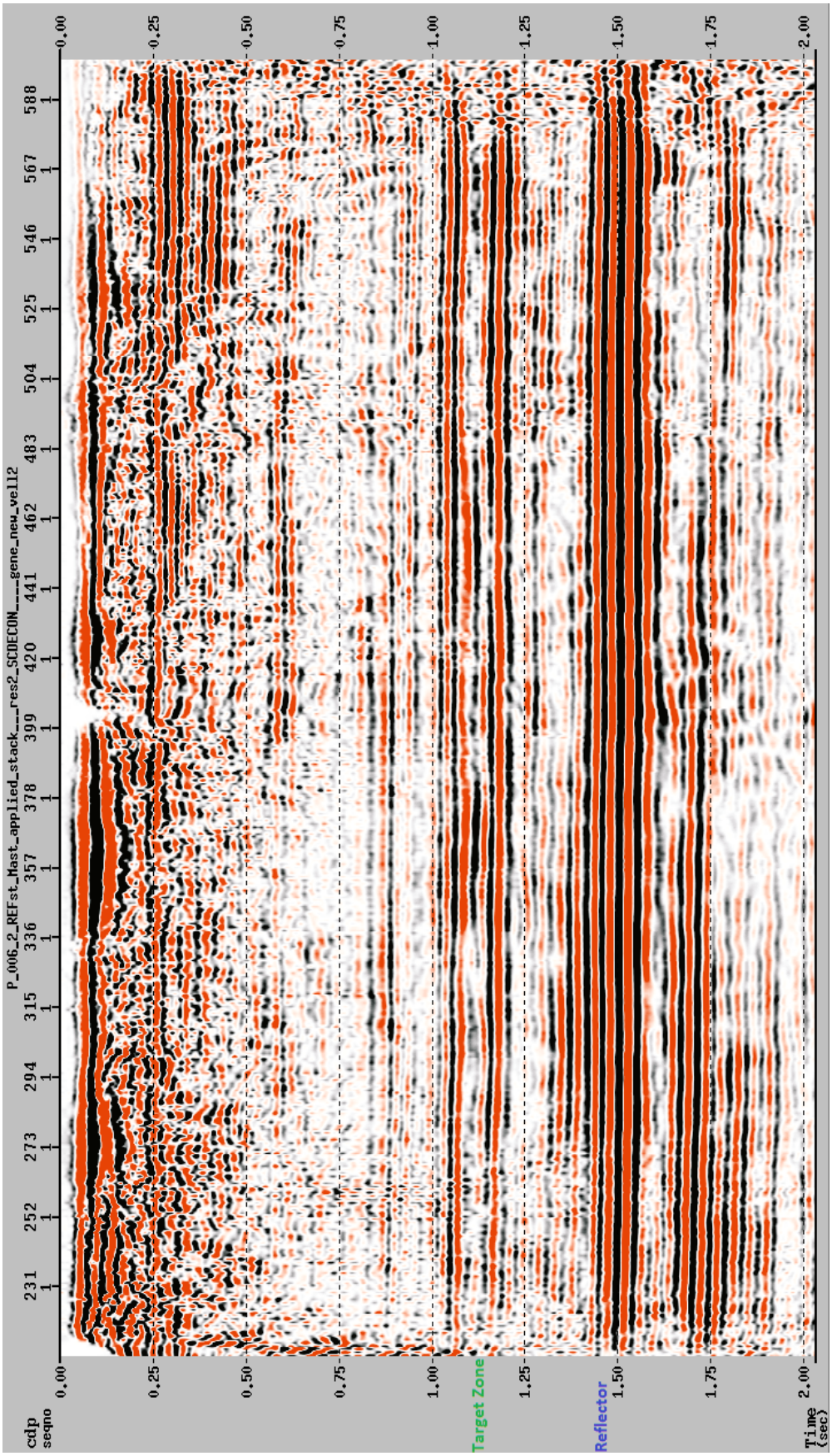

Figure 2.33. Stacked section with floating datum and improved velocities.

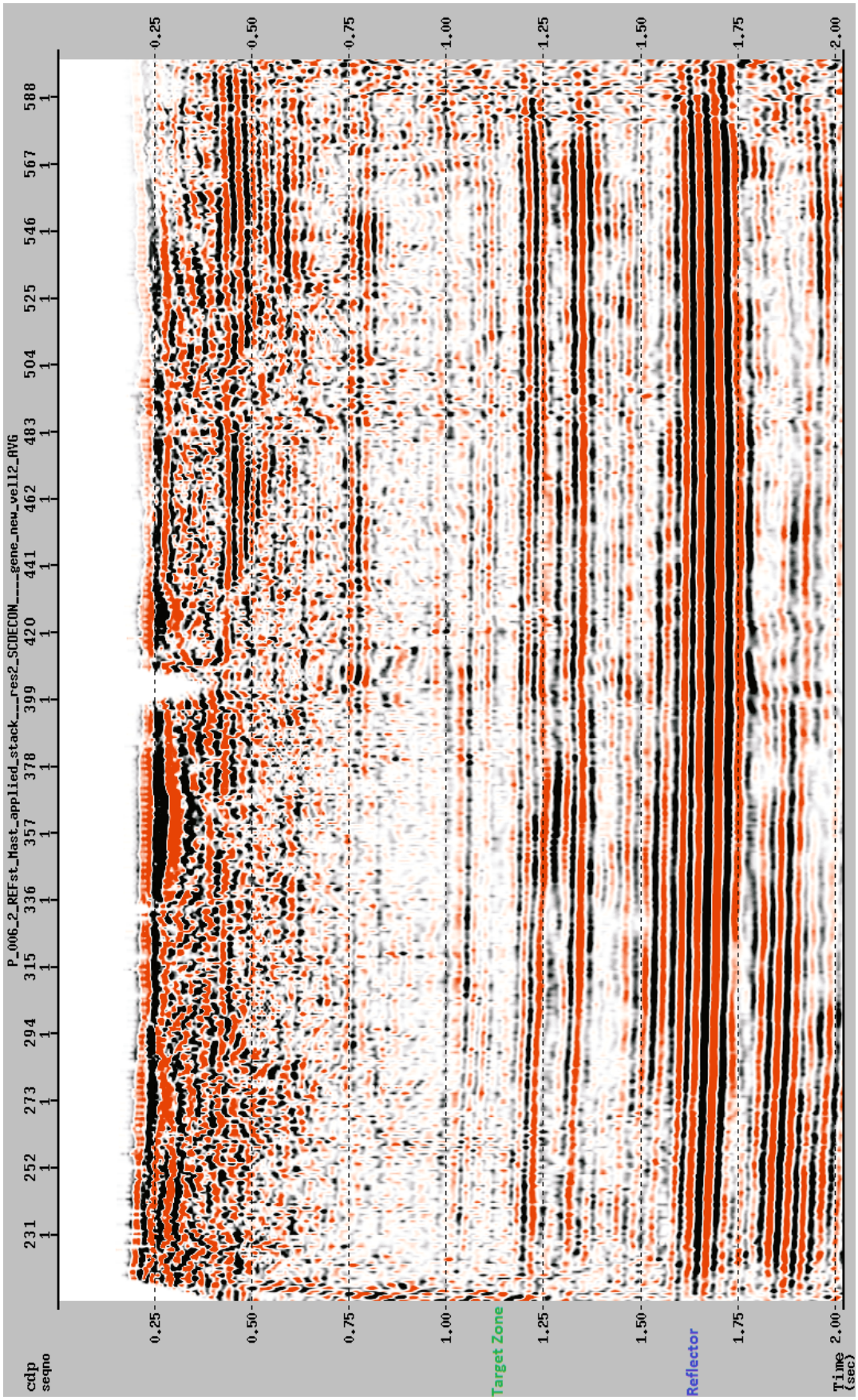

Figure 2.34. Stacked section fixed to a reference flat datum. The seismic data were shifted back to a flat datum.

Time migration is commonly used to image the subsurface since it is faster and less sensitive to velocity errors than depth migration (Dell et al., 2012). Depth migration is generally used for strong lateral variations that are associated with complex structures (Yilmaz, 2001).

Prestack migration is used for areas that have complex geological structures with CMP stacking problems because the common mid-point (CMP) is not the same as the common reflection-point (Bording and Lines, 1997). On the other hand, poststack migration offers less accurate images of the subsurface that have complex geological structures even though it is much less expensive than prestack migration (Yilmaz, 2001).

A number of migration algorithms are available in seismic processing. Deciding what type of migration should be used depends on three main factors: cost, needs regarding frequency content of seismic data, and maximum dip to migrate. All migration methods work based on two stages. The first stage is to generate an extrapolated seismic wavefield from the back projection of the seismic data by using the wave equation and determining a velocity field. The second stage involves using an algorithm to move reflectors to their correct positions by using an extrapolated seismic wavefield (Zhou, 2014).

In this study, 2D Kirchhoff time migration was used to image the subsurface. There are two important parameters affecting the performance of Kirchhoff migration: aperture width and maximum dip to migrate (Yilmaz, 2001). Aperture is defined as a part of seismic data to what extent filters or specified functions are applied. In Kirchhoff migration, seismic data are represented by a summation of amplitudes along the diffraction hyperbolas that are obtained by RMS velocities (Rastogi et al., 2000). Yilmaz (2001) defines the aperture as the spatial extent that the real summation path covers. Maximum dip is defined as the depth (in time) desired in the migrated section.

The issues encountered in the Blackfoot field are the lithology discrimination between the sand reservoir and the neighboring shales because of their similar P-wave anomalies and the state of stratigraphically thin beds (Okonkwo, 2014). To reveal seismic thin

beds, there are two key parameters, i.e., the frequency bandwidth of the data and the bed thickness (Sajid and Ghosh, 2014). Spectral whitening, which is also known as balancing or broadening, is used to obtain the frequency content wider and higher resolution.

In this study, the spectral whitening was applied to the migrated sections to enhance the resolution and appearance of the data. Both prestack time migration (PSTM) and poststack time migration were applied during the process. Figures 2.35 and 2.36 show the migrated sections of the 2D Kirchhoff poststack and prestack time migration with spectral whitening, respectively. The aperture, maximum dip to migrate, and other related parameters were tested to obtain the optimum image of the reservoir.

The area of interest is enlarged to better display the Glauconitic sand reservoir (Figure 2.37). According to the obtained results, PSTM (left) reveals the channel cuts (reservoir) more observable and offers stronger amplitudes in the target zone than the poststack time migration (right).

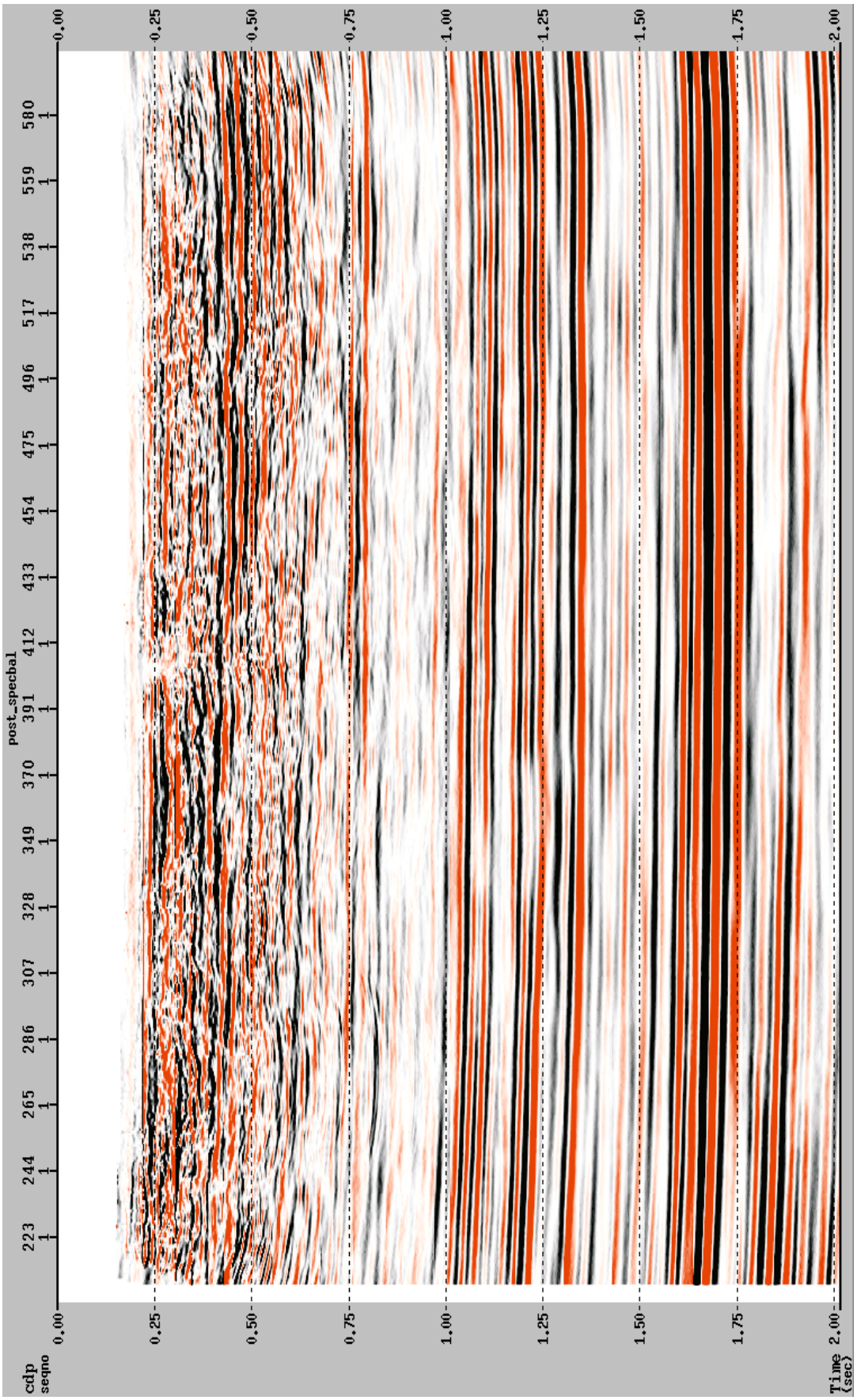

Figure 2.35. 2D Kirchhoff poststack time migrated section with spectral whitening.

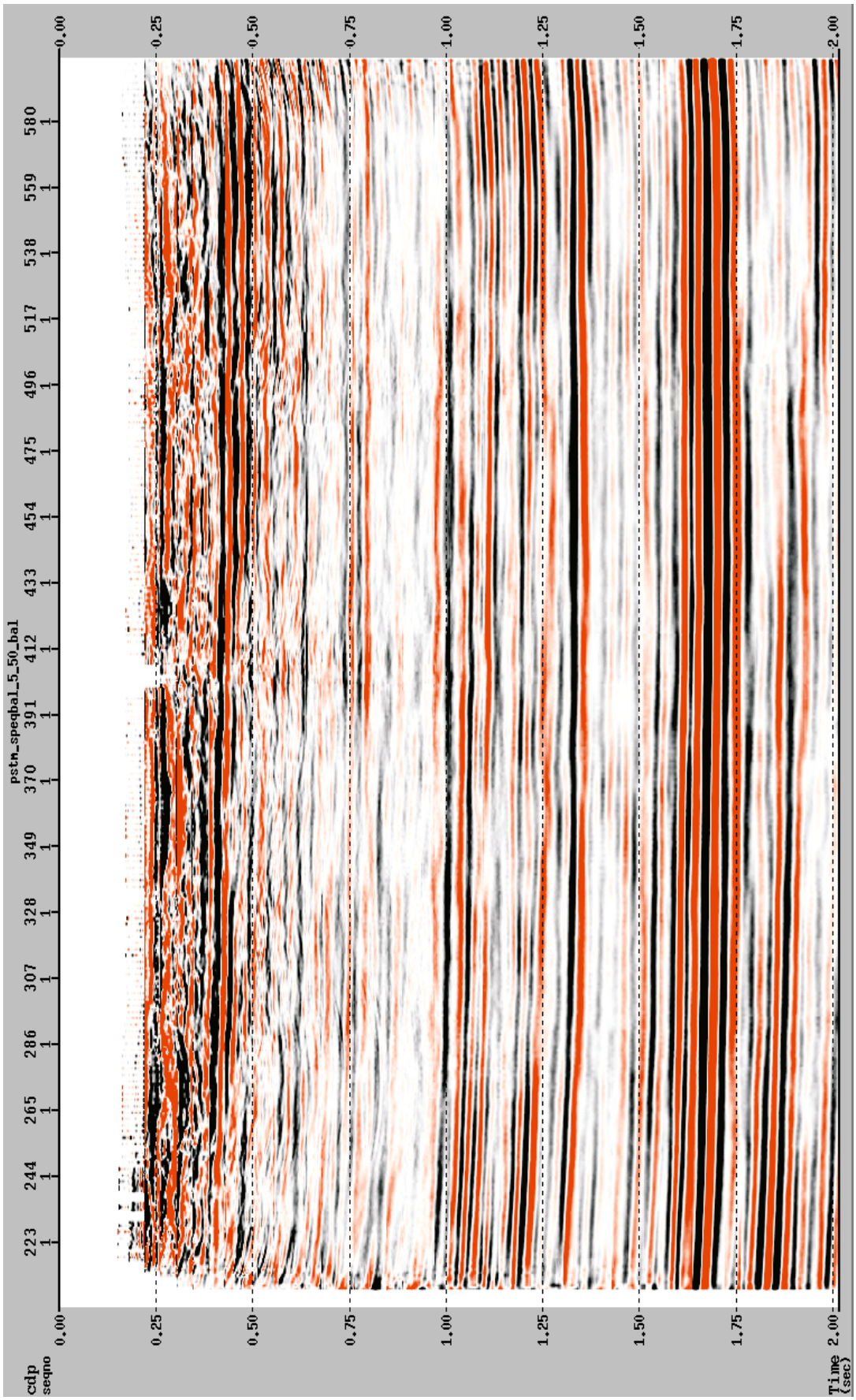

Figure 2.36. 2D Kirchhoff prestack time migrated section with spectral whitening.

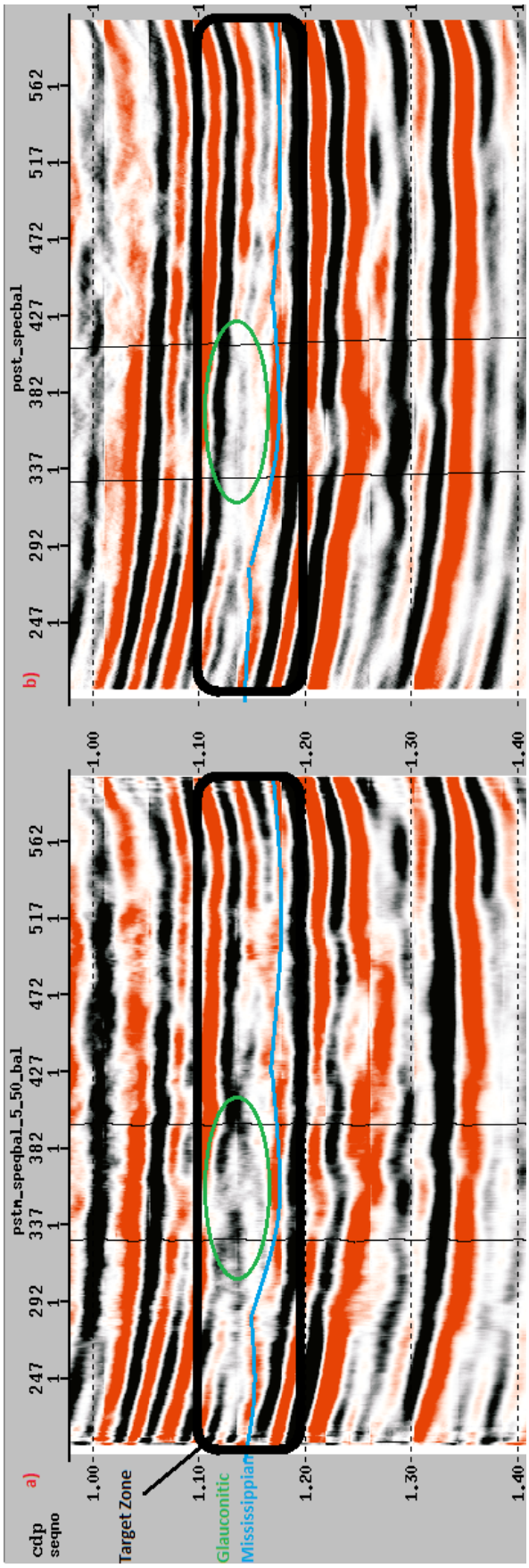

Figure 2.37. Enlarged display of the target zone. a) 2D Kirchhoff prestack time migration. b) 2D Kirchhoff poststack time migration. PSTM displays the reservoir (channel cuts) clearer than the poststack time migration.

3. MULTICOMPONENT SEISMIC PROCESSING

3.1. BACKGROUND

Before 1970s, seismic exploration for oil and gas reservoirs was limited to the recording only P-wave energy, which is a single component in the vertical direction (Sheriff and Geldart, 1995). Thereafter, S-wave recording (i.e., benefitting from all the components possible from both vertical and horizontal directions) was added to searching oil and gas. The concepts of the multicomponent acquisition, processing, and interpretation were developed, and the multicomponent seismic survey gained wide acceptance.

The multicomponent seismic technology uses horizontally and vertically polarized geophones and sources and provides more information about the subsurface than the conventional P-wave alone.

Multicomponent seismic survey records both the P-wave energy in the vertical direction and the S-wave energy in the horizontal direction. In this context, S-waves have two modes, i.e., SH and SV (Figure 3.1).

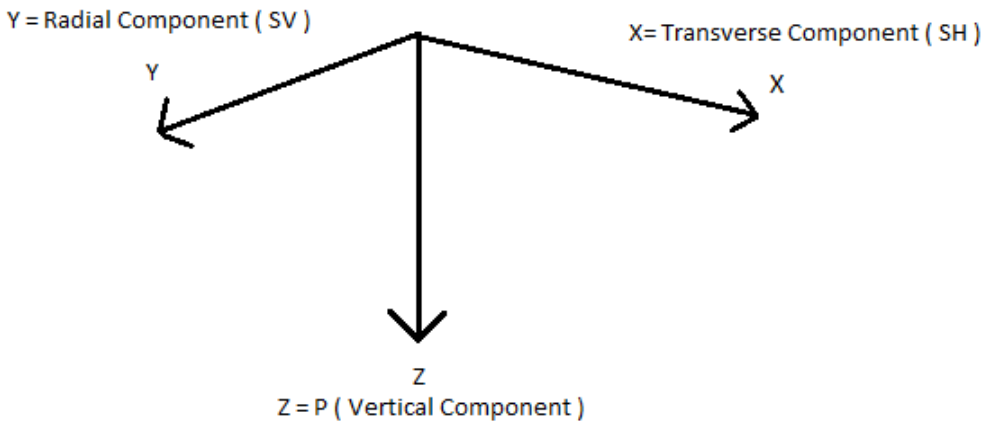

Figure 3.1. Diagram showing the vertical, radial, and transverse componets.

To acquire multicomponent seismic data, various survey geometries are utilized in the seismic exploration industry. These geometries include 2-component (2C), 3-component (3C), 4-component (4C), 6-component (6C), and 9-component (9C) for both 2D and 3D surveys. Table 3.1 shows the survey geometry to obtain 9C multicomponent seismic data.

SV, or the radial component, refers to the vertical S-wave while SH, or the transverse component, refers to the horizontal S-wave. The horizontal (radial and transverse) and vertical directions are represented by X, Y, and Z. Several other acquisition geometries to acquire the multicomponent seismic data include (Farfour and Yoon, 2016):

1. 3C denotes the recording of a source in the vertical direction and geophones in X, Y, and Z directions (Z / XYZ).

2. 4C is used for marine surveys and implies the same design as 3C with an additional measuring of the hydrophone (H) component.

3. 6C is acquired with sources in two directions (YZ) and 3C geophones in XYZ directions.

Table 3.1. Survey geometry to obtain 9C seismic data. This geometry is only accurate in Cartesian coordinates; that is, line direction is X-axis, and the line perpendicular to it is Y-axis.

Sources - Receivers	Z / Vertical (P)	X / Radial (SV)	Y / Transverse (SH)
Z / Vertical (P)	P-P	P-SV	P-SH
X / Radial (SV)	SV-P	SV-SV	SV-SH
Y / Transverse (SH)	SH-P	SH-SV	SH-SH

To capture these modes of P-wave and S-wave energies, specific geophones and survey orientations are used. Figure 3.2 shows an example of a 3C geophone. Figure 3.3 displays the survey design of vibroseis trucks when the multicomponent seismic data are recorded.

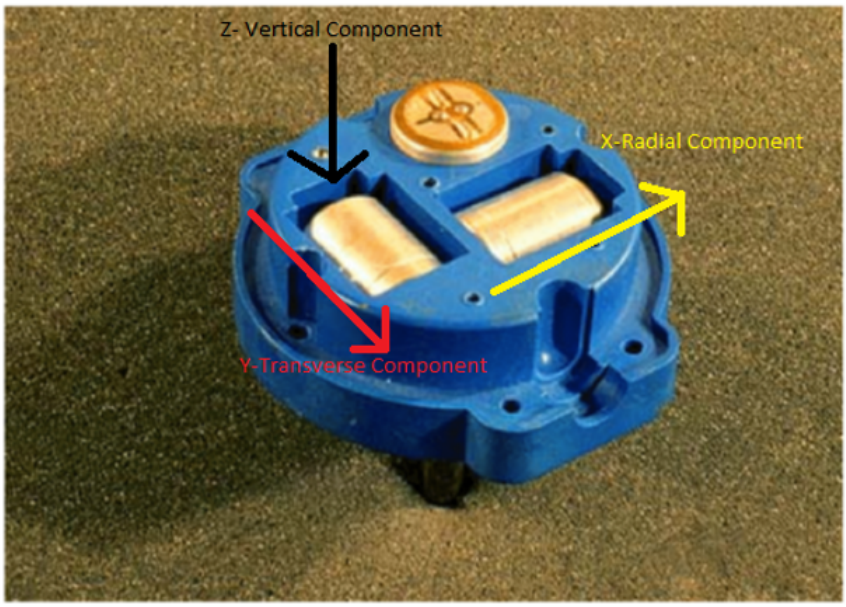

Figure 3.2. Example of a 3C geophone (Stewart, 2014).

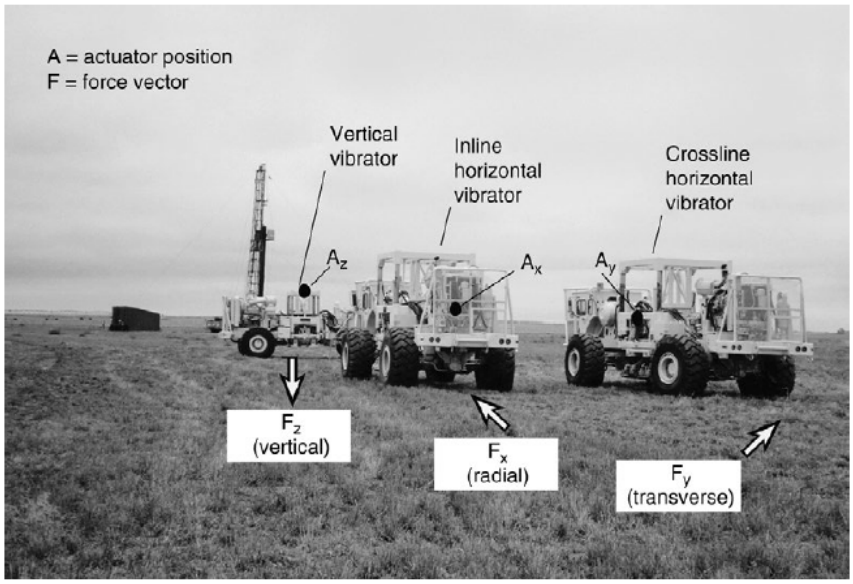

Figure 3.3. Design of vibroseis trucks while multicomponent seismic survey is performed (Hardage et al., 2011).

3.2. THE MAIN CHARACTERISTICS OF CONVERTED WAVE PROCESSING

The processing of the multicomponent seismic data is more complex than the conventional processing of P-wave data. The complexity stems from the differences in the characteristics of the propagation of P-waves and S-waves within the subsurface. Hence, the processing S-wave is not as straightforward as the P-wave processing (Eaton and Stewart, 1989). In this chapter, the main aspects of the converted wave processing, which include common-conversion point (CCP) imaging, asymptotic binning, statics corrections for receivers, anistropy, and rotation to radial/transverse components will be discussed in detail.

3.2.1. Common-Conversion Point (CCP) Processing. In the conventional P-wave (vertical component) processing, Snell's law indicates that the incidence angle (downgoing wave) and the reflection angle (upgoing wave) are the same. Thus, the processing P-waves benefits from the fact that the reflection point is the midpoint between the receiver and source. The processing of converted S-waves is more complicated than that of conventional P-wave. The complication arises because the propagation velocity of downgoing P waves is not the same as the propagation velocity of upgoing S waves (Farfour and Yoon, 2016). Consequently, the concepts involved in the common midpoint method (CMP) method are not applicable to the processing of converted waves.

Figure 3.4 displays the raypaths for the CMP and CCP imaging. In the converted wave processing, for instance P-SV, the downgoing wave (P-wave) propagates at a velocity that is higher than that of the upgoing wave (SV-wave). As a consequence, the reflection point (CCP) occurs closer to the receiver. However, SV-P wave is taken into account, the downgoing wave (SV-wave) propagates at a velocity that is lower than that of the upgoing wave (P-wave). In this case, the reflection point is closer to the source than to the receiver (Hardage et al., 2011).

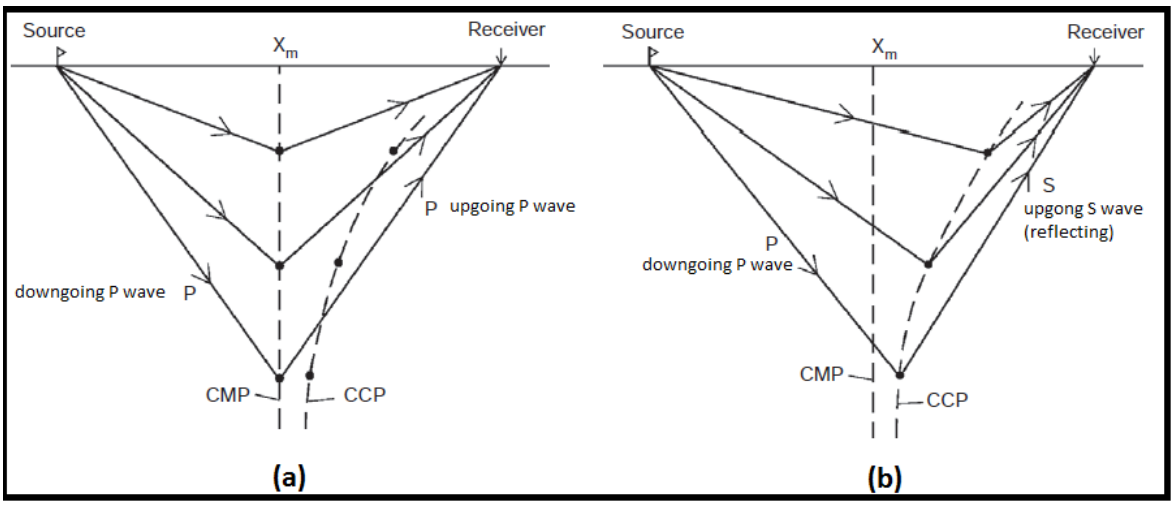

Figure 3.4. Raypaths for a) common midpoint (the vertical dashed line), and b) common-conversion point (the curved dashed line) (Hardage et al., 2011).

The fundamental assumption in the CMP processing is valid for SH-SH and SV-SV modes when the nine-component (9C) data are acquired since the velocities of downgoing and upgoing waves are the same (Hardage et al., 2011). For this reason, SH-SH and SV-SV processing is no different than the processing of the conventional P-wave.

3.2.2. Positive and Negative Offset. Offset is defined as the direction of the raypath from the source to the receiver. In this context, a positive offset is referred to as a raypath from the source to the receiver. On the other hand, a negative offset is defined as the raypath from the receiver to the source. In the CMP method, the lengths of the travel times are equal to each other for both positive and negative offsets because of the same velocities and travel times (Hardage et al., 2011) (Figure 3.5).

A different approach is performed when a converted wave is processed since the length of the raypaths are not the same in the CCP method. Figure 3.6 illustrates the positive and negative offsets involved in the P-SV imaging.

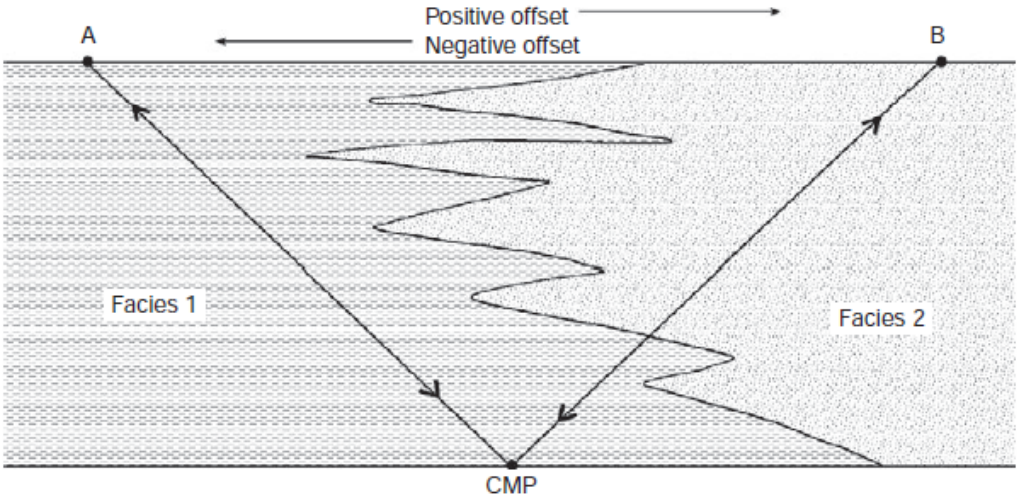

Figure 3.5. Raypaths in the CMP method. Since the length of the raypaths are the same for positive and negative offsets, the travel times are equal to each other (Hardage et al., 2011).

In Figure 3.6, the velocities and travel times of the downgoing P-wave are determined by facies 1. At the same time,the velocities and travel times of the upgoing SV-wave are governed by facies 2. This situation is concluded with different velocities of migration and stacking in the CCP method (Hardage et al., 2011).

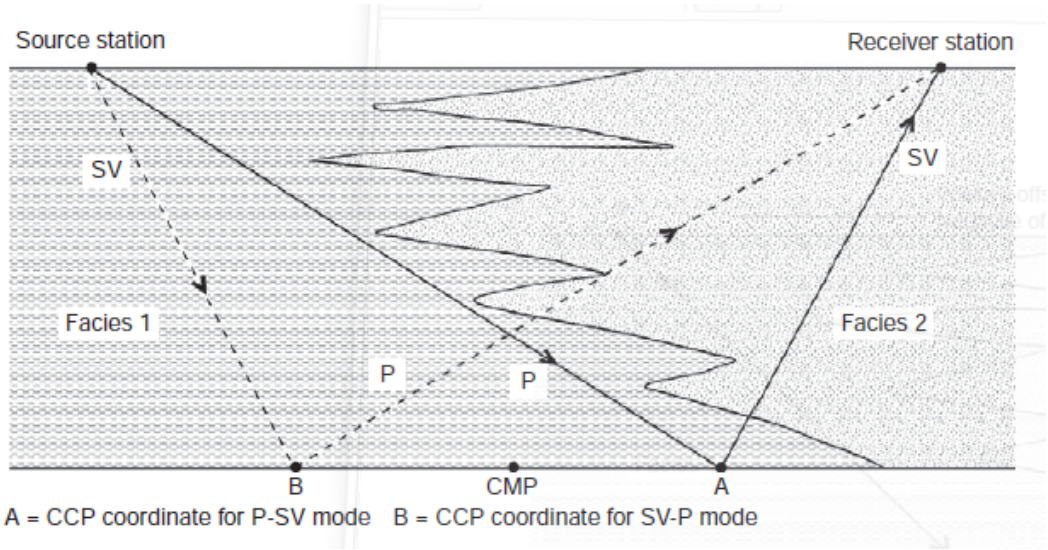

Figure 3.6. Raypaths in the CCP method. The raypaths are not the same for positive and negative offsets because of the different travel times and velocities (Hardage et al., 2011).

As a result of this distinction between positive and negative offsets in the processing of the converted waves, the multicomponent seismic data are processed as two different data volumes for both of the offsets. The stacking and migration velocities are computed differently for each offset. Finally, after obtaining the images of both volumes, these two images are summed to acquire a total offset image of the subsurface (Hardage et al., 2011). The interpreters generally prefer to obtain all of these three offset images i.e., positive, negative, and total offset image on account of the fact that some essential geological information about the subsurface could be observed better in one of these offset images than in the other two images (Hardage et al., 2011).

3.2.3. Asymptotic Binning. Bins are defined as small areas that are sorted by the common midpoints between the sources and the receivers in the conventional P-wave processing. Traces that have a common bin are then stacked or summed to produce the output CMP bin for that particular bin. As mentioned previously, the reflection point is the midpoint between the source and receiver in the CMP method since the raypaths of downgoing and upgoing waves are the same (symmetrical). On the other hand, for a converted wave, the raypaths of upgoing and downgoing waves are not the same. This leads to the reflection point being closer to the receiver station for P-SV converted mode as Snell's law indicated (Hardage et al., 2011). In the multicomponent seismic processing, since the conventional CMP method is not applicable, the CCP binning is calculated to sort the data by the common conversion points of the traces. There are a number binning methods in the converted-wave processing. One common method that is frequently used is called asymptotic binning (Schafer, 1992). In the asymptotic binning, the location of the reflection point (conversion point) changes with depth. This point is closer to the receiver station at shallow depths of the subsurface; however, it is almost vertical for the deeper parts (Hardage et al., 2011) (Figure 3.7).

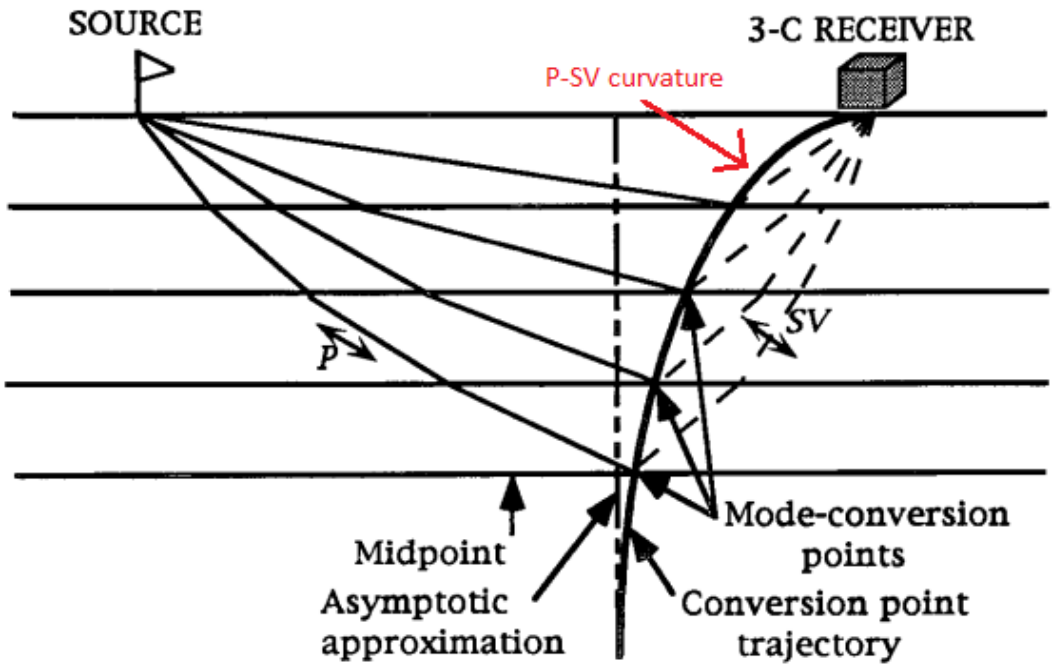

Figure 3.7. Diagram illustrating reflection point (conversion point) and asymptotic binning approach (Schafer, 1992).

Figure 3.7 demonstrates the approximation used to calculate the CCP coordinates of traces in the asymptotic binning. After calculating the coordinates of the CCP points, traces are then summed by assuming the entire trace is aligned vertically at the calculated coordinates. This approach provides a correct image for the deeper part of the subsurface, but it does not provide a correct image of the subsurface for the shallower parts (Hardage et al., 2011).

3.2.4. Gamma Functions. The curvature of P-SV converted-wave displayed in Figure 3.7 is controlled by the ratio of the P-wave and S-wave velocities in the CCP imaging. Thus, it is required to determine the Vp/Vs ratio for the seismic imaging to locate the CCP coordinates. This ratio is called gamma function, or gamma ratio, in converted-mode wave processing (Hardage et al., 2011).

Due to the fact that the velocities are offset-direction dependent in the CCP method, the two separate gamma ratios are calculated for the positive-offset and negative-offset data in 2D seismic. In 3D multicomponent seismic data processing, an additional gamma function is calculated for the reciprocal azimuth (Hardage et al., 2011).

3.2.5. Receiver Refraction Statics. The correction of static time shifts, or statics, is a key problem in the processing of the converted wave data. Due to the lower velocity of S-wave in the near subsurface, receiver statics can be large as 100–200 ms (Lu and Hall, 2003) (Figure 3.8). These static time shifts are caused by lateral variations in the near subsurface (thickness) and velocities of P and S waves (Tatham and McCormack, 1991).

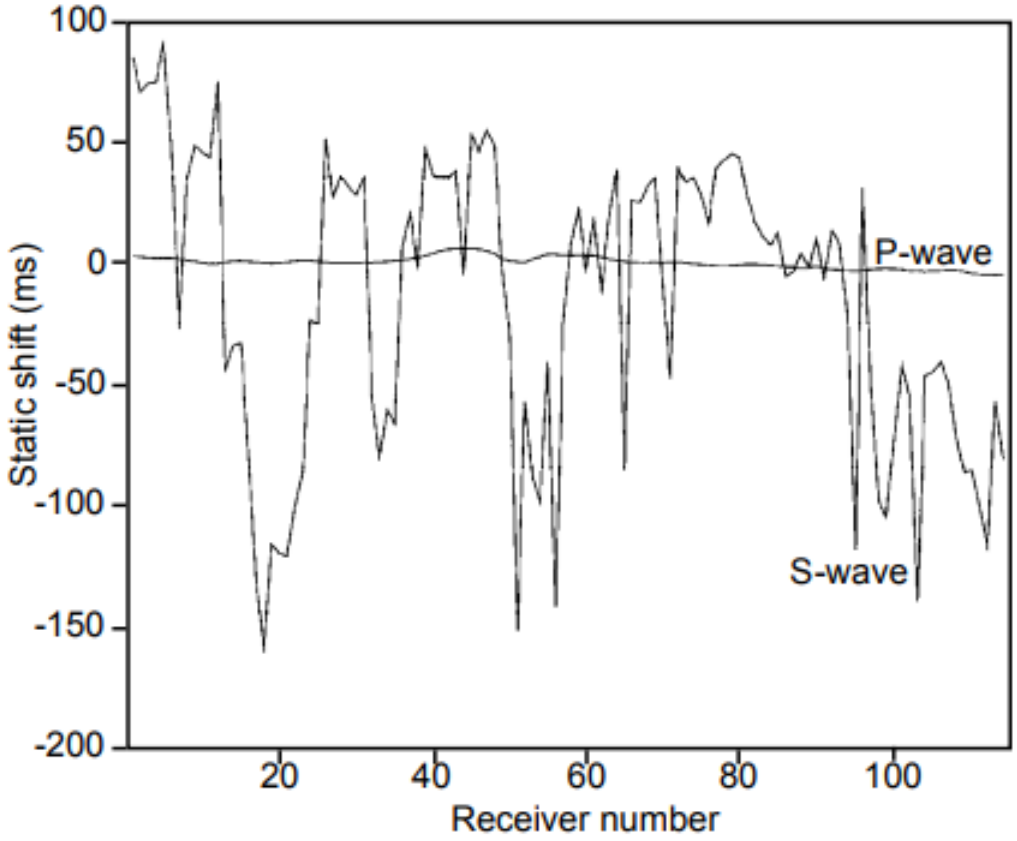

Figure 3.8. Demonstration of P-wave and S-wave receiver statics calculated from the vertical component and the radial component, respectively (Isaac, 1996).

A converted wave, for instance P-SV, consists of downgoing P-wave and upgoing S-wave. This situation expresses that shot statics are computed from P-wave velocities as in the P-P processing, and it can be used again for the processing of P-S data. However, receiver statics are calculated from S-wave velocities, and shear wave velocities change more laterally in the near subsurface than those of compressional waves. This causes difficulties to compute receiver statics in the P-S data and affects the frequency content of the seismic data severely (Lu and Hall, 2003).

Shear wave statics are generally ten times larger than the compressional wave statics for the same location (Tatham and McCormack, 1991). There are several emerging methods to estimate the receiver statics in the processing P-S data.

3.2.6. Anisotropy. If a medium is defined as an anisotropic, the elastic properties of the medium change with direction (or angle). On the contrary, isotropic medium is described as the independence of properties such as velocities on direction.

In this context, there are two main cases of anisotropy in seismic method: vertically transverse isotropy (VTI) and horizontally transverse isotropy (HTI). The former indicates that the elastic properties (or fabrics) of the medium are uniform horizontally within the layer. However, these properties vary vertically from one direction to another. In VTI, the velocities of the horizontal and vertical directions are not the same. The latter states that the properties of the medium are uniform vertically, but they vary horizontally from one lateral direction to another (Yilmaz, 2001). Figure 3.9 illustrates the vertical and horizontal transverse anisotropy.

The algorithms involved in the seismic data processing are founded on the assumption that the earth is isotropic. However, the earth itself is in reality anisotropic nearly everywhere. The influence of disregarding the anisotropy on seismic data during the processing stage is dependent on the magnitude and the type of the anisotropy (Tatham and McCormack, 1991).

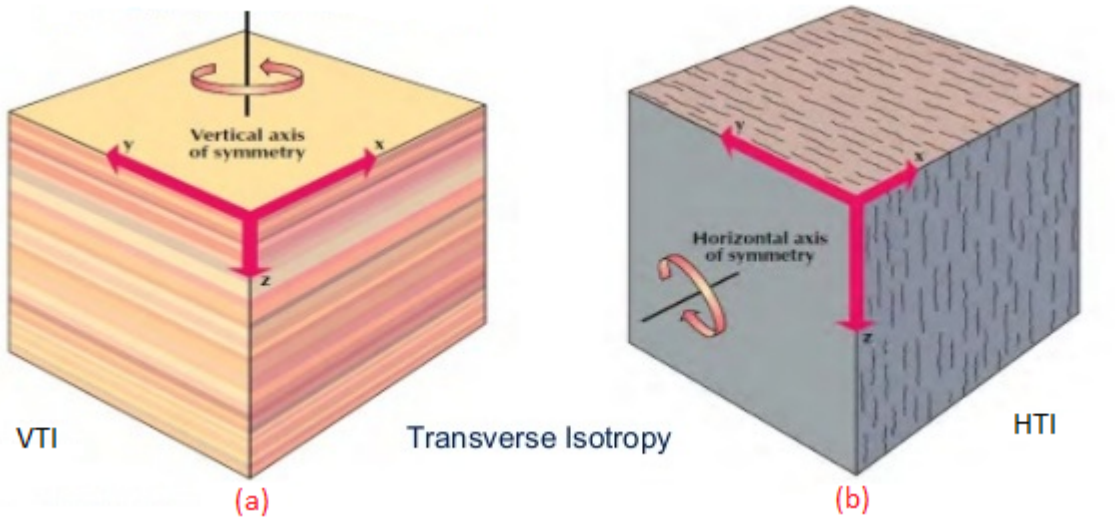

Figure 3.9. Schematic diagram of anisotropy. a) Vertical transverse isotropy (VTI). b) Horizontal transverse isotropy (HTI) (sch, 2017).

Additionally, the phenomenon of shear wave splitting, also known as a seismic birefringence, is caused by seismic anisotropy, where a shear wave passes through an anisotropic layer or medium. When a shear wave splitting occurs, the S-wave is divided into two modes that have different velocities and particle motion, i.e., fast and slow shear wave (Eaton and Stewart, 1989). The velocities of seismic waves generally are slower when seismic waves cross a boundary, and they are higher when seismic waves propagate along with the boundary or fractures in the subsurface. The attribute information of seismic anisotropy, such as the degree of anisotropy and polarization directions, is obtained from the analysis of shear wave splitting. The seismic birefringence may cause some degradation in the quality of S-wave data. For this reason, the rotation of the horizontal components of a shear wave data is used to compensate the effect of seismic anisotropy (Fang and Brown, 1996). Two modes of shear waves, fast and slow, are separated through the rotation step.

3.2.7. Rotation of Data. A multicomponent seismic survey consists of data obtained from not only a vertical geophone to record P-wave energy but also horizontal geophones to acquire S-wave energy. This is achieved by the multicomponent geophones, which are called 3C, to record seismic waves. Figure 3.10 displays the top view of a 3C geophone. The plus signs express the directions to generate a positive output (peak).

Figure 3.10. Top view of a 3C-geophone to obtain multicomponent seismic data. The positive output is generated through the positive signs (Guevara and Stewart, 1998).

The modern acquisition methods to obtain multicomponent seismic data are based on the alignment in the same orientation to provide data that have the same direction and polarity for each component. Geophone orientation is a critical step in the multicomponent seismic processing, especially in 3C-3D seismic data. The effective processing of the data is highly dependent on the correct orientation of geophones to provide accurate amplitude values (Guevara and Stewart, 1998). The two main configurations used for the orientation of the data are Cartesian configuration and Galperin configuration. The latter was developed as a tool that is mainly used for 3C borehole surveys by E.I. Galperin (Ralston and Steeples, 2002).

The Cartesian configuration is composed of three orthogonal axis or elements, i.e., one vertical (Z) and two horizontal (radial (X) and transverse (Y)). The required parameter to rotate data into the transverse and radial components is the directional azimuth calculated from the source to the receiver (Hardage et al., 2011). Figure 3.11 illustrates the procedure used in the source/receiver orientations.

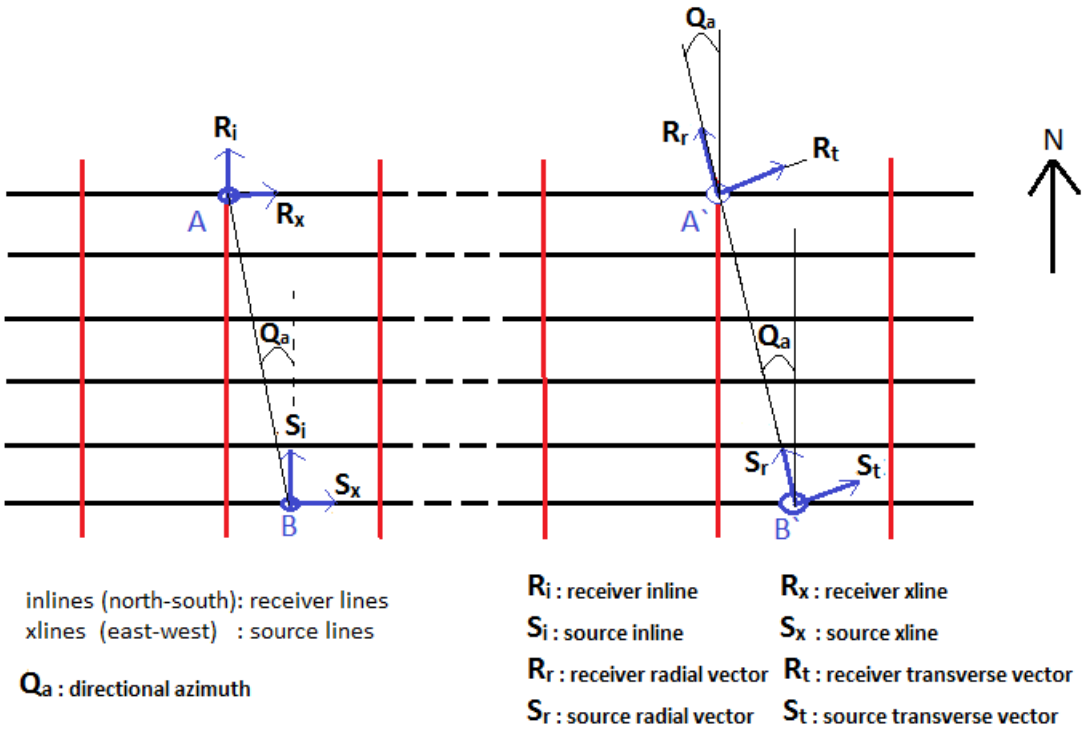

Figure 3.11. Diagram displaying the procedure to rotate source and receivers into radial and transverse coordinates (Modified from (Hardage et al., 2011)).

As mentioned previously, a 3-C geophone consists of three orthogonal channels that correspond to one vertical (Z) component and two horizontal (H1 and H2) components. The horizontal elements, H1 and H2, measure the shear wave components in the north-south and east-west direction, respectively. Rotation is performed to correct polarity changes by applying a coordinate transformation from the field coordinates (inline-crossline) to the natural coordinates (radial-transverse components) (Hardage et al., 2011).

In Figure 3.11, data acquisition coordinates are defined as inlines and crosslines. The source lines are laid out in the east-west direction (crosslines), and the receiver lines are spread out in the direction of north-south (inlines). The directional azimuth (Qa) is computed from the receiver station (A) to the source station (B) and used to rotate the data into radial and transverse components at both source and receiver stations. This angle is

measured clockwise from the north. The coordinates of all the receiver and source stations are required to calculate the directional azimuth (Qa). The calculated rotations are based on the assumption that the vectors of Ri, Rx, Si, and Sx are orthogonal (Hardage et al., 2011).

In a 2D survey, the horizontal elements of a 3-component geophones, H1 and H2, are generally laid out parallel (H1) and perpendicular (H2) to the acquisition direction. A previous study indicates that the SH-SH and SV-SV components of the seismic data can easily be acquired in a 2D survey by applying the survey acquisition plane described in Figure 3.12 (Hardage et al., 2011).

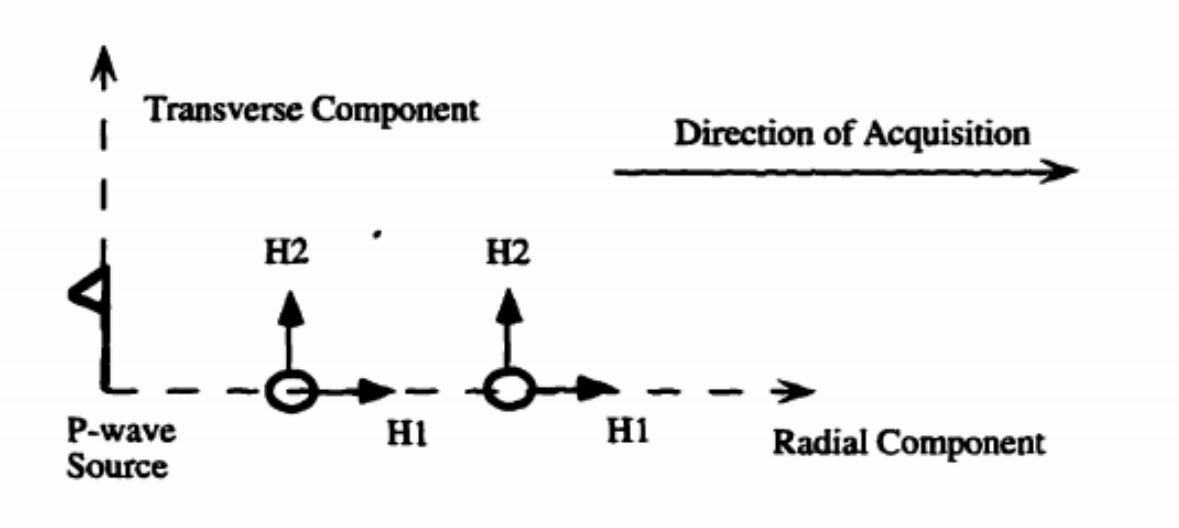

Figure 3.12. Diagram illustrating 3C-2D survey. H1 and H2 are horizontal components of 3C geophone. The channel H1 is aligned parallel to the direction of acquisition, and H2 is aligned perpendicular to the acquisition direction (Larson, 1996).

However, in a 3D survey, the natural components of the data, radial and transverse, are not oriented in the same direction as the horizontal channels of 3C geophones (H1 and H2). Thus, the rotation of the seismic data is required in a 3D survey.

3.3. THE APPLICATIONS OF MULTICOMPONENT SEISMIC METHOD

Multicomponent seismic data provide more information regarding the subsurface than the conventional P-wave method by capturing the seismic wavefield more thoroughly with the multicomponent geophones and sources that have not only vertical component but also horizontal components. The key principle in the multicomponent seismic exploration lies in the fact that the wave modes are needed to be addressed as vectors since three modes of seismic waves (P, SV, and SH) propagate through the earth with different velocities and directions (Hardage et al., 2011).

Since three seismic wave modes travel through the real earth with different velocities and directions, these modes offer unique information that is dependent upon the direction of the wave mode analyzed. The information regarding the subsurface such as elastic parameters, porosity, and anisotropy is provided by different wave modes due to their dependence on the directions (Hardage et al., 2011).

The multicomponent seismic method has gained a wide acceptance in seismic exploration industry since it offers more thoroughly information about the subsurface, and a number of successful applications have lately been implementing it (Farfour and Yoon, 2016). The applications of the multicomponent seismic method include the following (Stewart et al., 1999):

1. To offer a more comprehensive imaging of shallow subsurface.
2. To analyze anisotropy parameters.
3. To observe changes in a reservoir.
4. To examine the fracture density and lithology by using Vp/Vs.
5. To provide an additional information on P-P seismic sections with the analysis Vp/Vs ratio and correlation.

6. To image gas chimneys, mud volcanoes, the interfaces that have low P wave contrast, and substantial changes in S-wave and faults that have high angles.

Figure 3.13 demonstrates an example of a multicomponent seismic application obtained from the Alba field in the North Sea. The target reservoir in the area is a sandstone, and the low P-wave contrast between the reservoir and surrounding area causes a failure to image the reservoir reflection. In the study, the S-wave image is superior to the P-wave image since it provided a significantly clearer seismic section to image the reservoir reflection (MacLeod et al., 1999).

Figure 3.14 shows a seismic section obtained from the Offshore Brazil. The P-wave seismic section displays the flat spot that is related to fluid contact (oil-water contact) and gas above it. Since the S-wave does not give anomalies to fluid or gas presence, features such as oil-water contact and gas cap are not observed on the seismic section obtained from the converted wave. This fact provides complementary information for verifying hydrocarbon presence (Farfour and Yoon, 2016).

Figure 3.15 displays another comparison of the P-P image with the P-S image from a 3D multicomponent survey. In the P-P section, it is observed that the shallow gas obscures reflections that are at the crest of the structure. On the other hand, the P-S section from a seabed survey distinctly reveals the large fault that goes through the structure at the crest with reflections that have high amplitudes (Barkved et al., 2004).

Another example of multicomponent seismic data is presented to correlate the P-P data and P-S data (Stewart et al., 1996). Figure 3.16 shows the correlation of sections obtained from the 3C-10 Hz geophones in the 3D Blackfoot survey. The correlation of the sections are well established by taking into account the major reflectors from the Cretaceous and deeper parts (Wabamun and Viking isochrons).

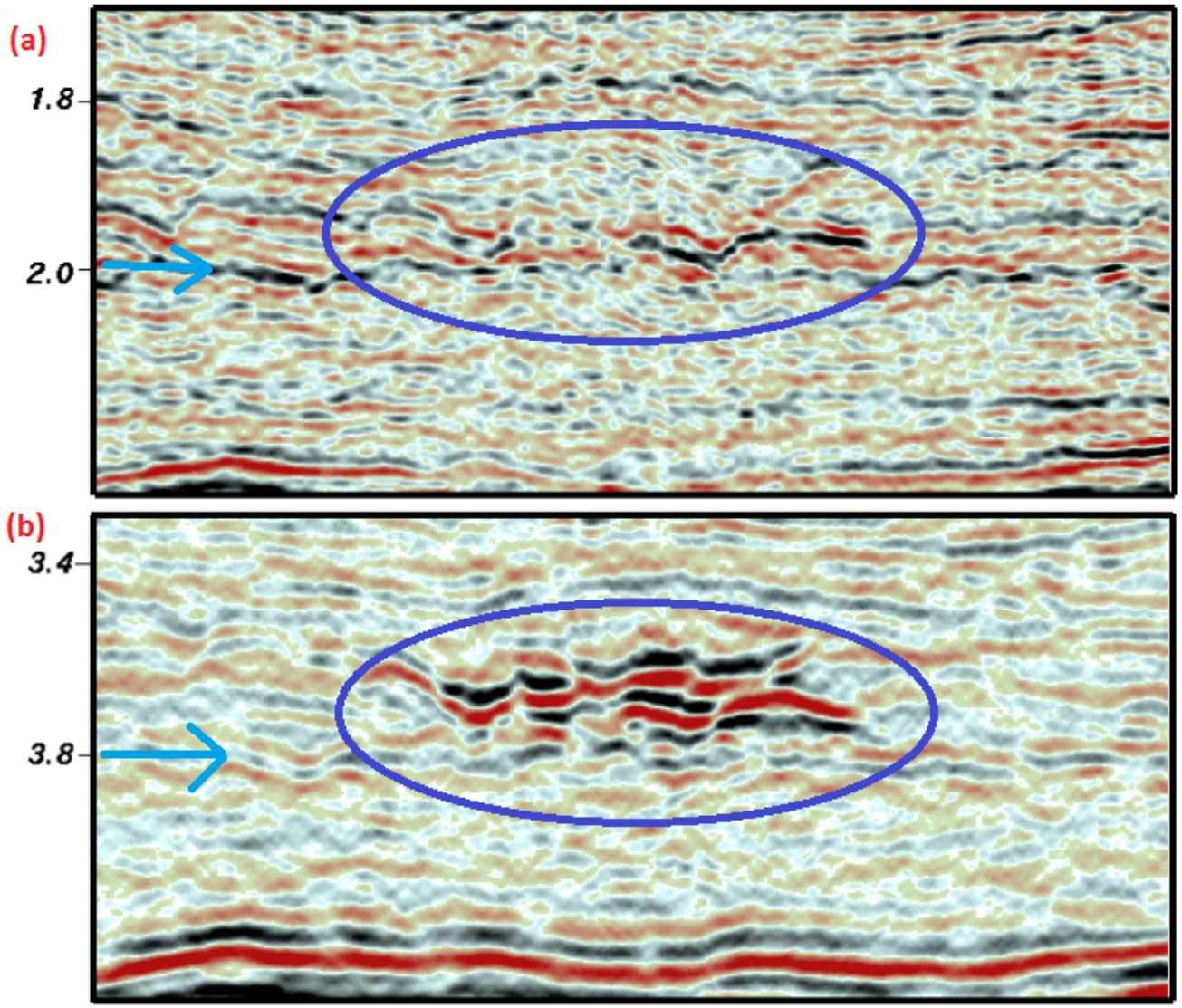

Figure 3.13. Seismic sections obtained from Alba Field. a) Streamer P-wave in 1989. b) Ocean bottom cable (OBC) shear wave in 1998. The reservoir reflection is imaged more clearly in S-wave data (MacLeod et al., 1999).

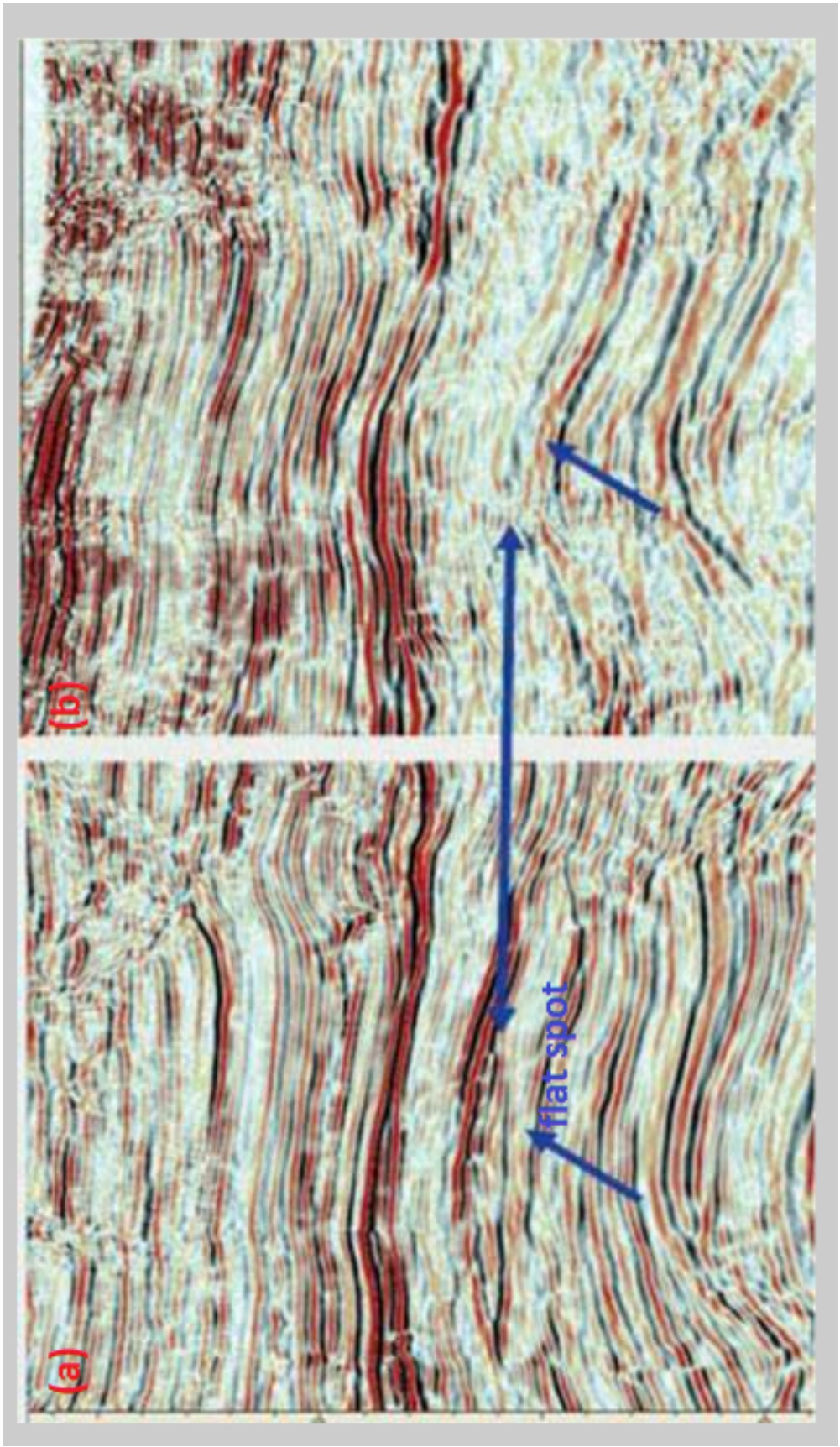

Figure 3.14. Seismic sections obtained from the Offshore Brazil. a) P-wave section. b) Shear wave section. The flat spot related to oil-water contact, and gas is not observed on the S-wave section (Cafarelli et al., 2006).

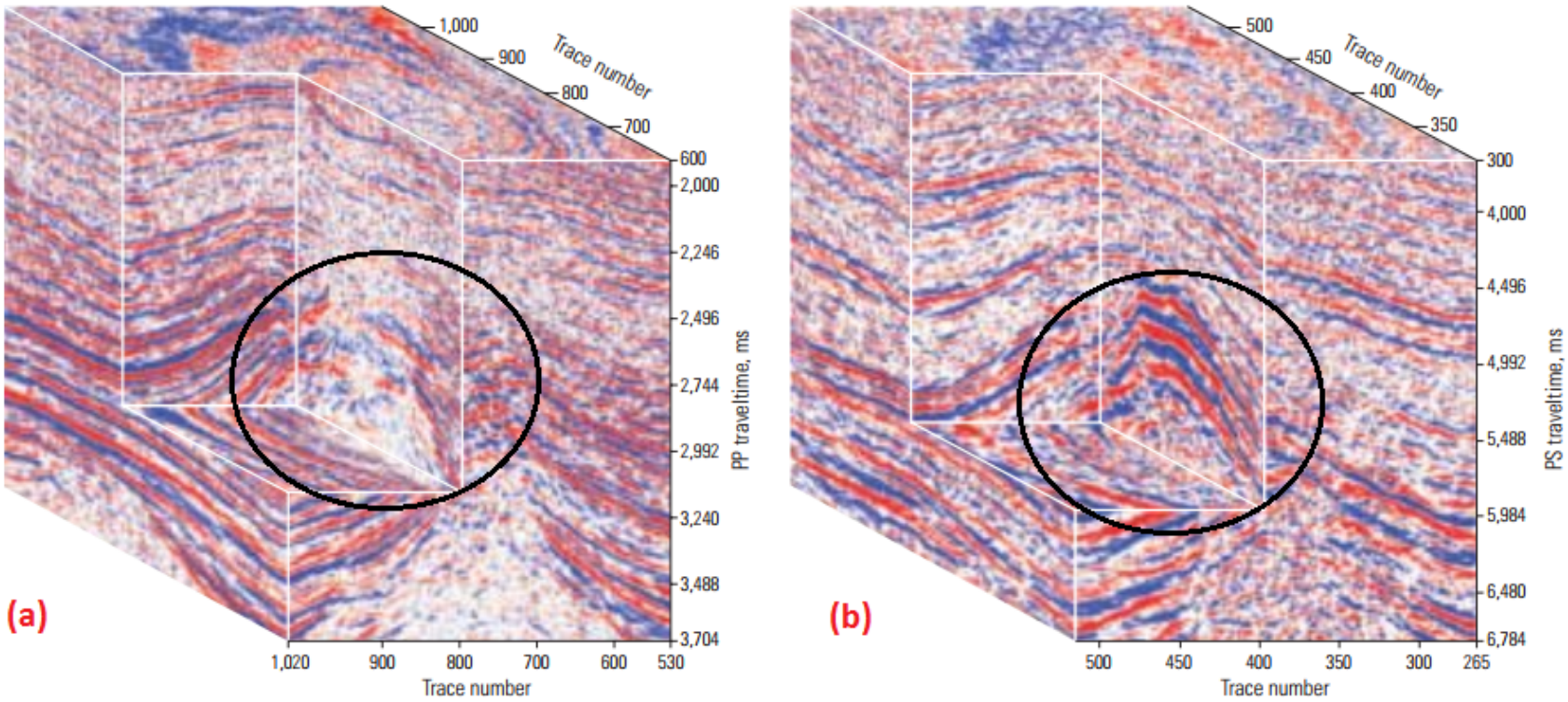

Figure 3.15. Seismic sections. a) P-P from towed-marine survey b) P-S from seabed survey. The fault going trough the structure at the crest is clearly revealed in P-S section. Also, P-S image offers the structure with reflections that have high amplitudes (Barkved et al., 2004).

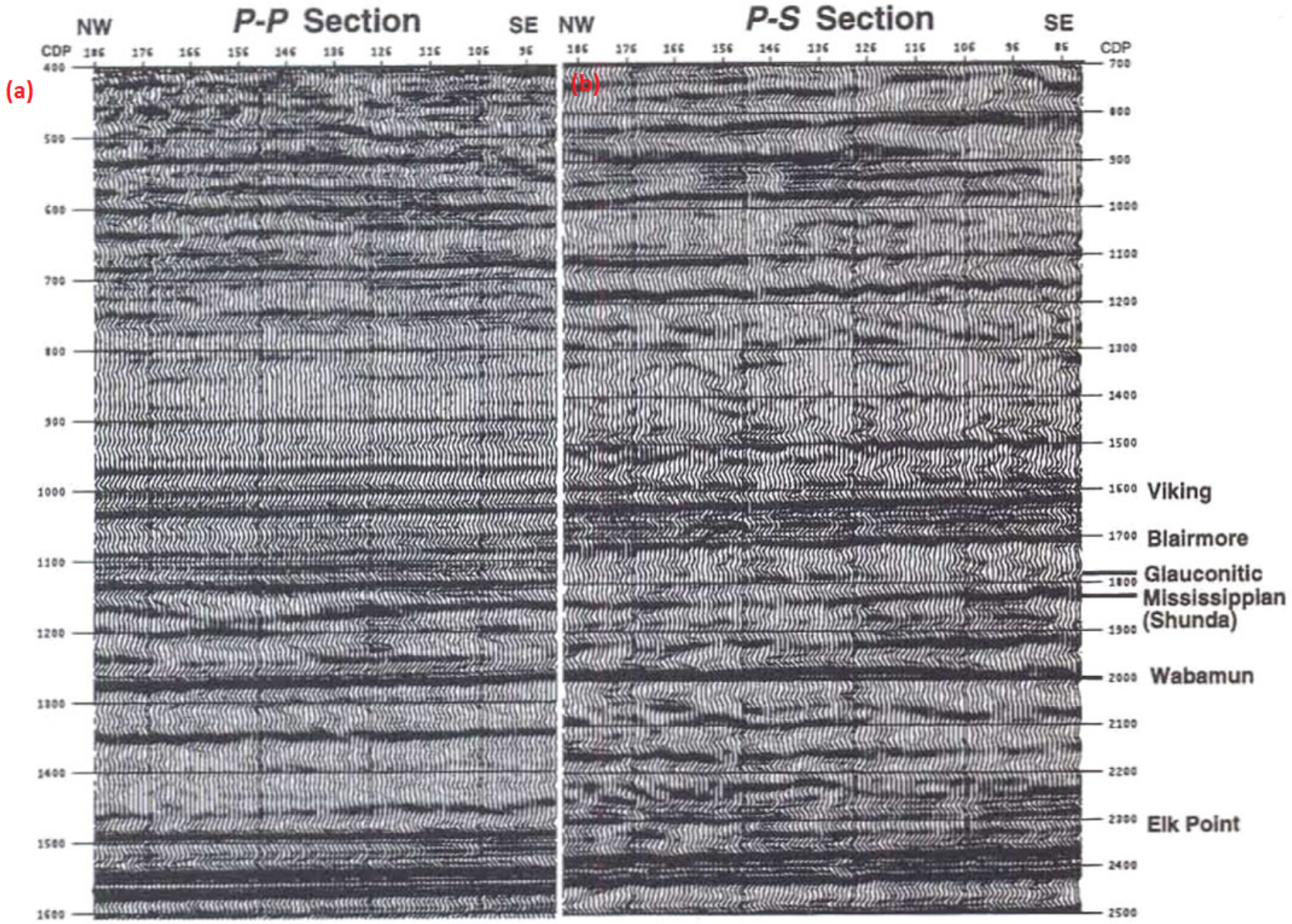

Figure 3.16. P-P and P-S seismic sections. a) P-P section. b) P-S section in the Blackfoot 3C-3D survey. The Wabamun and Viking isochrons proves that the correlation of the P-P and P-S sections are established well (Stewart et al., 1996).

In summary, multicomponent seismic exploration methods have been used for searching hydrocarbon resources since the 1980s (Stewart et al., 1999). The real data examples obtained from the multicomponent data (Figure 3.13 – 3.16) are proven to be valuable in many areas where conventional P-wave methods have encountered difficulties to indicate gas presence and complex geological conditions (Farfour and Yoon, 2016). Due to its increasing successful applications and the developments in the acquisition, processing, and interpretation techniques, the multicomponent seismic technology is increasingly utilized in the oil/gas industry.

4. CONCLUSIONS

The 2 Hz vertical component data obtained from the Blackfoot 3C-2D survey was reprocessed to better image the reservoir, the Glauconitic sand formation, which is at approximately 1150 ms. The two main areas that were taken into consideration in the processing of the seismic data were the target reservoir, the Glauconitic sand formation and the major reflector, which is at about 1550 ms. The obtained results and seismic sections were compared by having taken into account the two main areas in question. The decisions were made based on the improvements of these two target zones on the seismic sections. The areas below 2000 ms were not taken into account during the processing stages.

The seismic data was imported into the software as a SEG-Y format. The data geometry was set accordingly. The dead shots and missing shots were omitted from the records. The noisy traces were removed, and the polarity reversals were corrected.

The spherical divergence correction (gain) was applied to compensate for decreases in the seismic wave amplitude because of the geometrical spreading of wavefronts. The time-variant suppression was applied and increased the signal-to-noise ratio. The data analyses were conducted to eliminate possible noises caused by air blasts, noise bursts, or cable. The obtained results indicate that the noises obscuring the seismic data have been attenuated notably, particularly the ground roll noise. Reflections have been revealed clearly.

Surface consistent and predictive deconvolutions were applied to the seismic data to sharpen the seismic events and increase the frequency bandwidth. Spectral analyses were also performed to examine the frequency recovery for both deconvolutions tested. The amplitude spectra show that there was an observable recovery in the frequency contents of

both methods. According to the seismic sections, the stacked section with surface consistent deconvolution offers better results when taking into account the target zones in question, and it was used for further processing steps.

Elevation and refraction static corrections were used to correct the long wavelengths. Each was stacked to determine the better seismic section for further processing steps. The obtained results indicate that the refraction static corrections offered a better seismic section on the target zones specified than elevation statics.

The constant velocity stack and semblance methods were used in the analysis of the velocities. After applying NMO correction on the common midpoint (CMP) gathers, the primary reflections of the seismic data were flattened.

The two iterations of residual corrections were performed to correct short wavelengths. Each iteration was followed by a velocity analysis to improve the velocity picks and attain better quality in the stacked section. The obtained seismic sections suggest that residual static corrections improved the seismic section significantly, particularly the target zone.

The final stacked section with a floating datum was obtained. The seismic section fixed to a reference flat datum was also obtained in order to effectively use the migration algorithm in the migration step. The seismic data and velocities were shifted back to a reference flat datum for the spatial interpolation.

Two-dimensional Kirchhoff prestack time migration (PSTM) and poststack time migration were applied to image the subsurface. As mentioned before, the reservoir in the Blackfoot Field has similar P-wave anomalies to the neighboring shales. For this reason, it is difficult to observe the reservoir on the P-wave section. Spectral whitening was applied to the migrated sections to enhance the resolution and appearance of the reservoir. The obtained migrated sections indicate that the prestack time migration method offered stronger amplitudes in the target zone than the poststack time migration. Additionally, the channel

cuts were observed more visible on the seismic section with the prestack time migration method. As a result, the PSTM succeeded and revealed the Glauconitic sand reservoir better than the poststack time migration.

BIBLIOGRAPHY

1. Sch., 2017, Transverse isotropy. http://www.glossary.oilfield.slb.com/Terms/h/horizontal_transverse_isotropy.aspx. accessed December 13, 2017.

2. Barkved, O., Bartman, B., Gaiser, J., Van Dok, R., Johns, T., Kristiansen, P., Probert, T., and Thompson, M., 2004, The many facets of multicomponent seismic data: Oilfield Review, **16(2)**, 42–56.

3. Bording, R. P. and Lines, L. R., 1997, *S*eismic modeling and imaging with the complete wave equation: SEG.

4. Cafarelli, B., Randazzo, S., Campbell, S., Sobreira, J. F. F., Guimaraes, M. A. G., Rodriguez, C., Johann, P., and Theodoro, C., 2006, Ultra-deepwater 4-C offshore Brazil, The Leading Edge, **25(4)**, 474–477.

5. Christopher, J., 2002, The heavy oil-production lower Cretaceous Mannville sandstones of the unity-biggar district, west-central Saskatchewan: Saskatchewan geological survey, Saskatchewan industry and resources, Misc. Rep, **4**, 107–117.

6. Connolly, C. A., Walter, L. M., Baadsgaard, H., and Longsta˙e, F. J. , 1990, Origin and evolution of formation waters, Alberta Basin, Western Canada sedimentary Basin. I. Chemistry: Applied Geochemistry, **5(4)**, 375–395.

7. Covre, M. R., Barros, T., and da Rocha Lopes, R., 2014, High resolution stacking of seismic data: IEEE, In Signal Processing Conference (EUSIPCO), Proceedings of the 22nd European, pages 1009–1013.

8. Cox, M., 1999, Static corrections for seismic reflection surveys: SEG.

9. Dell, S., Gajewski, D., and Vanelle, C., 2012, Prestack time migration by common-migrated-reflector-element stacking: Geophysics, **77(3)**, S73–S82.

10. Dufour, J., Squires, J., Edmunds, A., and Shook, I., 1998, Integrated geological and geophysical interpretation of the Blackfoot area, southern Alberta: SEG, Expanded Abstracts , 1949-4645.

11. Dutta, S., Rao, B., Parasuman, K., Babu, B., and Parasad, K., 2010, 3D pre-stack merging: A case history in Cauvery Basin: Biennial International Conference Exposition on Petroleum Geophysics, page 110.

12. Dyson, I., and Christopher, C., 1994, Sequence stratigraphy of an incised-valley fill: the neoproterozoic seacli˙ sandstone, adelaide geosyncline, south Australia, 209-222, 10.2110/pec.94.12.0209.

13. Eaton, D. W. and Stewart, R. R., 1989, Aspects of seismic imaging using P-SV converted waves: CREWES Project Research Report, **6**, 68–92.

14. Eberhart-Phillips, D., Han, D.-H., and Zoback, M. D., 1989, Empirical relationships among seismic velocity, effective pressure, porosity, and clay content in sandstone: Geophysics, **54(1)**, 82–89.

15. Fang, K. and Brown, R. J., 1996, A new algorithm for the rotation of horizontal components of shear-wave seismic data: CREWES Project Research Report, page 12.

16. Faquan, F. and Yusheng, Z., 2011, Highly effective refractor residual static corrections and its applications: SEG, In Nonrecurring Meetings 2011, International Geophysical Conference, Shenzhen, China, pages 11–11.

17. Farfour, M. and Yoon, W. J., 2016, A review on multicomponent seismology: A potential seismic application for reservoir characterization: Journal of Advanced Research, **7(3)**, 515–524.

18. Gadallah, M. R. and Fisher, R. L., 2005, Applied seismology: A comprehensive guide to seismic theory and application: Pennwell Books.

19. Gallant, E., Stewart, R., Malcolm, B., and Lawton, D., 1996, Acquisition of the Blackfoot broad-band seismic survey: CREWES Project Research Report.

20. Gorek, S. J., Stewart, R. R., and Harrison, M. P. , 1995, Processing the Blackfoot broad-band 3-C seismic data: Technical report, Tech. rep., Consortium for Research in Elastic Wave and Exploration Seismology.

21. Guevara, S. E. and Stewart, R. R., 1998, Multicomponent seismic polarization analysis: CREWES Project Research Report, **10**.

22. Hardage, B. A., DeAngelo, M. V., Murray, P. E., and Sava, D., 2011, Multicomponent Seismic Technology: SEG.

23. Hatherly, P. J., Urosevic, M., Lambourne, A., and Evans, B. J., 1994, A simple approach to calculating refraction statics corrections: Geophysics, **59(1),**156–160.

24. Isaac, J. H., 1996, Seismic methods for heavy oil reservoir monitoring: Geology and Geophysics, University of Calgary.

25. Kaufman, H., 1953, Velocity functions in seismic prospecting: Geophysics, **18(2)**, 289–297.

26. Larson, G. A., 1996, Acquisition, processing, and interpretation of PP and PS 3-D seismic data: M.S. Thesis, University of Calgary.

27. Li, Q.-Z., 2017, High-resolution seismic exploration: SEG.

28. Lu, H.-x. and Hall, K., 2003, Tutorial: Converted wave (2D PS) processing: Technical report, CREWES Project Research Report.

29. Lu, H.-x. and Maier, R., 2009, Revisiting the Blackfoot 3C-2D broad-band seismic data. CREWES Project Research Report, **21**.

30. MacLeod, M., Hanson, R., Bell, C., and McHugo, S., 1999, The Alba field ocean bottom cable seismic survey: Impact on development: The Leading Edge, **18(11)**, 1306–1312.

31. Margrave, G. F., 1995, Estimates of the signal band of the Blackfoot broad-band data.

32. Mawdsley, M. J., Earner, A. L., Zaitlin, B. A., et al., 1996, Exploration for incised valley channel sandstones of the lower cretaceous (Alberta, Canada) using 3D seismic: Risks and opportunities: In 1996 SEG Annual Meeting, SEG.

33. Miller, S. L., Aydemir, E., and Margrave, G. F., 1995, Preliminary interpretation of P- P and P-S seismic data from the Blackfoot broad-band survey: Technical report, CREWES Project Research Report.

34. Mossop, G. D. and Shetsen, I., 1994, Geological atlas of the Western Canadian sedimentary basin: Published jointly by the Canadian Society of Petroleum Geologists and the Alberta Research Council, in sponsorship Association with the Alberta Department of Energy and the Geological Survey of Canada.

35. O'Haver, T., 2007, Intro to signal processing-deconvolution: University of Maryland at College Park.

36. Okonkwo, O. S., 2014, Improved interpretation of an incised valley system-channel delineation and thickness estimation using spectral inversion, Blackfoot Field, Alberta, Canada: PhD thesis, University of Calgary.

37. Peacock, K. and Treitel, S., 1969, Predictive deconvolution: Theory and practice: Geophysics, **34(2),** 155-169.

38. Ralston, M. and Steeples, D., 2002, A three-component acquisition system: Geophysics.

39. Rastogi, R., Yerneni, S., and Phadke, S., 2000, Aperture width selection criterion in Kirchhoff migration.

40. Regulator, A. E., 2015, Alberta's Energy Reserves 2015 and Supply/Demand 2014-2023: Statistical Series, (ST) 2015–98.

41. Sajid, M. and Ghosh, D., 2014, A fast and simple method of spectral enhancement: Geophysics, **79(3)**, V75–V80.

42. Schafer, A. W., 1992, A comparison of converted-wave binning methods using a synthetic model of the highwood structure, Alberta: Technical report, CREWES Project Research Report.

43. Sheriff, R. E. and Geldart L. P., 1995, Exploration Seismology: Cambridge University Press.eri˙, R., 2004, What 1995, Exploration Seismology: Cambridge University

44. Stewart, R., 1995, The Blackfoot broad-band 3-C seismic survey: Introduction: CREWES Project Research Report.

45. Stewart, R., Ferguson, R., Miller, S., Gallant, E., and Margrave, G., 1996, The Blackfoot seismic experiments: Broad-band, 3C-3D, and 3-D VSP surveys: Canadian Society of Exploration Geophysics, **21(6)**, 7–10.

46. Stewart, R. R., 2014, Multicomponent passive: Technical report, IRIS.

47. Stewart, R. R., Gaiser, J. E., Brown, R. J., and Lawton, D. C., 1999, Converted-wave seismic exploration: a tutorial: CREWES Project Research Report.

48. Stockwell, J., 2012, A course in geophysical image processing with seismic unix: Center for Wave Phenomena.

49. Taner, M. and Koehler, F., 2001, Velocity spectra: Digital computer derivation and applications of velocity functions: Geophysics, **(8),** 859–881.

50. Tatham, R. H. and McCormack, M. D., 1991, Multicomponent seismology in petroleum exploration: SEG.

51. Ulrych, T. J. and Matsuoka, T., 1991, The output of predictive deconvolution: Geophysics, **56(3)**, 371-377.

52. Wood, J. M. and Hopkins, J. C., 1992, Traps associated with paleovalleys and interfluves in an unconformity bounded sequence: Lower cretaceous glauconitic member, southern Alberta, Canada (1): AAPG Bulletin, **76(6),** 904–926.

53. Yang, G., Lawton, D., Stewart, R., Miller, S., Potter, C., and Simin, V., 1996, Interpretation and analysis of the Blackfoot 3C-3D seismic survey. CREWES Project Research Report, 8.

54. Yilmaz, O., 2001, Seismic data analysis: Processing, inversion, and interpretation of seismic data: SEG, page 2065.

55. Zheng, Y. et al., 2000, Migration redatuming and velocity conversion: In 2000 SEG Annual Meeting, SEG.

56. Zhou, H.-W., 2014, Practical seismic data analysis: Cambridge University Press.

57. Zhu, X., Gao, R., Li, Q., Guan, Y., Lu, Z., and Wang, H., 2014, Static corrections methods in the processing of deep reflection seismic data: Journal of Earth Science, 25(2), 299–308.

VITA

Onur Akturk was born in Istanbul, Turkey. He graduated from Istanbul University with a bachelor's degree in geophysical engineering in 2013. He had an internship at the department of the Earthquake Research Center in the Istanbul Metropolitan Municipality.

Upon graduating, he was awarded a scholarship from the Turkish Petroleum Co-operation (TPAO) to pursue a master's degree in the field of the multicomponent seismic processing in 2014. He completed the intensive English program at Rice University. In January 2016, he started studying as a graduate student in the department of Geosciences and Geological and Petroleum Engineering at Missouri University of Science and Technology. He worked on the reprocessing of the 2 Hz vertical component data obtained from the Blackfoot 3C-2D survey acquired in Alberta during his studies. He received the MS in Geology and Geophysics from Missouri University of Science and Technology in May 2018.